



THE UNIVERSITY *of* EDINBURGH

## Edinburgh Research Explorer

### **CtBP1-Mediated Membrane Fission Contributes to Effective Recycling of Synaptic Vesicles**

**Citation for published version:**

Ivanova, D, Imig, C, Camacho, M, Reinhold, A, Guhathakurta, D, Montenegro-Venegas, C, Cousin, MA, Gundelfinger, ED, Rosenmund, C, Cooper, B & Fejtova, A 2020, 'CtBP1-Mediated Membrane Fission Contributes to Effective Recycling of Synaptic Vesicles', *Cell Reports*, vol. 30, no. 7, pp. 2444-2459.e7. <https://doi.org/10.1016/j.celrep.2020.01.079>

**Digital Object Identifier (DOI):**

[10.1016/j.celrep.2020.01.079](https://doi.org/10.1016/j.celrep.2020.01.079)

**Link:**

[Link to publication record in Edinburgh Research Explorer](#)

**Document Version:**

Peer reviewed version

**Published In:**

Cell Reports

**General rights**

Copyright for the publications made accessible via the Edinburgh Research Explorer is retained by the author(s) and / or other copyright owners and it is a condition of accessing these publications that users recognise and abide by the legal requirements associated with these rights.

**Take down policy**

The University of Edinburgh has made every reasonable effort to ensure that Edinburgh Research Explorer content complies with UK legislation. If you believe that the public display of this file breaches copyright please contact [openaccess@ed.ac.uk](mailto:openaccess@ed.ac.uk) providing details, and we will remove access to the work immediately and investigate your claim.



CtBP1-mediated membrane fission contributes to effective recycling of synaptic vesicles

Daniela Ivanova<sup>1,2,3#</sup>, Cordelia Imig<sup>4\*</sup>, Marcial Camacho<sup>5\*</sup>, Annika Reinhold<sup>5</sup>, Debarpan Guhathakurta<sup>3</sup>, Carolina Montenegro-Venegas<sup>2</sup>, Michael A. Cousin<sup>6</sup>, Eckart D. Gundelfinger<sup>2,7</sup>, Christian Rosenmund<sup>5</sup>, Benjamin Cooper<sup>4</sup>, Anna Fejtova<sup>1,2,3,8</sup>

1 RG Presynaptic Plasticity, Leibniz Institute for Neurobiology, Magdeburg, Germany

2 Department of Neurochemistry and Molecular Biology, Leibniz Institute for Neurobiology, Magdeburg, Germany

3 Molecular Psychiatry, Department of Psychiatry and Psychotherapy, University Hospital Erlangen, Friedrich-Alexander-Universität Erlangen-Nürnberg (FAU), Germany

4 Department of Molecular Neurobiology, Max Planck Institute of Experimental Medicine, 37075 Göttingen, German

5 Institute of Neurophysiology, Charité-Universitätsmedizin Berlin, Berlin, Germany

6 Centre for Discovery Brain Sciences, Hugh Robson Building, George Square, University of Edinburgh, UK, EH9 9XD

7 Center for Behavioral Brain Science and Medical Faculty, Otto von Guericke University Magdeburg, Germany

8 Lead contact

# Present address: Centre for Discovery Brain Sciences, Hugh Robson Building, George Square, University of Edinburgh, UK, EH9 9XD

Corresponding author: Anna.Fejtova@uk-erlangen.de

\*Equally contributing authors

**Summary (150 words)** Compensatory endocytosis of released synaptic vesicles (SVs) relies on coordinated signaling at the lipid-protein interface. Here, we address the synaptic function of C-

terminal binding protein 1 (CtBP1), a ubiquitous regulator of gene expression and membrane trafficking, in cultured hippocampal neurons. In the absence of CtBP1 synapses formed in higher density and showed changes in SV distribution and size. The increased basal neurotransmission and enhanced synaptic depression could be attributed to a higher vesicular release probability and a smaller fraction of release-competent SVs, respectively. Rescue experiments with specifically targeted constructs indicated that while synaptogenesis and release probability were controlled by nuclear CtBP1, the efficient recycling of SVs relied on its synaptic expression. The ability of presynaptic CtBP1 to facilitate compensatory endocytosis depended on its membrane fission activity and the activation of the lipid-metabolizing enzyme PLD1. Thus, CtBP1 regulates SV recycling by promoting a permissive lipid environment for compensatory endocytosis.

**Keywords: (up to 10)**

Compensatory endocytosis, CtBP1, Bassoon, PLD1, synaptic vesicle recycling, membrane fission, short-term plasticity, synaptic vesicle pools, presynapse

**Introduction:**

C-terminal binding protein 1 (CtBP1) is a ubiquitously expressed dual-function protein that acts as a transcriptional corepressor in the cell nucleus and as a regulator of membrane fission in the cytoplasm (Chinnadurai, 2009; Valente et al., 2013). It is expressed in most types of neurons, where it shows a distinct localization to nuclei and presynapses (Hubler et al., 2012; tom Dieck et al., 2005). Presynaptic CtBP1 is localized in the vicinity of the active zone via its direct binding to two large, highly homologous active zone scaffolding proteins: bassoon (Bsn) and piccolo (Pclo) (Ivanova et al., 2015; tom Dieck et al., 2005). A dynamic synapto-nuclear shuttling of CtBP1, induced by changes in its affinity to Bsn and regulated by neuronal activity and cellular NAD/NADH ratio was shown to control the expression of a variety of neuroplasticity-related genes (Ivanova et al., 2016; Ivanova et al., 2015). While the importance of CtBP1-dependent transcriptional regulation of neuroplasticity genes emerged from recent studies (Garriga-Canut et al., 2006; Ivanova et al., 2016; Ivanova et al., 2015), the role of synaptic CtBP1 is still elusive. Here we hypothesize that in addition to being implicated in the remote control of gene expression, synaptic CtBP1 might directly contribute to neurotransmitter release and SV recycling. The involvement of CtBP1 in various membrane fission processes at the Golgi and plasma membrane in non-neuronal cells is in support of this view (Valente et al., 2013). Although the mechanism of CtBP1-mediated fission remains controversial, an increasing body of evidence suggests that it induces formation of vesicular carriers by recruiting and orchestrating numerous enzymes that

promote local lipid reorganization leading to membrane bending (Valente et al., 2013). This is mechanistically distinct from the principle of torsional force utilized in dynamin-mediated fission, most commonly implied in SV recycling (Antonny et al., 2016; Renard et al., 2018). Despite the well-established role of dynamin in SV fission, recent findings suggest that dynamin-independent forms of endocytosis might occur at hippocampal synapses (Gan and Watanabe, 2018; Wu et al., 2014). Moreover, a crosstalk and cooperativity between dynamin-mediated fission, actin cytoskeleton-mediated vesicle reformation and lipid reorganization by lipid-modifying enzymes in the execution of SV recycling were recently suggested (Puchkov and Haucke, 2013; Soykan et al., 2017; Wu et al., 2016).

In this study, we investigate the potential role of synaptic CtBP1 in the regulation of SV fusion and recycling. Using knock down (KD), knock out (KO) and complementation approaches we demonstrate that while loss of nuclear CtBP1 expression increases synaptogenesis and release probability of SVs, the depletion of synaptic CtBP1 leads to defects in SV retrieval, accompanied by an enlargement of the docked synaptic vesicles and pronounced synaptic depression during sustained neurotransmission. Functional experiments and super-resolution imaging indicate that synaptic CtBP1 acts at the same membrane domain as dynamin to promote SV recycling. Our results revealed a crucial requirement for CtBP1-mediated membrane fission and the activity of Phospholipase D1 (PLD1) in this process. Finally, we show that CtBP1 phosphorylation by the signaling kinase p21 (RAC1) activated kinase 1 (Pak1) provides a molecular switch controlling its re-distribution from the active zone protein Bsn to the endocytic effector PLD1, thus fine-tuning its membrane trafficking activity and potentially linking presynaptic exo- and endocytic processes.

## **Results:**

### **CtBP1 contributes to synaptic vesicle retrieval and regulates the size of the total recycling pool**

To assess whether the absence of CtBP1 affects synaptic structure and function we used a previously established RNA-interference approach in cultured hippocampal neurons (Ivanova et al., 2015). Significant downregulation of CtBP1, but no obvious differences in the morphology and the expression of pre- and post-synaptic markers or CtBP2, a close homologue of CtBP1, were observed between controls expressing scrambled shRNA (scr) and CtBP1 knock down (CtBP1KD) neurons expressing target shRNAs: CtBP1KD944 or CtBP1KD467 (Figure 1A,B; Figure S1A-D). Likewise, no regulation of synaptic proteins and CtBP2 were observed in homogenates or P2 fractions obtained from brains of *CtBP1* knock out animals (Figure S2A,B).

91 To assess SV turnover in the absence of CtBP1 we applied a fluorophore-coupled antibody  
92 recognizing the luminal domain of the integral SV protein synaptotagmin 1 (Syt1 Ab) to living  
93 neurons. Syt1 Ab binds to its epitope which is transiently accessible upon SV fusion with the  
94 plasma membrane until its internalization during compensatory endocytosis. The fluorescence  
95 intensity of the internalized Syt1 Ab provides an estimate of SV recycling at individual synapses  
96 (Kraszewski et al., 1995; Lazarevic et al., 2011). The Syt1 Ab uptake driven by endogenous  
97 activity (network activity-driven release) was reduced by about 50% in CtBP1KD neurons as  
98 compared to controls (30 min incubation; Figure 1C,D). To address the potential contribution of  
99 an increased neuronal network activity to this phenotype and isolate presynaptic effects, we also  
100 measured the spontaneous (i.e. action potential-independent) SV recycling within 30 min in the  
101 presence of TTX and the pool of all fusion-competent vesicles (total recycling pool, TRP) upon  
102 brief depolarization with 50 mM KCl. In both conditions Syt1 Ab uptake was strongly reduced  
103 (~50%) in CtBP1KD (Figure 1C), indicating an impairment in both evoked and spontaneous SV  
104 recycling at CtBP1-deficient synapses.

105 To monitor SV recycling by an alternative approach we expressed scr and CtBP1KD944 and  
106 CtBP1KD467 from a bicistronic vector together with ratio:sypHy (sypHy) (Figure 1E). SypHy is an  
107 indicator composed of the SV protein synaptophysin 1, fused to pH-sensitive GFP in one of the  
108 luminal domains and tdimer 2 in the cytoplasmic domain which allows its visualization prior to  
109 stimulation (Granseth et al., 2006; Rose et al., 2013). The fluorescence of sypHy increases upon  
110 SV exocytosis and decays following SV endocytosis and re-acidification. To determine the sizes  
111 of the readily releasable pool (RRP) and the recycling pool (RP) we utilized bafilomycin A1, a  
112 blocker of the vesicular proton pump that prevents the re-acidification of endocytosed SVs and  
113 thus the decline of sypHy fluorescence (Burrone et al., 2006). Exocytosis of the SVs from RRP  
114 and RP was evoked by the sequential delivery of 40 and 200 action potentials (AP) at 20 Hz  
115 (Figure 1E-G). In CtBP1KD neurons around 14% of the sypHy positive SVs fused upon  
116 stimulation with 40 AP at 20 Hz (i.e. RRP), which was comparable to control neurons. The  
117 delivery of additional 200 AP triggered exocytosis of ~50% of all sypHy-labeled SVs in controls,  
118 but only ~30% in CtBP1KD neurons, indicating a role of CtBP1 in the control of TRP (comprising  
119 RRP and RP). Alkalization with ammonium chloride, which de-quenches all sypHy-positive SVs,  
120 revealed no differences in its expression between CtBP1KD and control neurons. (Figure 1E-G)  
121 An analogous analysis performed in cultured neurons isolated from constitutive *Ctbp1* KO mice  
122 recapitulated the results of the KD approach and confirmed the significant reduction of TRP in  
123 CtBP1-deficient synapses (Figure S2C-E).

To assess potential changes in the kinetics of SV exo-endocytosis in the absence of CtBP1, we monitored syHy responses evoked by a train of 200 AP at 5, 20 or 40 Hz in neurons expressing CtBP1KD944, CtBP1KD467 or scrambled shRNA (Figure 1H-K). Several stimulation rates were tested since distinct molecular mechanisms have been proposed to mediate SV retrieval at different stimulation frequencies (Cousin, 2017; Kononenko and Haucke, 2015; Soykan et al., 2017). Whereas the time course of exocytosis was indistinguishable between CtBP1KD and control groups, the syHy fluorescence decay was significantly slower in CtBP1KD neurons at all frequencies tested (Figure 1I-K) suggesting a role of CtBP1 in SV endocytosis. Analogous experiments in cultured neurons from constitutive *Ctbp1* KO mice confirmed this conclusion (Figure S2G). Taken together, these results suggest that CtBP1 contributes to SV retrieval at a broad range of neuronal firing frequencies and is specifically required for maintaining the size of TRP during sustained neuronal activity.

#### **Deletion of CtBP1 induces changes in SV size and distribution**

Next, we performed an ultrastructural analysis of small glutamatergic spine synapses in 4-5 weeks old cultured hippocampal slices obtained from *Ctbp1* KO mice and their wild-type (WT) siblings. A combination of rapid cryo-fixation, automated freeze substitution, and 3D-electron tomographic analysis was designed to accurately reveal vesicular organization at presynaptic active zones (AZ) with nanometer precision, while circumventing the introduction of morphological artefacts associated with conventional electron microscopy preparation methods requiring dehydration of the tissue at room temperature (Korogod et al., 2015; Murk et al., 2003). An analysis of gross synaptic morphology and the number of SVs in individual presynaptic glutamatergic terminals revealed no differences between *Ctbp1* KO and WT synaptic profiles (Figure 2A–G). Electron tomographic analysis, however, revealed changes in the distribution of SVs in KO versus WT synapses (Figure 2H-K). The KO synaptic profiles showed a significant increase in the number of membrane-proximal SVs (within 0-5, 0-40, 50-100 and 0-100 nm of the AZ, Figure 2L, P and Table 1). It is important to note that no statistically significant differences in the number of vesicles within 0-2nm of the AZ were observed (Figure 2M), which is the morphological correlate of RRP. Analyses of individual SVs revealed a small, but significant increase in the diameter of docked SVs (Figure 2O), however no change in SV size was seen when comparing all synaptic vesicles within 0-200 nm (Table1). Altogether, these data suggest that loss of CtBP1 does not affect the overall number of SVs in the presynaptic terminals, but triggers their redistribution from membrane-distal to membrane-proximal areas. They also indicate that CtBP1 regulates the size uniformity of docked SVs.

## **Distinct roles of nuclear and synaptic CtBP1 in neurotransmission**

Since we observed changes in the diameter of docked SVs and the size of TRP we next determined the effect of CtBP1 depletion on neurotransmission. We first compared the AP-evoked excitatory postsynaptic currents (EPSCs) in cultures of autaptic hippocampal neurons transduced with CtBP1KD944 shRNA or scrambled shRNA as a control. Unexpectedly, CtBP1KD944 neurons exhibited greater amplitudes of EPSC compared to controls (Figure 3A). To examine whether the increase in EPSC amplitude reflected an increase in the amount of glutamate loaded into SVs or changes in postsynaptic receptors we analyzed mEPSCs, which represent single fusion events. Neither the amplitudes nor the charges of mEPSCs were affected by CtBP1-depletion indicating that the observed increase in EPSC amplitude cannot be attributed to any major changes in vesicular neurotransmitter content or postsynaptic properties (Figure 3B,C, Table 2). In support of the latter conclusion, quantitative live immunolabeling of autaptic neurons with an antibody recognizing the extracellular epitope of GluAs did not uncover any significant differences in the surface expression of AMPA receptors between the groups (Figure 3E,F). The mEPSC frequency was not significantly altered in CtBP1KD944 neurons (Figure 3D). However, the number of morphological synapses assessed as a number of co-localizing synapsin-GluA puncta in CtBP1KD944 neurons was slightly higher suggesting increased synaptogenesis in the absence of CtBP1 (Figure 3E,G). The increased synapse number might contribute, at least in part, to the increase of EPSC amplitude observed in these neurons.

Next we measured postsynaptic current evoked by application of hypertonic sucrose, leading to the release of all docked SVs (RRP) (Rosenmund and Stevens, 1996). We detected unchanged sucrose-evoked currents (Figure 3H,I), which is in line with unchanged RRP measured by synHy imaging (Figure 1E-G) and with the unchanged number of morphologically docked SVs (Figure 2M). The unchanged total RRP charge, but significantly higher EPSC charge evoked by an injection of a single AP implies an increased mean vesicular release probability (P<sub>vr</sub>, Figure 3J). Increased P<sub>vr</sub> is predictive of an increased synaptic transmission upon isolated stimuli but leads to an enhanced short-term depression upon repeated stimulation. To explore this possibility, we recorded synaptic responses induced by a 25 ms spaced pair of APs (Figure 3K). In line with the elevated P<sub>vr</sub>, the paired pulse ratio (i.e. the ratio of the peak amplitude of the second to the first evoked EPSC; PPR), was significantly decreased in CtBP1KD944 neurons, confirming a higher degree of synaptic depression. We also analyzed the depression of neurotransmission during sustained neuronal activity by recording the EPSCs evoked by a train of 50 stimuli at 10 Hz (Figure 3L). At this frequency only minor depression of EPSC amplitudes was evident in controls

(scr), while a pronounced rundown of neurotransmission was measured upon depletion of CtBP1 (CtBP1KD944), which is in line with the high initial Pvr and increased PPR measured in CtBP1KD944 neurons. Thus, depletion of CtBP1 promotes synaptogenesis and elevates Pvr resulting in increased evoked neurotransmission and contributing to the strongly enhanced short-term depression.

We have previously shown that nuclear CtBP1 acts as a transcriptional corepressor and regulates the expression of plasticity-related genes which might affect synaptogenesis and neurotransmission (Ivanova et al., 2015). To discriminate between the effects of nuclear and synaptic CtBP1 on synaptic transmission, we expressed CtBP1944KD together with RNAi-resistant variants of CtBP1 that were sorted predominantly to the synapses (EGFP-CtBP1) or only to the nucleus (YFP-CtBP2(NLS)-CtBP1). In EGFP-CtBP1, the N-terminal fusion of EGFP interferes with its nuclear localization, while it leaves the synaptic targeting unaffected (Figure S3A) (Ivanova et al., 2015; Verger et al., 2006). The chimeric protein YFP-CtBP2(NLS)-CtBP1 which bears the NLS signal of CtBP2, the paralogue of CtBP1 in vertebrates, fused to almost full length CtBP1, showed a restricted nuclear localization (Figure S3A) (Verger et al., 2006). While expression of synaptic EGFP-CtBP1 on a KD background led to a further increase of EPSC amplitude, expression of nuclear YFP-CtBP2(NLS)-CtBP1 fully rescued the EPSC amplitude (Figure 3A). These data indicate that the increased size of the evoked response in CtBP1KD944 neurons is a result of the depletion of the nuclear rather than the synaptic pool of CtBP1. Similarly, the increased number of morphological synapses as well as Pvr and PPR were substantially normalized upon expression of nuclear YFP-CtBP2(NLS)-CtBP1, indicating that depletion of nuclear CtBP1 leads to increased synaptogenesis and elevated Pvr (Figure 3G,J,K). Expression of YFP-CtBP2(NLS)-CtBP1 also normalized the altered expression of the immediate early gene *Arc* and neurotrophin *BDNF* in CtBP1KD944 neurons (Figure S3B,C), suggesting a link between CtBP1-controlled gene expression and the regulation of synaptic efficacy. We observed an intermediate increase in Pvr and PPR upon expression of synaptic EGFP-CtBP1 (Figure 3G,J,K), which further supports the notion that nuclear and not synaptic CtBP1 controls synapse formation and/or maintenance and Pvr. The expression of EGFP-CtBP1 also led to an increase in mEPSC frequency, which might be a consequence of the concomitant strong elevation in synapse number and Pvr (Figure 3D,J,K).

To our surprise, the expression of the nuclear construct YFP-CtBP2(NLS)-CtBP1 in CtBP1KD944 neurons that normalized the evoked neurotransmission and significantly decreased Pvr assessed upon single or paired-pulse stimulation (Figure 3A,J,K), did not revert the strikingly elevated



depression during the train of 50 stimuli at 10Hz (Figure 3L). In contrast, expression of synaptic EGFP-CtBP1 in CtBP1KD944, which further enhanced the evoked neurotransmission and left the increased Pvr largely unaffected, increased the steady state response to 10Hz stimulation by about 7% (of initial response) compared to CtBP1KD944 (Figure 3L). This is comparable with data obtained at calyx of held, where complete block of endocytosis decreased steady state response by 10% (Hosoi et al., 2009). Taken together, the complementation experiments revealed that nuclear CtBP1 has an inhibitory effect on basal neurotransmission due to its negative effect on synapse number and SV fusion competency. Interestingly, the nuclear expression of CtBP1 (YFP-CtBP2(NLS)-CtBP1) left the enhanced depression of neurotransmission during repetitive stimulation unaffected, while expression of synaptic EGFP-CtBP1 ameliorated the effect of CtBP1 depletion. Since, the synaptic rundown during repetitive stimulation is determined not only by the Pvr, but also by the size and refill capacity of the total recycling pool of SVs, we next addressed the involvement of synaptic and nuclear CtBP1 in SV retrieval in the following imaging experiments.

#### **Synaptic CtBP1 is required for normal SV recycling and short-term plasticity of release.**

To directly determine the contribution of synaptic and nuclear CtBP1 to the defect in the retrieval of the fused SVs observed in CtBP1KD neurons we performed imaging experiments in neurons, where CtBP1 KD was complemented by expression of synaptic or nuclear rescue constructs. Synaptically-localized EGFP-CtBP1 expressed on CtBP1KD944 background led to ~80% restoration of Syt1 Ab uptake driven by network activity. In contrast, the expression of nuclear YFP-CtBP12(NLS)-CtBP1 failed to rescue Syt1 Ab uptake in CtBP1KD944 neurons (Figure 4A, B). In addition, the expression of EGFP-CtBP1 with aspartate 355-to-alanine mutation (D355A), which impairs the fission activities of CtBP1 (Bonazzi et al., 2005), also failed to restore the Syt1 Ab uptake in CtBP1KD neurons (Figure 4A,B), suggesting that the function of CtBP1 in fission is required for normal SV recycling. Next, we tested the ability of synaptic vs. nuclear CtBP1 expression to rescue the aberrant exo-endocytosis observed upon depletion of endogenous CtBP1 (Figure 1H-K) To this end we used a sensor composed of synaptophysin fused to the monomeric, orange pH-sensitive mOrange2 (sypmOr2), which we co-expressed with the EGFP and YFP-labeled rescue constructs (Figure 4C,D). The fluorescence recovery after stimulation with 200 APs at 20 Hz was significantly retarded in CtBP1KD944: it did not reach full recovery during the time of imaging and had a greater recovery halftime compared to the controls (Figure 4C,D). The expression of synaptic EGFP-CtBP1 on CtBP1KD944 background fully rescued the normal SV retrieval, while nuclear YFP-CtBP2(NLS)-CtBP1 or the fission mutant EGFP-

CtBP1D355A failed to do so (Figure 4C,D). Altogether, these data indicate that synaptic localization and intact fission activities of CtBP1 are crucial for its role in SV retrieval.

To re-evaluate the altered short-term plasticity measured by the electrophysiological recordings of CtBP1-depleted autaptic neurons (Figure 3L), we monitored the exocytosis of endogenous syt1 during a train of 200 AP at 10 Hz using an antibody against its luminal domain coupled to CypHer5E (Syt1 Ab-CypHer). CypHer5E is a pH sensitive dye with maximal fluorescence at acidic pH in the vesicle lumen and fluorescence decline upon SV exocytosis (Hua et al., 2011). Experiments were performed in the presence of bafilomycin A1 (Figure 4E) or folimycin (Figure S4) to block SV reacidification and thus visualize net SV fusion. To normalize for potential differences in the initial release probability and thus uncover the contribution of SV retrieval, the response amplitudes after a reference train of 40 APs at 20 Hz, which leads to the release of RRP (unchanged between control and CtBP1KD, Figures 1G, 2I,M 3H,I), were used for normalization as described previously (Hua et al., 2013). This reference pulse was followed by a brief recovery period and a test stimulus of 200 AP at 10 Hz. The amplitudes of the fluorescence responses to 200 AP were strongly reduced in CtBP1KD944 compared to the control for stimuli delivered at 5, 10 or 40Hz (Figure 4E,F and S4A,B). The expression of YFP-CtBP2(NLS)-CtBP1 on CtBP1KD944 background did not improve this decrease, while the responses in KD neurons expressing EGFP-CtBP1 construct were not significantly different from control (Figure 4E,F). These experiments further supported the view that synaptic CtBP1 is required for efficient SV recycling during sustained neuronal activity.

#### **Dynamin-dependent SV recycling is unaffected in CtBP1-deficient neurons.**

The GTPase dynamin plays a key role in the reformation of SVs by catalyzing the fission of SV membranes from the plasma membrane and endosomal structures (Gan and Watanabe, 2018; Kononenko and Haucke, 2015). In non-neuronal cells, CtBP1 was described as an accessory protein in the assembly of dynamin-independent fission machinery, which includes molecules like ADP ribosylation factor (Arf), phospholipase D (PLD) and lysophosphatidic acid acyltransferase (LPAAT) (Haga et al., 2009; Pagliuso et al., 2016; Valente et al., 2012). To investigate a possible link of CtBP1 to the established presynaptic endocytic machinery, we assessed the nanoscale localization of CtBP1 in respect to other membranous structures implicated in SV recycling. To this end, we performed super-resolution dual-color STED microscopy of neurons labeled with antibodies against CtBP1, the SV protein Syt1 and several endocytic markers followed by co-localization modeling. Dynamin1 labeling was used to visualize the classic endocytic machinery

(Figure 5A). Since many of the components of the CtBP1-associated fission machinery were shown to coordinate the endosomal trafficking of membrane proteins, we also labeled the neurons with markers for early (rab5), late (rab7) and recycling (rab22) endosomes (Figure 5A). Prior to staining, neuronal cultures were first silenced with APV ((2*R*)-amino-5-phosphonovaleric acid; (2*R*)-amino-5-phosphonopentanoate) and CNQX (6-cyano-7-nitroquinoxaline-2,3-dione) for 10 minutes, in order to reduce the intersynaptic variability induced by the endogenous network activity. We analyzed the distance of CtBP1 to other markers at rest and also monitored the co-localization in cells fixed 30 seconds after stimulation with 200 AP at 40 Hz (Figure S5). Overall, CtBP1 localized in the proximity (0-200 nm) of dynamin1 and Syt1, while all endosome markers we probed for were much more distant (100-500 nm) (Figure 5A,B and S5A-E). Synaptic stimulation did not affect the co-localization of CtBP1 with dynamin1 and Syt1 but led to a significant increase in the distance between CtBP1 and endosome markers rab5 and rab7, but not rab22 (Figure S5A-E). Thus, CtBP1 likely acts at the membrane domain marked by Syt1 and dynamin1 indicating its potential role in the retrieval of exocytosed SVs. The poor baseline co-localization of CtBP1 with the endosomal markers rab5, rab7 and rab22, and subsequent increase of distance upon neuronal stimulation, suggests a role of CtBP1 in the formation of vesicular carriers rather than its constitutive association with intracellular membranous structures.

Given the fact that CtBP1 was reported to regulate membrane trafficking in dynamin-independent exocytic and endocytic pathways (Bonazzi et al., 2005), the high synaptic co-localization with dynamin1 was unexpected. Therefore, in order to test whether CtBP1 contributes to the presynaptic dynamin-dependent endocytosis, we quantified the Syt1 Ab-CypHer uptake in control and CtBP1KD944 neurons treated with the potent dynamin inhibitors dynole 34-2 (Figure 5C,D). As inhibition of dynamin increases the membrane stranding of SV proteins due to an impaired retrieval (Raimondi et al., 2011) we used Syt1 Ab-CypHer uptake to determine specifically the fraction of Syt1 retrieved through dynamin-independent endocytosis. Dynole 34-2 had a comparable effect in control and in CtBP1KD944 neurons, and reduced the Syt1 Ab-CypHer Ab uptake by more than 80% (Figure 5D). The large effect of dynamin inhibition in both conditions confirms the principal requirement of dynamin for efficient SV retrieval at the presynapse. However, as the effects of CtBP1KD and dynole 34-2 were not completely additive but rather cooperative and considering the high degree of co-localization observed for CtBP1 and dynamin, we propose that despite their involvement in independent machineries they might act in concert at the same membrane domain to mediate effective SV retrieval.

#### **CtBP1 promotes retrieval of SVs by activation of presynaptic PLD1**

Given the established role of CtBP1 in membrane trafficking in non-neuronal cells, we hypothesized a role of CtBP1-based fission machinery in SV recycling. To test this hypothesis, we first treated control and CtBP1-depleted neurons with brefeldin A (BFA), a fungal antibiotic interfering with the intracellular membrane trafficking. BFA targets several proteins involved in membrane trafficking, including CtBP1. It induces ADP-ribosylation of CtBP1 (also known as BFA-ADP-ribosylation substrate, shortly BARS), which interferes with the assembly of CtBP1-based fission complex and results in inhibition of endocytic vesicle formation (Colanzi et al., 2013; Spano et al., 1999). We applied BFA (2.5 $\mu$ M) only five minutes prior to and during the image acquisition, which we reasoned is a too short time period to influence synaptic function by changes in gene expression or soma-to-synapse trafficking. Thus, the effect of BFA treatment more likely reflected an acute inhibition of CtBP1 and the associated fission machinery at the presynapse. In agreement with previous reports (Kononenko et al., 2013; Park et al., 2016) (but see (Kim and Ryan, 2009) for lack of effect of BFA on vGLUT-pHluorin), BFA treatment affected significantly the post-stimulus fluorescence decay of syHy in control neurons (Figure 6A) indicating that BFA slows down the retrieval of exocytosed SVs. In contrast, the syHy fluorescence decay was not further affected by BFA in CtBP1KD neurons (Figure 6B), suggesting that CtBP1-based fission machinery mediates to a great extent the effect of BFA.

The precise molecular mechanism of CtBP1-mediated membrane trafficking is still not fully understood. It was suggested that CtBP1-based fission complex drives membrane budding and fission by catalyzing the remodeling of membrane lipids, which leads to formation of fission-prone membrane domains. In non-neuronal cells, CtBP1 was shown to interact and activate the phosphodiesterase activity of phospholipase D1 (PLD1), an enzyme catalyzing the conversion of phosphatidylcholine (PC) into the fusogenic phosphatidic acid (PA) (Donaldson, 2009; Haga et al., 2009; Raben and Barber, 2017). Although PLD1 was shown to play a role in the control of neurotransmitter release in *Aplysia* (Humeau et al., 2001) and in the secretion of neuropeptides in chromaffin cells (Zeniou-Meyer et al., 2007), its function in the regulation of SV recycling in mammalian synapses has not been investigated yet. Therefore, next we tested the involvement of PLD1 in SV recycling and its link to CtBP1-dependent SV retrieval. Acute application of VU 0155069 (1 $\mu$ M for 5 min), a specific inhibitor of PLD1, led to a two-fold decrease in the rate of syHy retrieval in control neurons, while it had no effect on the endocytosis rate in CtBP1KD neurons (Figure 6C,D).

Considering the activity-induced recruitment of CtBP1 to nanodomains co-labeled with dynamin1 and Syt1 and its dissociation from the endosome markers rab5 and rab7 we hypothesized that

CtBP1 localizes to the membrane proximal regions, where endocytosis of newly released SV proteins takes place. To address this by independent means we performed imaging with fluorescently labeled mCLING: a lipophilic reacidification-independent probe suitable for STED nanoscopy of endocytic organelles (Revelo et al., 2014). We loaded mCLING into the synapses of APV and CNQX silenced (for 10min) control and CtBP1KD944 neurons by stimulation with 200 AP at 40 Hz and fixed them 30 seconds later. The mCLING labeling was notably reduced in the synapses in CtBP1KD944 neurons in comparison to the control (Figure 6E,F), but was again evident upon the expression of shRNA resistant EGFP-CtBP1 construct on CtBP1KD944 background (Figure 6G). We next performed dual-color STED nanoscopy followed by co-localization modelling to assess the co-distribution of mCLING and EGFP-CtBP1 (Figure 6G). This analysis revealed a significant negative correlation between the intensity of mCLING and the distance to individual EGFP-CtBP1 puncta, which supports a role of CtBP1 in SV endocytosis (Figure 6I).

Phosphorylation of CtBP1 at serine 147 (S147), mediated by the kinase Pak1, was found to strongly increase the capacity of CtBP1 to stimulate membrane fission by increasing its ability to activate PLD1 (Haga et al., 2009; Liberali et al., 2008). To test the importance of this regulation at the presynapse we compared the mCLING labeling in neurons expressing the RNAi resistant EGFP-CtBP1 or EGFP-CtBP1S147A construct on CtBP1KD944 background. The mCLING labeling was reduced by 80% in cells expressing EGFP-CtBP1S147A as compared to cells expressing EGFP-CtBP1 (Figure 6G,H) indicating lower ability of this mutant to rescue stimulus-induced membrane retrieval upon CtBP1KD. Moreover, the co-distribution between mCLING and S147A mutant was shifted towards higher distances compared to EGFP-CtBP1 (Figure 6J), which likely reflects impaired recruitment to the sites of endocytosis. Taken together these data indicate that the presence of CtBP1 at the endocytic sites and its phosphorylation at S147 are key factors determining the efficacy of SV retrieval.

### **Phosphorylation of CtBP1 regulates its distribution between the CAZ and the presynaptic endocytic sites.**

Previous studies showed that the presynaptic scaffolding proteins Bsn and Pclo recruit CtBP1 to synapses via a direct interaction (Ivanova et al., 2015; tom Dieck et al., 2005). Despite the tight functional coupling between SV fusion and endocytosis, it is well established that the two processes take place at distinct membrane domains within the presynapse (Haucke et al., 2011; Maritzen and Haucke, 2018). Thus, the association of CtBP1 with Bsn and Pclo, which are

established components of the SV release sites, is seemingly in disagreement with the proposed function of CtBP1 in SV endocytosis. To address this apparent ambiguity, we performed the following series of experiments. First, we performed co-immunoprecipitation (CoIP) of Bsn with EGFP-CtBP1, overexpressed in primary cortical cultures in basal state or upon a treatment with the Pak1 inhibitor IPA3 for 1 h (Figure 7A). At basal state a considerable CoIP of CtBP1 with PLD1 but only a low binding to Bsn were detected. The IPA3 treatment visibly reduced the overall serine/threonine phosphorylation of CtBP1 (Figure 7C,D). Consistent with the requirement for Pak1-dependent phosphorylation of CtBP1 for its association with PLD1, IPA3 reduced the CoIP of PLD1 with CtBP1 to an undetectable minimum but increased the association of CtBP1 with Bsn (Figure 7A and B). This indicates that the phosphorylation of CtBP1 by Pak1 acts as a molecular switch which triggers its dissociation from Bsn and binding to PLD1. To further test this hypothesis, we compared the nanoscale co-localization of EGFP-CtBP1 or S147A mutant with endogenous Bsn at synapses of acutely silenced neurons before and upon stimulation with 200 AP at 40 Hz. Consistent with our previously published observations, stimulation led to a tighter co-localization of EGFP-CtBP1 and Bsn (Figure 7E,F) (Ivanova et al., 2015). EGFP-CtBP1S147A showed a greater co-localization with Bsn than EGFP-CtBP1 in silenced cells and no effect on its co-distribution with Bsn was observed upon stimulation (Figure 7E,F). This supports our view that Pak1-mediated phosphorylation of S147 favors a redistribution of CtBP1 from Bsn towards PLD1, thus, promoting SV retrieval through activation of PLD1.

## **Discussion:**

### **Nuclear CtBP1 restricts synaptogenesis, while synaptic CtBP1 promotes SV retrieval**

In this study we investigated the effect of CtBP1 depletion on synaptic function using knock down and knock out approaches. Neurons lacking CtBP1 had normal overall morphology but showed a significant shift in the distribution of SVs towards the AZ and an enlargement of the docked SVs at rest. Interestingly, a similar change in the distribution of SVs was also observed after treatment with BFA (Ramperez et al., 2017), which as shown here inhibits SV recycling via CtBP1, and upon depletion of Arf6, a component of the CtBP1-dependent fission machinery and an alternative activator of PLD1 (Haga et al., 2009; Tagliatti et al., 2016; Valente et al., 2012). Thus, it is tempting to speculate that insufficient PLD1 activity in the absence of CtBP1 might cause this phenotype. The efficiency of fission during vesicle budding crucially affects the size of the resulting vesicular structures. In line with that, enlarged SVs were observed in mutants of dynamin, AP180 and syndapin, which have been implicated in different steps of SV reformation,

like fission, recruitment of the clathrin-coat or induction/sensing of membrane curvature (Ferguson et al., 2007; Koch et al., 2011; Zhang et al., 1998). Thus, an involvement of CtBP1 in the fission of the SV membranes, might explain the changes in SV size observed in *Ctbp1* KO synapses.

Interference of CtBP1 expression in cultured neurons revealed its multifaceted role in the regulation of synaptogenesis and neurotransmission. A rescue strategy with CtBP1 fusion proteins selectively sorted to nucleus or synapses revealed distinct roles for CtBP1 in these spatially separated neuronal compartments. Nuclear CtBP1 restricted synaptogenesis and presynaptic vesicular release probability possibly by repressing the expression of plasticity-related genes, such as neurotrophins or neurotransmitter receptors (Ivanova et al., 2015). In line with that, the expression of the nuclear rescue construct YFP-CtBP2(NLS)-CtBP1 could normalize the higher number of morphologically identified excitatory synapses, the enlarged amplitudes of the evoked EPSC and the higher Pvr and PPR that were observed in CtBP1KD944 neurons. Notably, the expression of the synaptic rescue (EGFP-CtBP1) on CtBP1KD944 background tended to enhance the effect of CtBP1 depletion on synapse density and EPSC amplitude, suggesting a dominant-negative effect of this construct on the nuclear functions of CtBP1. One possible explanation of this effect is that the EGFP-CtBP1 binds to the nuclear CtBP1-interacting partners and promotes their cytoplasmic retention. However, expression of this construct on CtBP1KD944 background compensated the defects in SV retrieval and ameliorated the enhanced short-term depression of neurotransmission upon repetitive stimulations. This indicates a positive effect of synaptic CtBP1 on neurotransmission. Based on this, we can speculate that the recently reported activity-induced redistribution of CtBP1 from nucleus to presynapses exerts a dual-positive effect on neurotransmission (Ivanova et al., 2015). Thus, during bursts of intense neuronal activity the reduced nuclear abundance of CtBP1 will lead to a release of the transcriptional block of neuroplasticity-related genes, while the enhanced synaptic targeting will facilitate SV recycling.

#### **CtBP1-mediated membrane fission and PLD1 activation are required for SV retrieval**

Our data indicate that CtBP1-mediated membrane fission and activation of PLD1 has an important contribution to the effective SV retrieval at the presynapse. We provide multiple evidences supporting this view: 1) CtBP1D355A fission-deficient mutant failed to rescue SV retrieval in CtBP1KD944, 2) CtBP1S147A mutant that cannot recruit PI4KIII $\beta$ /ARF6 and activate PLD1 failed to rescue endocytosis visualized with mCLING and 3) the pharmacological inhibition

of CtBP1-based fission complex using BFA or inhibition of PLD1 activity phenocopied the aberrant SV retrieval observed in CtBP1KD. Our data also indicate a role of PLD1 in SV recycling at hippocampal synapses. PLD1 was detected in synaptic plasma membranes isolated from rat synaptosomes and interference with PLD1 was shown to affect acetylcholine release from nerve ganglia in *Aplysia* (Humeau et al., 2001). However, PLD1 was mainly discussed in the context of exocytosis in neurons and chromaffin cells (Zenou-Meyer et al., 2007). Our data indicate a role of PLD1 in SV retrieval in hippocampal synapses and reveal a requirement for CtBP1-mediated activation of PLD1 in this process. The activation of PLD1 depends on Pak1-mediated phosphorylation of CtBP1. It is unclear whether and how Pak1 activity is regulated at the presynapse but based on our findings we can speculate that the level of presynaptic Pak1 activity could regulate the SV retrieval and thereby modulate short-term plasticity of neurotransmission. Interestingly, the phosphorylation of S147 of CtBP1 by Pak1, which is necessary for PLD1 activation, also induces dissociation of CtBP1 from Bsn, which anchors it to the active zones. This suggests that Pak1 activity might induce a rapid activation of PLD1 in the vicinity of presynaptic release sites and thereby link SV fusion and retrieval in time, space and extent.

#### **CtBP1-mediated lipid reorganization in SV retrieval**

CtBP1-based fission machinery was proposed to act in a dynamin-independent manner at the Golgi and plasma membrane in non-neuronal cells (Bonazzi et al., 2005; Haga et al., 2009; Yang et al., 2008). However, the fluid phase endocytosis switched from a CtBP1-dependent to a dynamin-dependent mechanism in fibroblasts in which CtBP1 was knocked out (Bonazzi et al., 2005), suggesting a tight interaction between these pathways. Thus, it is possible that CtBP1- and dynamin-based fission machineries converge in their action at the presynapse, where particularly potent endocytosis is required for sustained SV replenishment. CtBP1 was suggested to mediate fission of target membranes by activation of lipid enzymes such as PLD1 and LPAAT, that generate curvature-inducing lipid modifications (Haga et al., 2009; Liberali et al., 2008; Pagliuso et al., 2016), and by their recruitment to the machinery, that initiates vesicular budding and tubulation (Valente et al., 2012). PLD1 and LPAAT catalyze production of the fusogenic PA, which, due to its conical shape, promotes negative membrane curvature necessary for vesicle fusion and fission (Kooijman et al., 2003). Besides its structural role, PA was also linked to the generation of PI(4,5)P<sub>2</sub>, the phospholipid involved in the recruitment of numerous proteins involved in endocytosis, including dynamin (Puchkov and Haucke, 2013). Specifically, PA activates PI kinases necessary for PI(4,5)P<sub>2</sub> production (Jenkins et al., 1994; Moritz et al., 1992) and intriguingly, one of them, PI4KIIIβ, is a component of the CtBP1-based fission complex in



non-neuronal cells (Valente et al., 2012). Thus, it is likely that CtBP1 promotes SV retrieval by recruitment and activation of multiple lipid-modifying enzymes, which drive the formation of a lipid environment permissive for compensatory endocytosis. The tight co-localization of CtBP1 and dynamin as well as the cooperative effect of the interference with their functions on SV recycling support this view. However, future studies will be needed to gain more insight into the mechanisms linking and regulating the different fission machineries involved in SV recycling.

## LEAD CONTACT AND MATERIALS AVAILABILITY

Further information and requests for resources and reagents can be directed to and will be fulfilled by the Lead Contact, Anna Fejtova ([Anna.Fejtova@uk-erlangen.de](mailto:Anna.Fejtova@uk-erlangen.de)).

## EXPERIMENTAL MODEL AND SUBJECT DETAILS

### ***Animals***

Cells and tissues used in this study were obtained from Wistar rats, Sprague-Dawley rats, C57BL/6N mice and *Ctbp1*<sup>tm1Sor</sup> (*Ctbp1* KO) mouse strain (Hildebrand and Soriano, 2002) backcrossed to C57BL/6N. Animals of both sex were used. Animal handling was performed according to the regulations of the European Committees Council Directive 86/609/EEC, Landesverwaltungsamt Sachsen-Anhalt, (AZ: T LIN-AF/2009), Berlin state government agency for Health and Social Services and the animal welfare committee of Charité Medical University Berlin, Germany (license no. T 0220/09).

### ***Lentiviral particle production***

Lentiviral particles were produced as described previously with slight modifications (Ivanova et al., 2015). HEK293T cells (ATCC CRL-3216) were grown in media containing 10% fetal bovine serum (FBS) to 80% confluence and transfected using the calcium phosphate method (Fejtova et al., 2009) with three vectors: FUGW-based transfer, psPAX2 packaging, and p-CMV-VSV-G pseudotyping vectors (ratio 2:1:1). Cells were incubated for 8 h at 37°C in 5% CO<sub>2</sub> atmosphere, before the FBS medium was replaced by Neurobasal (NB) medium, containing B27, antibiotics, and 0.8 mM glutamine. Virus-containing media was collected at day 3 and 4, passed through 0.45 µm filter and used either directly for transducing primary neurons or stored at -80°C.

### ***Primary cultures and treatments***

Primary dissociated hippocampal and cortical cultures from rat embryos and C57BL/6N and *CtBP1* KO neonatal mice of were prepared as described in (Ivanova et al., 2015; Lazarevic et al., 2011).

Autaptic cultures from P0-P2 C57BL/6N mice were grown on coverslips with a dotted pattern of astrocytic microislands (Bekkers and Stevens, 1991). To grow neurons individually, 0.15% agarose solution was spread on 30 mm coverslips. Coating solution containing collagen and poly-D-lysine in acetic acid was stamped onto the agarose, thus creating small islands of substrate with a diameter of about 100  $\mu$ m. Hippocampi were dissected out and digested with 25 U/ml of papain for 60 min at 37°C. After papain inactivation, hippocampi were mechanically dissociated in Neurobasal-A medium containing B-27, Glutamax and penicillin/streptomycin. To obtain a desirable distribution of neurons, astrocytes and neurons were plated onto the coverslips with a density of 50000 and 3000 cells/coverslip, respectively. To knock down *CtBP1*, neurons were infected 24 hours later with lentiviruses expressing scrambled, shRNA against *CtBP1* or the rescue constructs EGFP-*CtBP1* and YFP-*CtBP2*(NLS)-*CtBP1*. Experiments were performed on DIV14 (electrophysiological recordings) or DIV16-21 (fixed and live-cell imaging).

Hippocampal neurons were co-transfected with syp mOrange2 and a plasmid expressing *CtBP1* scr, *CtBP1*KD944 or *CtBP1*KD944 along with shRNA-resistant EGFP-*CtBP1*, EGFP-*CtBP1*D355A or YFP-*CtBP2*(NLS)-*CtBP1* at DIV6 using Lipofectamine 2000 (Thermo Fisher Scientific) as recommended by the manufacturer. The neurons were used for live imaging 8 to 10 days after the transfection.

For the treatments, the following drugs were used: d-(-)-2-amino-5-phosphonopentanoic acid (APV, 50  $\mu$ M; Tocris), 6-cyano-7-nitroquinoxaline-2,3-dione disodium (CNQX, 10 $\mu$ M; Tocris), bafilomycin A1 (1 $\mu$ M, Merck/Millipore), folimycin/concanamycin A (80nM, Tocris), brefeldin A (2.5  $\mu$ M, Tocris), VU 0155069 (PLD1 inhibitor, 1 $\mu$ M, Tocris). Neurons were pre-treated with these inhibitors for 5 minutes before imaging and the inhibitors were kept in the imaging buffer during the whole imaging assay. IPA 3 (50  $\mu$ M, Tocris) was applied for 1h before the cells were collected or lysed for western blotting. The inhibitors of dynamin, Dynole 34-2 (30  $\mu$ M, Abcam) was applied for 1h during Syt1 Ab-CypHer uptake. The fixable endocytosis marker mCLING (ATTO647N-labelled in Figure 6G and H and DY654-labelled in Figure 6E and F, 1:100, Synaptic Systems) was applied to neurons in extracellular solution containing 50  $\mu$ M APV and 10  $\mu$ M CNQX, for 2 min before cells were stimulated with 200 AP at 40 Hz. To eliminate unspecific labeling neurons were washed three times with extracellular solution and fixed within 30 seconds after stimulation with a mixture of 4% paraformaldehyde (PFA) and 0.2% glutaraldehyde, as recommended by the manufacturer.

## METHOD DETAILS

### ***Antibodies***

The following primary antibodies were used in this study: **Mouse antibodies against:** CtBP1 (immunocytochemistry (ICC) 1:1,000, Western blotting (WB) 1:5,000, BD Biosciences, 612042), CtBP2 (WB 1:2000 BD Biosciences, 612044) synaptotagmin1 luminal domain Oyster 550 or CypHer5E-labeled (ICC 1:200, Synaptic Systems, 105311 and 105311CpH), rab5 (ICC 1:500, Synaptic Systems, cells stained with this antibody were fixed with ice-cold methanol for 10 min, followed by rehydration in PBS for 20 min, 108011), rab7 (ICC 1:1,000, Abcam, ab50533), phosphoserine/threonine (WB 1:1000, BD Biosciences, 612548), GluA Oyster 550-labeled (ICC 1:200, Synaptic Systems, 182411 C3),  $\alpha$ -tubulin (WB 1:1000, Sigma Aldrich); **Rabbit antibodies against:** CtBP1 (ICC 1:1,000, WB 1:1,000, Synaptic Systems, 222002), GFP (ICC 1:1,000, WB 1:5,000, Abcam, ab 6556), SV2B (ICC 1:200, Synaptic Systems, 119103), GAPDH (WB 1:3000, Abcam, ab37168), synaptotagmin1 luminal domain Oyster 550-labeled (ICC 1:200, Synaptic Systems, 105103C3), synaptotagmin 1 luminal domain (WB 1:1000, Synaptic Systems, 105102), dynamin1 (ICC 1:1000, Abcam, ab3456), rab22a (ICC 1:1000, Abcam, ab137093), Phospholipase D (WB 1:1000, Cell Signaling technologies, 3832S), , Homer1 (ICC 1:500, Synaptic Systems, 160003); **Guinea pig antibodies against:** synapsin 1, 2 (ICC 1:1,000, Synaptic Systems, 106004), synaptophysin 1 (ICC 1:1,000, Synaptic Systems, 101004), Piccolo (WB 1:2000, Dick et al, 2001).

The following secondary cross-adsorbed antibodies were used in this study: Alexa 488- (ICC: 1:1,000), Cy3-(ICC: 1:1,000), Cy5-(ICC: 1:2,000), Alexa 680- (WB 1:20,000) conjugated whole IgGs against mouse, rabbit and guinea pig were obtained from Invitrogen/Mol. Probes, IRDye™ 800CW (WB 1:20,000) and Atto 647N (1:500, 610-156-121 and 611-156-122) from Rockland and Abberior STAR 580 (1:100, 2-0002-005-1 and 2-0012-005-8) from Abberior GmbH.

### ***DNA constructs***

EGFP-tagged CtBP1 was generated by cloning the sequence for CtBP1-S into pEGFPC vector. Subsequently, the DNA cassette containing EGFP-CtBP1 was shuttled into FUGW H1 lentiviral vector (Leal-Ortiz et al., 2008), replacing EGFP coding sequence. The shRNAs against CtBP1 and YFP-CtBP2(NLS)-CtBP1 constructs were reported previously (Ivanova et al., 2015; Verger et al., 2006). All point mutations, including the silent point mutations for the rescue experiments,

were introduced by inverse PCR using primers containing the mutations and CtBP1-S coding sequence cloned in pBluescriptII SK-(AgilentTechnologies). The ratio:syHy construct and syp mOrange2 used in this study were reported in (Lazarevic et al., 2017; Rose et al., 2013) and (Egashira et al., 2015), respectively. All constructs were verified by sequencing.

### **Ultrastructural analysis**

Organotypic hippocampal slice cultures from *Ctbp1* KO and WT littermates were prepared at postnatal day 0 and were cryo-fixed after 4-5 weeks in vitro under cryo-protectant conditions (20% bovine serum albumin in culture medium) using the High Pressure Freezing device HPM100 (Leica), and cryo-substituted in Freeze Substitution Processor EM AFS2 (Leica) according to previously published protocols (Imig and Cooper, 2017; Imig et al., 2014). For 2D analyses of synaptic morphology, electron micrographs were acquired from 60 nm-thick plastic sections with a transmission electron microscope (Zeiss LEO 912-Omega) operating at 80 kV. For 3D electron tomographic analysis of docked SV, 200 nm-thick plastic sections were imaged in a JEM-2100 transmission electron microscope (JEOL) operating at 200 kV. SerialEM (Mastronarde, 2005) was used to acquire single-axis tilt series ( $-60^{\circ}/-55^{\circ}$  to  $\pm 55^{\circ}/\pm 60^{\circ}$ ;  $1^{\circ}$  increments) at 25,000 fold magnification with an Orius SC1000 camera (Gatan, Inc.). Tomograms reconstructed from tilt series using the IMOD package (Kremer et al., 1996) had a voxel size of  $x,y,z = 1.82$  nm. Tomogram acquisition and analyses were performed blindly. Quantifications were done manually using ImageJ (National Institutes of Health). The smallest SV distances from the outer leaflet of the SV membrane to the inner leaflet of the AZ plasma membrane were measured using the straight line tool of the ImageJ software. Only SVs observed to be in physical contact at their midline with the presynaptic membrane were considered docked (0-2 nm distance). The mean SV diameter was calculated from the area of the SV measured at its midline to the outer leaflet of the SV membrane using the elliptical selection tool of ImageJ.

For illustrative purposes, images depicting tomographic sub-volumes represent an overlay of seven consecutive tomographic slices produced using the slicer tool of the 3dmod software of the IMOD software package to generate an approximately 13 nm thick sub-volume.

### **Quantitative real-time PCR**

Quantitative real-time PCR was performed as described in (Ivanova et al., 2015). Total RNA was extracted from primary cortical cultures (DIV16) superinfected on the day of plating with lentiviral particles driving the expression of scrambled, shRNA944 and YFP-CtBP2(NLS)-CtBP1, using RNeasy Plus Mini Kit (Qiagen) and following the instructions of the manufacturer. The transcript

levels of BDNF and Arc were analyzed by a customized version of Rat Synaptic Plasticity RT<sup>2</sup> Profiler PCR Array (Qiagen). To calculate the expression of BDNF and Arc in relation to a reference gene we used  $\Delta\Delta$ CP method. We used the 'second derivative maximum analysis' method, available in the software of Roche LightCycler480, to determine the crossing point (CP) of the PCR. The expression of lactate dehydrogenase A was used as a reference to calculate the relative mRNA levels of BDNF and Arc.

### ***Biochemical experimental work***

Cortical neurons with cell density 10 million per 75-cm<sup>2</sup> flask were superinfected with lentiviral particles, driving the expression of EGFP-CtBP1. Cells (DIV16) were lysed in 10mM Tris-HCl, 150mM NaCl, 2% SDS, 1% deoxycholate and 1% Triton X-100 containing complete protease inhibitors (Roche), and PhosStop (Roche) and co-immunoprecipitations were performed using MicroMACS anti-GFP MicroBeads and MicroColumns (Miltenyi Biotec) according to the instructions from the manufacturer.

Crude synaptosomal fraction (P2) was prepared as follows: First, cell or mouse brain homogenates were prepared in HEPES-buffered sucrose (4 mM HEPES pH 7.4, 0.32 M sucrose) and centrifuged at 1000 x g for 10 min to pellet the nuclear fraction (P1). The supernatant was then centrifuged at 12000 g for 20 min to give the crude synaptosomal pellet (P2). The crude synaptosomal fraction (P2) was lysed in 10 mM Tris-HCl, 150mM NaCl, 2% SDS, 1% deoxycholate and 1% Triton X-100 containing complete protease inhibitors (Roche), and PhosStop (Roche) and further subjected to IP or western blotting.

Protein samples were separated on 5–20% Tris-glycine gels, or 3.5–8% Tris-acetate gels as described previously (Ivanova et al., 2015) or on 10% (Bio-Rad TGX-Stain free gels) and blotted onto Millipore Immobilon FL PVDF membranes by tank or semidry blotting. Immunodetection was performed on Odyssey Infrared Scanner (LI-COR). For the quantification of the immunoblots the integrated density (ID) of signals was measured using ImageJ by setting rectangular ROIs with identical size around or using Image Studio Software (LI-COR). Samples of each experimental group were always loaded and quantified on the same membrane. TCE total protein stain used for normalization in Figure 1B. In Figure S2A GAPDH or  $\alpha$ -tubulin were used for normalization in homogenates and P2 fraction, respectively. The values for ID of CtBP1 or Pak1 (Figure 7A-D) were normalized to the corresponding expression levels of the two proteins in each experimental group. The antibodies used for immunodetection and the molecular weight of the markers are indicated in the figures.

## ***Microscopy and image analysis***

Immunostaining of neurons was performed as described in (Lazarevic et al., 2011). For quantifications, identical antibodies solutions were used for all coverslips from the same experiment. For the co-localization analysis, neurons were silenced with APV and CNQX for 10 minutes, in order to minimize the effect of the ongoing activity on the variance between synapses and then stimulated with 200 AP at 40 Hz. Cells were fixed within 30 seconds after the end of stimulation.

Staining with synaptotagmin 1 antibody (Syt1 Ab uptake) was performed by incubating the cells with fluorescently-labelled primary antibody dissolved in extracellular solution, containing 119 mM NaCl, 2.5 mM KCl, 2 mM CaCl<sub>2</sub>, 2 mM MgCl<sub>2</sub>, 30 mM glucose, and 25 mM HEPES, pH 7.4 for 30 min at 37°C (Lazarevic et al., 2011) before fixation. For the imaging with CypHer5E-labeled anti-synaptotagmin1 antibody, cells were incubated with the antibody diluted in a buffer containing 120 mM NaCl, 5 mM KCl, 2 mM MgCl<sub>2</sub>, 2 mM CaCl<sub>2</sub>, 10 mM glucose, and 18 mM NaHCO<sub>3</sub>, pH 7.4 for 2-3 hours at 37°C prior imaging.

Epifluorescence images were acquired on a Zeiss Axio Imager A2 microscope with Cool Snap EZ camera (Visitron Systems) controlled by VisiView (Visitron Systems GmbH) software.

Confocal images in Figure S2A were acquired on a Leica SP5 confocal microscope. The format of the images was 2048x2048 pixels display resolution, 8 bit dynamic range, for acquisition 63x objective, NA 1.40 and 2x optical zoom were used, which results in a voxel size of approximately 50 nm.

Dual-color STED images (1024x1024 pixels display resolution, 8 bit dynamic range) were acquired on a Leica TCS SP8-3X gated STED microscope using a HC APO CS2 100x objective, NA 1.40, and 5x optical zoom, corresponding to a voxel size of approximately 23 nm. 16 times line averaging was applied on frames acquired at a scan speed 600 Hz. The built-in pulsed white light laser of the setup was used to excite Abberior STAR 580 and Atto 647N at 561 nm and 650 nm, respectively. The detection was done at 580-620 nm for Abberior STAR 580 and 660-730 nm for Atto647N. Both dyes were depleted using a pulsed 775 nm depletion laser. Time-gated detection of 0.5-1 ns to 6 ns was set for both STED channels. All raw data were subsequently deconvolved using the calculated point spread function (PSF) of the system and the Classic Maximum Likelihood Estimation (CMLE) algorithm with Huygens Professional (SVI,15.10.1). In brief, after an automatic background correction, the signal to noise ratio was set to 15 and the optimized iteration mode of the CMLE was run until a quality threshold of 0.05 was reached. The deconvolved datasets were corrected for a chromatic aberration in z, using the Chromatic Aberration Corrector (CAC) in Huygens.

The co-localization analysis was performed on the deconvolved STED stacks using Imaris 8.3 (Bitplane, Oxford Instruments). To detect punctate staining as spots Imaris spot detection algorithm was applied as follows: the sensitivity for the detection of the spots in each channel was determined by an automatically generated threshold and the spots diameter was set to 0.06  $\mu\text{m}$ . The distances between the spots in the two channels were measured using a customized version of the Imaris XTension Spots Colocalize, which determines the co-localization between the spots within a user-defined distance (1  $\mu\text{m}$ ) and bins the data into several bins with equal width (100 nm).

For quantifications, the same detector settings were used for all coverslips quantified in one experiment. From each culture, images from at least two different coverslips were acquired and quantified to minimize experimental variability. The nuclear fluorescence was assessed as established before (Ivanova et al., 2015). ImageJ (NIH) and OpenView software (Tsurriel et al., 2006) were used for quantitative immunofluorescence analysis. After removing the background by threshold subtraction in ImageJ, synaptic puncta were defined with OpenView software by setting rectangular regions of interest (ROI) with identical dimensions around local intensity maxima in the channel with staining for synapsin or any of the other synaptic markers that were used (GluA, homer1, synaptophysin, SV2B). Mean immunofluorescence (IF) intensities were measured in the synaptic ROIs in all corresponding channels using the same software and normalized to the mean IF intensities of the control group for each of the experiments. The number of synapses per unit of dendrite length was determined as follows: First synapsin puncta along 30  $\mu\text{m}$  of proximal dendrite, was detected using Find Maxima function in ImageJ, by setting the same noise tolerance to all images quantified in one experiment; Mean IF intensities of GluA were measured in circular ROIs set around the local intensity maxima in the image with synapsin staining; The number of GluA puncta co-localizing with synapsin was calculated by applying an identical intensity threshold for GluA detection between the different conditions within an experiment.

### ***pHluorin imaging and analysis***

The pHluorin imaging was performed with hippocampal cultures DIV16 to 20, transduced with lentiviral particles on the day of plating.

The coverslips were removed from the cell culture plates and mounted in an imaging chamber (Warner instruments), supplied with a pair of platinum wire electrodes, 1 cm apart, for electrical stimulation. The imaging was performed at 26°C in extracellular solution, containing 119 mM NaCl, 2.5 mM KCl, 25 mM Hepes pH7.4, 30 mM glucose, 2 mM  $\text{MgCl}_2$  and 2 mM  $\text{CaCl}_2$ , 10  $\mu\text{M}$  6-cyano-7-nitroquinoxaline-2,3-dione disodium (CNQX, Tocris) and 50  $\mu\text{M}$  d-(-)-2-amino-5-

phosphonopentanoic acid (APV, Tocris), on inverted microscope (Observer. D1; Zeiss-as described above) equipped with an EMCCD camera (Evolve 512; Photometrics) controlled by MetaMorph Imaging (MDS Analytical Technologies) and VisiView (Visitron Systems GmbH) software, using 63x objective. EGFP ET filter set (exciter 470/40, emitter 525/50, dichroic 495 LP, Chroma Technology Corp.) and Cy5 ET filter set (exciter 620/60, emitter 700/75, dichroic 660 LP, Chroma Technology Corp.) were used for imaging of the pHluorin and CypHer5E, respectively. Cultures were stimulated with a train of 40 or 200 action potentials (1 ms, constant voltage pulses) at 5, 20 or 40 Hz using S48 stimulator (GRASS Technologies). The alkaline trapping method was used for quantification of the recycling vesicle pools. In brief, the stimulation of sypHy expressing neurons was done in presence of bafilomycin A1 (1  $\mu$ M, Merck/Millipore), a specific inhibitor of the vesicular V-type ATPase. Exocytosis of RRP was triggered by delivering of 40 AP at 20 Hz. Following a 2 min break after the end of the first train of stimuli TRP was released by stimulation with 200 AP at 20 Hz. The relative sizes of RRP and TRP were determined as fractions of the total sypHy-expressing pool measured after addition of alkaline imaging buffer (60 mM NaCl in the extracellular solution was replaced with 60 mM NH<sub>4</sub>Cl). Fluorescent images were acquired at 1 Hz (Figure 1I) and 10 Hz (Figures 1F,J,K, 4E, 6A-D, S2C,G, and S4). Imaging of hippocampal neurons transfected with syp mOrange2 (Figure 4C) was performed in a modified extracellular solution (136-mM NaCl, 2.5 mM KCl, 2 mM CaCl<sub>2</sub>, 1.3 mM MgCl<sub>2</sub>, 10 mM glucose, and 10 mM HEPES, 10  $\mu$ M CNQX, 50  $\mu$ M APV, pH 7.4) on inverted Zeiss Axio Observer.Z1 epifluorescence microscope, equipped with Zeiss AxioCam 506 camera controlled by ZEISS ZEN 2 software, using EC Plan-Neofluar 40x oil immersion objective (NA 1.3) and a DsRED filter set (exciter 538-562, beam splitter 570, emitter 570-640). Cultures were stimulated with a train of 200 AP delivered at 20 Hz (100 mA, 1 ms pulse width) and fluorescent images were acquired at 0.5 Hz. Synaptic puncta responding to stimulation were identified by subtracting an average of the first several frames of the baseline from an average of several frames at the end of stimulation. The mean IF intensities were measured in ROIs with an identical size, placed automatically over each responding synapse using a self-written macro in ImageJ. The data traces were determined after removing the background by threshold subtraction and correction for bleaching, calculated from the bleaching of unresponsive boutons from the same coverslip. The half times for endocytosis ( $t_{1/2}$ ) were determined by applying a single exponential fit to the decay phases of the data traces using GraphPad Prism5 and the following equation:  $F_t = F_{stim} \cdot \exp(-t/\tau)$ ,  $t_{1/2} = \ln(2) \cdot \tau$ , where  $F_{stim}$  is the fluorescence intensity at the end of stimulation and  $\tau$  is the time constant for endocytosis.



## Electrophysiology

Whole-cell voltage clamp recordings were performed between 14 and 18 days in vitro (DIV) in autaptic neurons at room temperature. Ionic currents were acquired using a Digidata 1440A digitizer and a Multiclamp 700B amplifier under the control of Clampex X software (Axon instrument). Series resistance was set at 70% and only neurons with series resistances below 10 M $\Omega$  were selected. Data were recorded at 10 kHz and low-pass filtered at 3 kHz. Borosilicate glass pipettes with a resistance around 3 M $\Omega$  were used and filled with an intracellular solution containing (in mM): 136 KCl, 17.8 HEPES, 1 EGTA, 4.6 MgCl<sub>2</sub>, 4 Na<sub>2</sub>ATP, 0.3 Na<sub>2</sub>GTP, 12 phosphocreatine, and 50 U/ml phosphocreatine kinase; 300 mOsm; pH 7.4. Autaptic neurons were continuously perfused with standard extracellular solution composed of (in mM): 140 NaCl, 2.4 KCl, 10 HEPES, 10 glucose, 2 CaCl<sub>2</sub>, 4 MgCl<sub>2</sub>; 300 mOsm; pH 7.4. Spontaneous release was measured by recording mEPSC for 30 s at a holding potential of -70 mV in the presence of 3 mM kynurenic acid to detect false positive events and for the equal amount of time in extracellular solution. Data were filtered at 1 kHz and analyzed using template-based miniature event detection algorithms implemented in the AxoGraph X software. Action potential-evoked release EPSCs were elicited by 2 ms somatic depolarization from -70 to 0 mV. To estimate the readily-releasable pool (RRP) size, 500 mM hypertonic sucrose added to standard extracellular solution, was applied for 5 s using a fast-flow system (Pyott and Rosenmund, 2002). For vesicular release probability (P<sub>vr</sub>) calculations, the ratio of EPSC charge to RRP charge was determined. Short-term plasticity was examined either by evoking 2 unclamped AP with 25 ms interval (40 Hz) or a train of 50 AP at an interval of 100 ms (10 Hz). All electrophysiological data were analyzed offline using Axograph X (Axograph Scientific).

## QUANTIFICATION AND STATISTICAL ANALYSIS

All quantitative results are given as means  $\pm$  standard errors of the mean (SEM) and normalised to the values of control. Statistical analyses were performed with Prism 7 and 8 (GraphPad Software, Inc.). The sample sizes (n numbers) were adjusted based on published studies using similar methodology. In the plots the interquartile range and median are depicted as boxes, minimal and maximal values as whiskers and + indicates mean. In Figure 2 F and G scatter dot plots show mean and 95% CI, and in 2 L and N bars indicate mean and SEM. Data points in curves in Figure 3L, 4C and E, 6A-D, are depicted as means and SEM. n numbers correspond to the number of cells (fixed cell imaging and electrophysiology experiments), individual coverslips (live cell imaging experiments), synaptic profiles (EM data), number of independent

immunoprecipitations (IP) or samples from independent animals (WB) and are indicated for each group in graphs. In graphs comparisons with the control are indicated above each box and, comparisons between the conditions are given as horizontal bars. The statistical tests were chosen after the distribution of the data sets was explored. The scoring and the statistical tests used to compute the P values are specified in the datatable. Significance is indicated using asterisks: nsP>0.05, \*P<0.05, \*\*P<0.01, \*\*\*P<0.001, \*\*\*\* P<0.0001.

## DATA AND CODE AVAILABILITY

Requests for data and the scripts used for the main steps of the analysis of the pHluorin and STED data should be directed to the Lead Contact Anna Fejtova and will be made available upon reasonable request.

**Acknowledgments:** The YFP-CtBP2(NLS)-CtBP1 construct was kindly provided by M.Crossley, University of Sydney, Australia. We thank Anika Dirks for help with maintenance of the *Ctbp1* KO mouse colony, Christiana Kontaxi for help with animal handling, Maria Jose for help with imaging, Oliver Kobler, Torsten Stoeter and SL ELMI for providing expertise in STED imaging and tools for analysis and Janina Juhle, Bettina Kracht, Anita Heine and Isabel Herbert for excellent technical assistance. We also thank Renato Frischknecht, all members of the Presynaptic plasticity group and the Department Neurochemistry and molecular biology at LIN for useful discussions. This research was supported by the German Research Council grant GRK2162 and FE1335-1 to AF, SFB 779 to AF, SFB958 to CR, Wellcome Trust grant to MAC (204954/Z/16/Z) and Leibniz SAW grants to AF and EDG.

## Author contributions:

Conceptualization: DI and AF; Methodology: DI, CI, MC, CMV, DG, MAC, BC, AF; Investigation: DI, CI, MC, AR, DG, BC; Writing original draft: DI and AF; Writing-Review-Editing: all authors; Funding acquisition: MAC, CR, EDG and AF

## Declaration of interest:

"The authors declare no competing interests"

## Figure legends

### Figure 1

#### Knock down of CtBP1 reduces SV recycling.

- A) Representative images showing that the general neuronal morphology and the localization of synaptic markers are not changed in CtBP1KD neurons.
- B) Representative Western blots of samples from rat neurons transduced with viruses expressing shRNAs: scr, CtBP1KD944 and KD467 together with syphHy. The immunoreactivity for CtBP1 and CtBP2 and TCE total protein stain used as a loading control are shown. While notable downregulation of CtBP1 is evident in KD samples compared to scr, no changes were detected for CtBP2.
- C) Quantification of the Syt1 Ab uptake driven by basal network activity, depolarization with 50 mM KCl or in the presence of 1  $\mu$ M TTX in scr, and knockdown cultures.
- D) Representative images of Syt1 Ab uptake driven by basal neuronal network activity in control (scr), CtBP1KD944 and CtBP1KD467 cultures.
- E) Representative images of neurons expressing syphHy used to determine SV pool sizes. Cells were imaged in the presence of bafilomycin A1 during stimulation with 40 AP at 20 Hz to release RRP. After a rest for 2 min a train of 200 AP at 20 Hz triggered the exocytosis of all release-competent vesicles (TRP). A final  $\text{NH}_4\text{Cl}$ -pulse that visualized all released and non-released syphHy-positive vesicles (total pool: TP) was used for normalization.
- F) Average syphHy-fluorescence (FsyphHy) traces reporting SV pool sizes from control and CtBP1KD neurons. RRP and TRP are given as fractions of TP.
- G) The mean values of RRP in scr, CtBP1KD944 and CtBP1KD467 did not differ significantly, but KD of CtBP1 leads to a significant reduction of TRP size.
- H) Images of syphHy showing SV exo-endocytosis at synapses in response to 200 AP at 5 Hz. The upper image shows the reference F of tdimer 2 before stimulation and the lower three the green F of syphHy before, during and after the stimulation.
- I-K) CtBP1 deletion results in slower retrieval of exocytosed SV. Peak-normalized syphHy responses to 200 AP at 5 Hz (I), 200 AP at 20 Hz (J) and 200 AP at 40 Hz (K) and respective single exponential fits of fluorescence decay are shown for each group. The estimated half times of endocytosis ( $t_{1/2}$ ) are plotted.
- Overlays are shown in the indicated colors. Scale bar is 10  $\mu$ m in A and 5  $\mu$ m in D, E and H.

### Figure 2

#### Ultrastructural analysis of synaptic morphology and SV distribution in *Ctbp1* KO and wild-type (WT) neurons

Synaptic profiles of glutamatergic spine synapses in high-pressure frozen and freeze substituted hippocampal organotypic slice cultures of *Ctbp1* knock out (KO) and wild-type (WT) animals were

analysed in electron micrographs of 60 nm-thick ultrathin sections (A-G) and by 3D electron tomography (H-P).

A and B) Electron micrographs of WT and respective *Ctbp1* KO synaptic profiles.

C to G) Mean values for number of SVs per synaptic profile(C), SV density(D), postsynaptic density (PSD) length (E), number of endosomes per synaptic profile(F,) and number of large dense-core vesicles (LDCVs) per synaptic profile(G).

H and I) Electron tomography sub-volumes of wild-type (H) and *Ctbp1* KO (I) synapses.

J and K) 3D models of synaptic profiles including orthogonal views of the active zone (AZ, white; docked SVs, red; nonattached SVs, gray).

L to P) Graphs show spatial distribution of SVs within 100 nm of the AZ (L), mean number of docked SVs (within 0–2 nm of the AZ) per AZ area (M), frequency distribution of SV diameters within 200 nm of the AZ (N), mean diameter of docked SVs (O) and mean number SV within 0–40 nm of the AZ per AZ area.

Scale bars: 200 nm in B) and 100 nm in I)

Figure 3

### **Synaptic and nuclear CtBP1 have distinct effects on neurotransmission and their deletion leads to pronounced short-term depression**

A) Averaged normalized evoked EPSC amplitudes from control, CtBP1KD944, EGFP-CtBP1 and YFP-CtBP2(NLS)-CtBP1 expressed in CtBP1KD944 neurons.

B) Example traces showing spontaneous EPSCs from control, CtBP1KD944 neurons, or neurons expressing EGFP-CtBP1 and YFP-CtBP2(NLS)-CtBP1 on CtBP1KD background.

C) Respective quantifications of average mEPSC amplitudes from the groups shown in (B).

D) Respective quantifications of mEPSC frequency from the groups shown in (B).

E) Autaptic neurons expressing the scrambled and CtBP1KD944 shRNA or the rescue variants: EGFP-CtBP1 or YFP-CtBP2(NLS)-CtBP1 on CtBP1KD944 background, were live stained for surface AMPA receptors and post fixation for synapsin to label presynapses. The overlays are shown in the indicated colors. Scale bar: 5µm

F and G) Quantification of the experiment in E. IF intensity of surface expressed GluA at synapses does not differ between conditions, but CtBP1KD944 and expression of EGFP-CtBP1 in CtBP1KD944 neurons increase the number of synapses.

H and I) Typical responses to application of 500mOsmM sucrose for 10sec (H) and average normalized sizes of RRP (I).

J) and K) Averaged normalized vesicular release probability (J) and PPR (K) in control, CtBP1KD944, and EGFP-CtBP1 and YFP-CtBP2(NLS)-CtBP1 expressed in CtBP1KD944 neurons.

L) Averaged normalized amplitudes of EPSC evoked by a train of stimuli at 10Hz.

Figure 4

### **Synaptic CtBP1 regulates SV recycling and short-term plasticity**

A) Syt1 Ab uptake was used to evaluate the efficacy of SV recycling in control, CtBP1KD944 and CtBP1KD944 neurons expressing the rescue constructs: EGFP-CtBP1 and YFP-

CtBP2(NLS)-CtBP1. Neurons were stained for synapsin to label synapses. Colored images represent overlays. Scale bar: 5µm.

- B) Expression of EGFP-CtBP1 rescues the Syt1 Ab uptake in CtBP1KD944 neurons up to 80% of the control levels. The fission deficient mutant EGFP-CtBP1D355A has a reduced rescue capacity compared to EGFP-CtBP1. Expression of the nuclear rescue: YFP-CtBP2(NLS)-CtBP1, does not compensate for the decreased Syt1 Ab uptake in CtBP1KD944.
- C) Average sympOrange2 responses to 200 AP at 20 Hz from control, CtBP1KD944 or CtBP1KD944 neurons expressing EGFP-CtBP1, EGFP-CtBP1D355A or YFP-CtBP2(NLS)-CtBP1.
- D) The endocytic half times,  $t_{1/2}$  from the experiment in (C) indicated that the rate of endocytosis was significantly lower in CtBP1KD944 compared to control. While expression of EGFP-CtBP1 in CtBP1KD944 cells rescued the endocytosis rate, expression of EGFP-CtBP1D355A or YFP-CtBP2(NLS)-CtBP1 did not.
- E) Visualization of short-term depression of exocytosis in CtBP1KD944 and upon expression of rescue constructs. Plotted are average Syt1 Ab-CypHer responses to 40AP at 20Hz (a reference response), followed by a 60s rest period and 200 AP at 10 Hz in the presence of bafilomycin A1. The traces were normalized to the amplitudes of the reference responses in each condition.
- F) The absence of synaptic CtBP1 led to a reduction of the plateau fluorescence responses in experiment E.

Figure 5

### **CtBP1 and dynamin act at the same membrane domain in an independent but likely cooperative manner**

- A) Orthographic views of the distribution of synaptic CtBP1 and the endocytic markers dynamin1, rab5, rab7, rab22 in neurons stimulated with 200 AP at 40 Hz. Punctate staining was detected as 'spots' and the co-localization was assessed as a distance from the CtBP1-labeled spots (synaptic distance) < 1 µm.
- B) The histogram shows the distribution of synaptic puncta co-localizing with CtBP1, binned according to the distance to CtBP1. A significantly smaller distance to CtBP1 is evident for dynamin1 (0-100 and 100-200 nm distance to CtBP1) compared to the other endosome markers.
- C) Images of Syt1 Ab-CypHer uptake in control and CtBP1KD944 neurons untreated or treated with dynole 34-2 (C, 30 µM) for 1h. Live staining for surface GluA receptors was used to mark synapses. Overlays are shown as colored images.
- D) Dynole 34-2 inhibits endocytosis in control and in CtBP1KD944 neurons. The residual endocytosis is significantly lower upon Dynole 34-2 application in CtBP1KD944 suggesting an interaction of treatments.

Scale bar is 0.1 µm in (A) and 5µm in (C).

Figure 6

### **CtBP1 promotes SV retrieval by activation of PLD1**

- A to D) Average syHy responses to 200 AP at 20 Hz were recorded and quantification of  $t_{1/2}$  of recovery was performed upon treatment with BFA (A,B) or PLD1 inhibitor (C,D) in control (A,C) or CtBP1KD944 neurons (B,D). SV retrieval was significantly delayed in BFA-treated neurons (A) but not further affected in BFA treated CtBP1KD944 neurons (B). Treatment with a PLD1 inhibitor affected SV retrieval in control neurons (C) but not in CtBP1KD944 neurons (D). The same controls were plotted in (A) and (C) as well as in (B) and (D), respectively.
- E) The endocytic probe mCLING-DY654 was loaded by stimulation of control and CtBP1KD944 neurons with 200AP at 40Hz. Synapses were stained with synapsin Ab. Synapses in CtBP1KD944 neurons show a reduction in the mCLING labeling.
- F) Quantification of synaptic mCLING IF in (E).
- G) Orthographic views of synaptic EGFP-CtBP1 or EGFP-CtBP1S147A (S147A) expressed in CtBP1KD944 neurons and the endocytic probe mCLING-ATTO647N, loaded by stimulation with 200 AP at 40 Hz.
- H) Quantification of the mCLING intensities from EGFP-CtBP1- and S147A-labeled synapses in G.
- I) Correlation of mCLING intensities and the distances to EGFP-CtBP1. The intensity of the endocytic probe was inversely correlated with the distance to EGFP-CtBP1.
- J) The histogram shows the distribution of mCLING puncta co-localizing with EGFP-CtBP1 or S147A, binned according to the distance mCLING-CtBP1. Note the shift in the histogram of EGFP-CtBP1 towards closer distances.

Scale bar is 2  $\mu$ m in E and 0.1  $\mu$ m in G.

Figure 7

#### **PAK1 phosphorylation mediates a switch in the association of CtBP1 with Bsn and PLD1**

- A and B) Inhibition of Pak1 increases the binding of EGFP-CtBP1 to Bsn and reduces its binding to PLD1. (A) Co-IP with EGFP antibodies was performed from neuronal cultures expressing EGFP-CtBP1 and treated or not with the Pak1 inhibitor IPA3 (50 $\mu$ M, 1h). (B) Quantification of the binding of Bsn to CtBP1.
- C and D) IP with EGFP antibodies was performed from whole cell lysates or P2 fractions of neuronal cultures expressing EGFP-CtBP1 and treated or not with the Pak1 inhibitor IPA3 (50 $\mu$ M for 1h). The Western blots were probed with a pan anti Ser/Thr Ab to visualize the phospho-Ser/Thr levels of CtBP1. Quantification of the Ser/Thr phosphorylation of CtBP1.
- E) The 2 color-STED images show a tighter co-localization of EGFP-CtBP1 with Bsn after stimulation with 200 AP at 40 Hz compared to cells at rest. EGFP-CtBP1S147A displays a tight co-localization with Bsn independently of neuronal activity.
- F) The histogram shows the relative distribution of Bsn puncta co-localizing with EGFP-CtBP1 or S147A at rest and upon stimulation.

Scale bar is 40 nm.

Figure S1

**Knock down of CtBP1 does not affect the overall expression of synaptic proteins and CtBP2**

- A) Synaptic abundance of pre- (SV2B, synapsin, synaptophysin) and post-synaptic markers (homer1, GluA) does not change in CtBP1KD neurons.
- B) Quantification of the effects shown in A)
- C) Nuclear CtBP2 does not change in CtBP1KD neurons.
- D) Quantification of the effects shown in C)

Scale bar is 5  $\mu$ m in A, and 10  $\mu$ m in C.

**Figure S2**

***Ctbp1* KO synapses have a reduced rate of SV endocytosis and a lower number of release-competent vesicles.**

- A) Immunoblot detection of synaptic proteins in brain homogenates (H) and crude synaptosomes (P2) from WT and *CtBP1* KO mice. GAPDH and  $\alpha$ -tubulin are loading controls.
- B) Quantification of the effects shown in A)
- C) Average syHy-fluorescence traces reporting SV pool sizes from neurons derived from WT and *Ctbp1*<sup>-/-</sup> mice.
- D) The mean values of RRP in WT and *Ctbp1*<sup>-/-</sup> did not differ significantly.
- E) Quantification of TRP size in WT and *Ctbp1*<sup>-/-</sup>.
- F) Neurons prepared from *Ctbp1*<sup>-/-</sup> animals and their WT siblings stained with an anti synapsin Ab, to label presynaptic terminals and pan anti GluA Ab to label postsynapses. Number of co-localizing synapsin and GluA puncta was slightly but not significantly increased in KO compared to control. The overlays are shown in the indicated colors. Scale bar: 5 $\mu$ m.
- G) Peak-normalized syHy responses to 200 AP at 20Hz. The half times: t<sub>1/2</sub> of endocytosis (bar graph) were smaller in WT neurons compared to *Ctbp1*<sup>-/-</sup>.

**Figure S3**

**Expression of YFP-CtBP2(NLS)-CtBP1 reverts the effect of CtBP1KD944 on gene expression.**

- A) Perspective views of 3D reconstructions of hippocampal neurons showing the synapto-nuclear distribution of the endogenous CtBP1 and the expressed rescue variants. Synapsin staining labels presynaptic terminals; DAPI labels nuclei. Note that EGFP-CtBP1 shows a decreased nuclear and an increased synaptic localization, whereas YFP-CtBP2(NLS)-CtBP1 is expressed only in the nucleus. For better visualization several EGFP-CtBP1-positive spots were removed from the planes above the nucleus. Overlays are shown in the indicated colors. Scale bar: 7 $\mu$ m.

B and C) YFP-CtBP2(NLS)-CtBP1 counteracts the increased expression of BDNF and Arc in CtBP1KD944 neuronal cultures.

Figure S4

### Frequency-dependent short-term synaptic depression at CtBP1-deficient synapses

A) and B) Average Syt1 Ab-CypHer responses to 50 AP at 20 Hz (a reference response), followed by a 60s rest period and 200 AP at 5 Hz (A) or 40 Hz (B) in the presence of 80 nM folimycin. The traces were normalized to the amplitudes of the reference response. KD of CtBP1 reduces the fluorescence responses to 200 AP at 5 Hz and even more pronouncedly at 40 Hz.

Figure S5

### Effect of synaptic stimulation on the co-localization of CtBP1 with the endocytic markers dynamin1, rab5, rab7, rab22 and the SV protein Syt1.

A - E) Cumulative plots showing the % of dynamin1, rab5, rab7, rab22 and Syt1 puncta co-localizing with CtBP1 in control (treated with 50μM APV and 10μM CNQX for 10 min) and stimulated (200AP at 40Hz) neurons, binned according to the distance to the CtBP1 labeled spots.

### Table 1: Ultrastructural analysis of synaptic morphology

#### 2D EM Analysis of Synaptic Morphology

	WT (N=3, n=159)	KO (N=4, n=146)	
# of SVs per profile	80.72 ± 3.244	89.21 ± 3.721	P = 0.098
terminal area ( x 0.01 μm <sup>2</sup> )	40.38 ± 1.182	41.19 ± 1.303	P = 0.845
# SVs / 0.01 μm <sup>2</sup> terminal area	1.993 ± 0.054	2.159 ± 0.064	P = 0.065
PSD length (nm)	373.7 ± 9.261	379.4 ± 9.421	P = 0.627
# of endosomes / terminal	0.843 ± 0.077	0.726 ± 0.082	P = 0.140
# of LDCVs / terminal	0.151 ± 0.034	0.24 ± 0.043	P = 0.083

N, number of animals; n, number of synaptic profiles; SV, synaptic vesicle; PSD, postsynaptic density; LDCV, large dense-core vesicle. (red P-values = Mann-Whitney test, black P-values = unpaired t-test)

#### 3D Electron Tomographic Analysis of Synaptic Vesicle Pools

	WT (N=3, n=26)	KO (N=4, n=25)	
# SVs within 0-2 nm of AZ	0.605 ± 0.092	0.876 ± 0.117	P = 0.075
# SVs within 0-5 nm of AZ	0.797 ± 0.109	1.213 ± 0.142	*P = 0.043
# SVs within 0-40 nm of AZ	1.821 ± 0.12	2.496 ± 0.168	**P = 0.002
# SVs within 0-100 nm of AZ	5.876 ± 0.267	7.307 ± 0.382	**P = 0.003



# SVs within 0-200 nm of AZ	14.65 ± 0.817	15.31 ± 0.811	P = 0.572
# SVs within 5-10 nm of AZ	0.214 ± 0.041	0.292 ± 0.07	P = 0.621
# SVs within 10-20 nm of AZ	0.264 ± 0.058	0.162 ± 0.037	P = 0.354
# SVs within 20-30 nm of AZ	0.213 ± 0.051	0.363 ± 0.069	P = 0.072
# SVs within 30-40 nm of AZ	0.345 ± 0.052	0.465 ± 0.07	P = 0.170
# SVs within 40-50 nm of AZ	0.531 ± 0.053	0.596 ± 0.081	P = 0.503
# SVs within 50-100 nm of AZ	3.54 ± 0.196	4.215 ± 0.245	*P = 0.036
# SVs within 100-150 nm of AZ	4.408 ± 0.331	4.175 ± 0.251	P = 0.579
# SVs within 150-200 nm of AZ	4.34 ± 0.328	3.827 ± 0.291	P = 0.249
AZ area (nm <sup>2</sup> )	40.900 ± 1.775	44.240 ± 2.276	P = 0.569
SV diameter (SVs within 0-200 nm of AZ)	44.95 ± 0.347	45.77 ± 0.38	P = 0.114
SV diameter (SVs within 0-100 nm of AZ)	44.98 ± 0.381	45.82 ± 0.426	P = 0.15

N, number of animals; n, number of tomograms; SV, synaptic vesicle; AZ, active zone. SV numbers within a certain distance of the AZ are normalized to 0.01  $\mu\text{m}^2$  of AZ area. Values indicate mean  $\pm$  SEM. (red P-values = Mann-Whitney test, black P-values = unpaired t-test)

	WT (n=63)	KO (n=100)	
SV diameter (docked SVs, 0-2 nm of AZ)	44.17 ± 0.64	46.08 ± 0.485	*P = 0.012

n, number of docked SVs averaged over all tomograms of a given genotype

Table 2: Electrophysiological analysis of autaptic cultures from CtBP1944KD and scr and upon expression of selective synaptic or nuclear rescue constructs

	SC	Kruskal-Wallis test	CtBP1KD944	Kruskal-Wallis test	EGFP-CtBP1	Kruskal-Wallis test	YFP-CtBP2(NLS)-CtBP1	Kruskal-Wallis test
mEPSC charge (fC)	110.5 $\pm$ 4.2 (n=69/5)	CtBP1KD944 P>0.99	104.4 $\pm$ 4.1 (n=70/5)	SC P>0.99	119.4 $\pm$ 9.8 (n=64/5)	SC P>0.99	110.3 $\pm$ 4.1 (n=62/5)	SC P>0.99
		EGFP-CtBP1 P>0.99		EGFP-CtBP1 P>0.99		CtBP1KD944 P>0.99		CtBP1KD944 P>0.99
		YFP-CtBP2(NLS)-CtBP1 P>0.99		YFP-CtBP2(NLS)-CtBP1 P>0.99		YFP-CtBP2(NLS)-CtBP1 P>0.99		EGFP-CtBP1 P>0.99
EPSC	35.4	CtBP1KD944	55.2	SC	78.1	SC	51.3	SC P=0.072

Charge (pC)	± 4.5 (n=77/5)	P=0.0018	± 5.9 (n=72/5)	P=0.0018	± 8.5 (n=62/5)	<0.0001	± 6.2 (n=63/5)	
		EGFP-CtBP1 P<0.0001		EGFP- CtBP1 P=0.4137		CtBP1KD94 4 P=0.4137		CtBP1KD944 P>0.99
		YFP- CtBP2(NLS)- CtBP1 P=0.072		YFP- CtBP2(NLS) -CtBP1 P>0.99		YFP- CtBP2(NLS) -CtBP1 P=0.0436		EGFP-CtBP1 P=0.0436
Pvr (%)	7.0 ± 0.5 (n=73/5)	CtBP1KD944 P<0.0001	15.8 ± 0.9 (n=64/5)	SC P<0.0001	14.2 ± 1.1 (n=52/5)	SC P<0.0001	11.6 ± 1.0 (n=62/5)	SC P>0.006
		EGFP-CtBP1 P<0.0001		EGFP- CtBP1 P>0.999		CtBP1KD94 4 P>0.999		CtBP1KD944 P=0.011
		YFP- CtBP2(NLS)- CtBP1 P>0.006		YFP- CtBP2(NLS) -CtBP1 P=0.011		YFP- CtBP2(NLS) -CtBP1 P=0.1925		EGFP-CtBP1 P=0.1925

1031 n, number of neurons / independent cultures analyzed

## 1032 References:

- 1033 Antonny, B., Burd, C., De Camilli, P., Chen, E., Daumke, O., Faelber, K., Ford, M., Frolov, V.A., Frost, A.,  
1034 Hinshaw, J.E., *et al.* (2016). Membrane fission by dynamin: what we know and what we need to know.  
1035 EMBO J 35, 2270-2284.
- 1036 Bekkers, J.M., and Stevens, C.F. (1991). Excitatory and inhibitory autaptic currents in isolated hippocampal  
1037 neurons maintained in cell culture. Proc Natl Acad Sci U S A 88, 7834-7838.
- 1038 Bonazzi, M., Spano, S., Turacchio, G., Cericola, C., Valente, C., Colanzi, A., Kweon, H.S., Hsu, V.W.,  
1039 Polishchuck, E.V., Polishchuck, R.S., *et al.* (2005). CtBP3/BARS drives membrane fission in dynamin-  
1040 independent transport pathways. Nat Cell Biol 7, 570-580.
- 1041 Burrone, J., Li, Z., and Murthy, V.N. (2006). Studying vesicle cycling in presynaptic terminals using the  
1042 genetically encoded probe synaptopHluorin. Nat Protoc 1, 2970-2978.
- 1043 Chinnadurai, G. (2009). The transcriptional corepressor CtBP: a foe of multiple tumor suppressors. Cancer  
1044 Res 69, 731-734.
- 1045 Colanzi, A., Grimaldi, G., Catara, G., Valente, C., Cericola, C., Liberali, P., Ronci, M., Lalioti, V.S., Bruno, A.,  
1046 Beccari, A.R., *et al.* (2013). Molecular mechanism and functional role of brefeldin A-mediated ADP-  
1047 ribosylation of CtBP1/BARS. Proc Natl Acad Sci U S A 110, 9794-9799.
- 1048 Cousin, M.A. (2017). Integration of Synaptic Vesicle Cargo Retrieval with Endocytosis at Central Nerve  
1049 Terminals. Front Cell Neurosci 11, 234.
- 1050 Dick O, Hack I, Altrock WD, Garner CC, Gundelfinger ED, Brandstatter JH (2001) Localization of the  
1051 presynaptic cytomatrix protein Piccolo at ribbon and conventional synapses in the rat retina: comparison  
1052 with Bassoon. J Comp Neurol 439: 224-234
- 1053 Donaldson, J.G. (2009). Phospholipase D in endocytosis and endosomal recycling pathways. Biochim  
1054 Biophys Acta 1791, 845-849.

1055 Egashira, Y., Takase, M., and Takamori, S. (2015). Monitoring of vacuolar-type H<sup>+</sup> ATPase-mediated proton  
1056 influx into synaptic vesicles. *J Neurosci* 35, 3701-3710.

1057 Fejtova, A., Davydova, D., Bischof, F., Lazarevic, V., Altmann, W.D., Romorini, S., Schone, C., Zuschratter, W.,  
1058 Kreutz, M.R., Garner, C.C., *et al.* (2009). Dynein light chain regulates axonal trafficking and synaptic levels  
1059 of Bassoon. *J Cell Biol* 185, 341-355.

1060 Ferguson, S.M., Brasnjo, G., Hayashi, M., Wolfel, M., Collesi, C., Giovedi, S., Raimondi, A., Gong, L.W., Ariel,  
1061 P., Paradise, S., *et al.* (2007). A selective activity-dependent requirement for dynamin 1 in synaptic vesicle  
1062 endocytosis. *Science* 316, 570-574.

1063 Gan, Q., and Watanabe, S. (2018). Synaptic Vesicle Endocytosis in Different Model Systems. *Front Cell*  
1064 *Neurosci* 12, 171.

1065 Garriga-Canut, M., Schoenike, B., Qazi, R., Bergendahl, K., Daley, T.J., Pfender, R.M., Morrison, J.F., Ockuly,  
1066 J., Stafstrom, C., Sutula, T., and Roopra, A. (2006). 2-Deoxy-D-glucose reduces epilepsy progression by  
1067 NRSF-CtBP-dependent metabolic regulation of chromatin structure. *Nat Neurosci* 9, 1382-1387.

1068 Granseth, B., Odermatt, B., Royle, S.J., and Lagnado, L. (2006). Clathrin-mediated endocytosis is the  
1069 dominant mechanism of vesicle retrieval at hippocampal synapses. *Neuron* 51, 773-786.

1070 Haga, Y., Miwa, N., Jahangeer, S., Okada, T., and Nakamura, S. (2009). CtBP1/BARS is an activator of  
1071 phospholipase D1 necessary for agonist-induced macropinocytosis. *EMBO J* 28, 1197-1207.

1072 Haucke, V., Neher, E., and Sigrist, S.J. (2011). Protein scaffolds in the coupling of synaptic exocytosis and  
1073 endocytosis. *Nat Rev Neurosci* 12, 127-138.

1074 Hildebrand, J.D., and Soriano, P. (2002). Overlapping and unique roles for C-terminal binding protein 1  
1075 (CtBP1) and CtBP2 during mouse development. *Mol Cell Biol* 22, 5296-5307.

1076 Hosoi N, Holt M, Sakaba T (2009) Calcium dependence of exo- and endocytotic coupling at a glutamatergic  
1077 synapse. *Neuron* 63: 216-229

1078 Hua, Y., Sinha, R., Thiel, C.S., Schmidt, R., Huve, J., Martens, H., Hell, S.W., Egner, A., and Klingauf, J.  
1079 (2011). A readily retrievable pool of synaptic vesicles. *Nat Neurosci* 14, 833-839.

1080 Hua, Y., Woehler, A., Kahms, M., Haucke, V., Neher, E., and Klingauf, J. (2013). Blocking endocytosis  
1081 enhances short-term synaptic depression under conditions of normal availability of vesicles. *Neuron* 80,  
1082 343-349.

1083 Hubler, D., Rankovic, M., Richter, K., Lazarevic, V., Altmann, W.D., Fischer, K.D., Gundelfinger, E.D., and  
1084 Fejtova, A. (2012). Differential spatial expression and subcellular localization of CtBP family members in  
1085 rodent brain. *PLoS One* 7, e39710.

1086 Humeau, Y., Vitale, N., Chasserot-Golaz, S., Dupont, J.L., Du, G., Frohman, M.A., Bader, M.F., and Poulain,  
1087 B. (2001). A role for phospholipase D1 in neurotransmitter release. *Proc Natl Acad Sci U S A* 98, 15300-  
1088 15305.

1089 Imig, C., and Cooper, B.H. (2017). 3D Analysis of Synaptic Ultrastructure in Organotypic Hippocampal Slice  
1090 Culture by High-Pressure Freezing and Electron Tomography. *Methods Mol Biol* 1538, 215-231.

1091 Imig, C., Min, S.W., Krinner, S., Arancillo, M., Rosenmund, C., Sudhof, T.C., Rhee, J., Brose, N., and Cooper,  
1092 B.H. (2014). The morphological and molecular nature of synaptic vesicle priming at presynaptic active  
1093 zones. *Neuron* 84, 416-431.

1094 Ivanova, D., Dirks, A., and Fejtova, A. (2016). Bassoon and piccolo regulate ubiquitination and link  
1095 presynaptic molecular dynamics with activity-regulated gene expression. *J Physiol* 594, 5441-5448.

1096 Ivanova, D., Dirks, A., Montenegro-Venegas, C., Schone, C., Altmann, W.D., Marini, C., Frischknecht, R.,  
1097 Schanze, D., Zenker, M., Gundelfinger, E.D., and Fejtova, A. (2015). Synaptic activity controls localization  
1098 and function of CtBP1 via binding to Bassoon and Piccolo. *EMBO J* 34, 1056-1077.

1099 Jenkins, G.H., Fiset, P.L., and Anderson, R.A. (1994). Type I phosphatidylinositol 4-phosphate 5-kinase  
1100 isoforms are specifically stimulated by phosphatidic acid. *J Biol Chem* 269, 11547-11554.

1101 Kim, S.H., and Ryan, T.A. (2009). Synaptic vesicle recycling at CNS synapses without AP-2. *J Neurosci* 29,  
1102 3865-3874.

1103 Koch, D., Spiwoks-Becker, I., Sabanov, V., Sinning, A., Dugladze, T., Stellmacher, A., Ahuja, R., Grimm, J.,  
 1104 Schuler, S., Muller, A., *et al.* (2011). Proper synaptic vesicle formation and neuronal network activity  
 1105 critically rely on syndapin I. *EMBO J* 30, 4955-4969.  
 1106 Kononenko, N.L., Diril, M.K., Puchkov, D., Kintscher, M., Koo, S.J., Pfuhl, G., Winter, Y., Wienisch, M.,  
 1107 Klingauf, J., Breustedt, J., *et al.* (2013). Compromised fidelity of endocytic synaptic vesicle protein sorting  
 1108 in the absence of stonin 2. *Proc Natl Acad Sci U S A* 110, E526-535.  
 1109 Kononenko, N.L., and Haucke, V. (2015). Molecular mechanisms of presynaptic membrane retrieval and  
 1110 synaptic vesicle reformation. *Neuron* 85, 484-496.  
 1111 Kooijman, E.E., Chupin, V., de Kruijff, B., and Burger, K.N. (2003). Modulation of membrane curvature by  
 1112 phosphatidic acid and lysophosphatidic acid. *Traffic* 4, 162-174.  
 1113 Kraszewski, K., Mundigl, O., Daniell, L., Verderio, C., Matteoli, M., and De Camilli, P. (1995). Synaptic  
 1114 vesicle dynamics in living cultured hippocampal neurons visualized with CY3-conjugated antibodies  
 1115 directed against the luminal domain of synaptotagmin. *J Neurosci* 15, 4328-4342.  
 1116 Kremer, J.R., Mastronarde, D.N., and McIntosh, J.R. (1996). Computer visualization of three-dimensional  
 1117 image data using IMOD. *Journal of structural biology* 116, 71-76.  
 1118 Lazarevic, V., Fienko, S., Andres-Alonso, M., Anni, D., Ivanova, D., Montenegro-Venegas, C., Gundelfinger,  
 1119 E.D., Cousin, M.A., and Fejtova, A. (2017). Physiological Concentrations of Amyloid Beta Regulate Recycling  
 1120 of Synaptic Vesicles via Alpha7 Acetylcholine Receptor and CDK5/Calcineurin Signaling. *Front Mol Neurosci*  
 1121 10, 221.  
 1122 Lazarevic, V., Schone, C., Heine, M., Gundelfinger, E.D., and Fejtova, A. (2011). Extensive remodeling of the  
 1123 presynaptic cytomatrix upon homeostatic adaptation to network activity silencing. *J Neurosci* 31, 10189-  
 1124 10200.  
 1125 Leal-Ortiz, S., Waites, C.L., Terry-Lorenzo, R., Zamorano, P., Gundelfinger, E.D., and Garner, C.C. (2008).  
 1126 Piccolo modulation of Synapsin1a dynamics regulates synaptic vesicle exocytosis. *J Cell Biol* 181, 831-846.  
 1127 Liberali, P., Kakkonen, E., Turacchio, G., Valente, C., Spaar, A., Perinetti, G., Bockmann, R.A., Corda, D.,  
 1128 Colanzi, A., Marjomaki, V., and Luini, A. (2008). The closure of Pak1-dependent macropinosomes requires  
 1129 the phosphorylation of CtBP1/BARS. *Embo J* 27, 970-981.  
 1130 Maritzen, T., and Haucke, V. (2018). Coupling of exocytosis and endocytosis at the presynaptic active zone.  
 1131 *Neurosci Res* 127, 45-52.  
 1132 Mastronarde DN (2005) Automated electron microscope tomography using robust prediction of specimen  
 1133 movements. *Journal of structural biology* 152: 36-51  
 1134 Moritz, A., De Graan, P.N., Gispen, W.H., and Wirtz, K.W. (1992). Phosphatidic acid is a specific activator of  
 1135 phosphatidylinositol-4-phosphate kinase. *J Biol Chem* 267, 7207-7210.  
 1136 Pagliuso, A., Valente, C., Giordano, L.L., Filograna, A., Li, G., Circolo, D., Turacchio, G., Marzullo, V.M.,  
 1137 Mandrich, L., Zhukovsky, M.A., *et al.* (2016). Golgi membrane fission requires the CtBP1-S/BARS-induced  
 1138 activation of lysophosphatidic acid acyltransferase delta. *Nature communications* 7, 12148.  
 1139 Park, J., Cho, O.Y., Kim, J.A., and Chang, S. (2016). Endosome-mediated endocytic mechanism replenishes  
 1140 the majority of synaptic vesicles at mature CNS synapses in an activity-dependent manner. *Scientific*  
 1141 *reports* 6, 31807.  
 1142 Puchkov, D., and Haucke, V. (2013). Greasing the synaptic vesicle cycle by membrane lipids. *Trends Cell*  
 1143 *Biol* 23, 493-503.  
 1144 Pyott, S.J., and Rosenmund, C. (2002). The effects of temperature on vesicular supply and release in  
 1145 autaptic cultures of rat and mouse hippocampal neurons. *J Physiol* 539, 523-535.  
 1146 Raben, D.M., and Barber, C.N. (2017). Phosphatidic acid and neurotransmission. *Advances in biological*  
 1147 *regulation* 63, 15-21.  
 1148 Raimondi, A., Ferguson, S.M., Lou, X., Armbruster, M., Paradise, S., Giovedi, S., Messa, M., Kono, N.,  
 1149 Takasaki, J., Cappello, V., *et al.* (2011). Overlapping role of dynamin isoforms in synaptic vesicle  
 1150 endocytosis. *Neuron* 70, 1100-1114.

1151 Ramperez, A., Sanchez-Prieto, J., and Torres, M. (2017). Brefeldin A sensitive mechanisms contribute to  
1152 endocytotic membrane retrieval and vesicle recycling in cerebellar granule cells. *J Neurochem* 141, 662-  
1153 675.

1154 Renard, H.F., Johannes, L., and Morsomme, P. (2018). Increasing Diversity of Biological Membrane Fission  
1155 Mechanisms. *Trends Cell Biol* 28, 274-286.

1156 Revelo, N.H., Kamin, D., Truckenbrodt, S., Wong, A.B., Reuter-Jessen, K., Reisinger, E., Moser, T., and  
1157 Rizzoli, S.O. (2014). A new probe for super-resolution imaging of membranes elucidates trafficking  
1158 pathways. *J Cell Biol* 205, 591-606.

1159 Rose, T., Schoenenberger, P., Jezek, K., and Oertner, T.G. (2013). Developmental refinement of vesicle  
1160 cycling at Schaffer collateral synapses. *Neuron* 77, 1109-1121.

1161 Rosenmund, C., and Stevens, C.F. (1996). Definition of the readily releasable pool of vesicles at  
1162 hippocampal synapses. *Neuron* 16, 1197-1207.

1163 Soykan, T., Kaempf, N., Sakaba, T., Vollweiler, D., Goerdeler, F., Puchkov, D., Kononenko, N.L., and  
1164 Haucke, V. (2017). Synaptic Vesicle Endocytosis Occurs on Multiple Timescales and Is Mediated by Formin-  
1165 Dependent Actin Assembly. *Neuron* 93, 854-866 e854.

1166 Spano, S., Silletta, M.G., Colanzi, A., Alberti, S., Fiucci, G., Valente, C., Fusella, A., Salmona, M., Mironov, A.,  
1167 Luini, A., *et al.* (1999). Molecular cloning and functional characterization of brefeldin A-ADP-ribosylated  
1168 substrate. A novel protein involved in the maintenance of the Golgi structure. *J Biol Chem* 274, 17705-  
1169 17710.

1170 Tagliatti, E., Fadda, M., Falace, A., Benfenati, F., and Fassio, A. (2016). Arf6 regulates the cycling and the  
1171 readily releasable pool of synaptic vesicles at hippocampal synapse. *eLife* 5.

1172 tom Dieck, S., Altroch, W.D., Kessels, M.M., Qualmann, B., Regus, H., Brauner, D., Fejtova, A., Bracko, O.,  
1173 Gundelfinger, E.D., and Brandstatter, J.H. (2005). Molecular dissection of the photoreceptor ribbon  
1174 synapse: physical interaction of Bassoon and RIBEYE is essential for the assembly of the ribbon complex. *J*  
1175 *Cell Biol* 168, 825-836.

1176 Tsuruel, S., Geva, R., Zamorano, P., Dresbach, T., Boeckers, T., Gundelfinger, E.D., Garner, C.C., and Ziv, N.E.  
1177 (2006). Local sharing as a predominant determinant of synaptic matrix molecular dynamics. *PLoS biology*  
1178 4, e271.

1179 Valente, C., Luini, A., and Corda, D. (2013). Components of the CtBP1/BARS-dependent fission machinery.  
1180 *Histochemistry and cell biology* 140, 407-421.

1181 Valente, C., Turacchio, G., Mariggio, S., Pagliuso, A., Gaibisso, R., Di Tullio, G., Santoro, M., Formiggini, F.,  
1182 Spano, S., Piccini, D., *et al.* (2012). A 14-3-3gamma dimer-based scaffold bridges CtBP1-S/BARS to  
1183 PI(4)KIIIbeta to regulate post-Golgi carrier formation. *Nat Cell Biol* 14, 343-354.

1184 Verger, A., Quinlan, K.G., Crofts, L.A., Spano, S., Corda, D., Kable, E.P., Braet, F., and Crossley, M. (2006).  
1185 Mechanisms directing the nuclear localization of the CtBP family proteins. *Mol Cell Biol* 26, 4882-4894.

1186 Wu, X.S., Lee, S.H., Sheng, J., Zhang, Z., Zhao, W.D., Wang, D., Jin, Y., Charnay, P., Ervasti, J.M., and Wu,  
1187 L.G. (2016). Actin Is Crucial for All Kinetically Distinguishable Forms of Endocytosis at Synapses. *Neuron* 92,  
1188 1020-1035.

1189 Wu, Y., O'Toole, E.T., Girard, M., Ritter, B., Messa, M., Liu, X., McPherson, P.S., Ferguson, S.M., and De  
1190 Camilli, P. (2014). A dynamin 1-, dynamin 3- and clathrin-independent pathway of synaptic vesicle  
1191 recycling mediated by bulk endocytosis. *eLife* 3, e01621.

1192 Yang, J.S., Gad, H., Lee, S.Y., Mironov, A., Zhang, L., Bezoussenko, G.V., Valente, C., Turacchio, G., Bonsra,  
1193 A.N., Du, G., *et al.* (2008). A role for phosphatidic acid in COPI vesicle fission yields insights into Golgi  
1194 maintenance. *Nat Cell Biol* 10, 1146-1153.

1195 Zeniou-Meyer, M., Zabari, N., Ashery, U., Chasserot-Golaz, S., Haeberle, A.M., Demais, V., Bailly, Y.,  
1196 Gottfried, I., Nakanishi, H., Neiman, A.M., *et al.* (2007). Phospholipase D1 production of phosphatidic acid  
1197 at the plasma membrane promotes exocytosis of large dense-core granules at a late stage. *J Biol Chem*  
1198 282, 21746-21757.

1199 Zhang, B., Koh, Y.H., Beckstead, R.B., Budnik, V., Ganetzky, B., and Bellen, H.J. (1998). Synaptic vesicle size  
1200 and number are regulated by a clathrin adaptor protein required for endocytosis. *Neuron* 21, 1465-1475.

1201

1202

CtBP1-mediated membrane fission contributes to effective recycling of synaptic vesicles

Daniela Ivanova<sup>1,2,3#</sup>, Cordelia Imig<sup>4\*</sup>, Marcial Camacho<sup>5\*</sup>, Annika Reinhold<sup>5</sup>, Debarpan Guhathakurta<sup>3</sup>, Carolina Montenegro-Venegas<sup>2</sup>, Michael A. Cousin<sup>6</sup>, Eckart D. Gundelfinger<sup>2,7</sup>, Christian Rosenmund<sup>5</sup>, Benjamin Cooper<sup>4</sup>, Anna Fejtova<sup>1,2,3,8</sup>

1 RG Presynaptic Plasticity, Leibniz Institute for Neurobiology, Magdeburg, Germany

2 Department of Neurochemistry and Molecular Biology, Leibniz Institute for Neurobiology, Magdeburg, Germany

3 Molecular Psychiatry, Department of Psychiatry and Psychotherapy, University Hospital Erlangen, Friedrich-Alexander-Universität Erlangen-Nürnberg (FAU), Germany

4 Department of Molecular Neurobiology, Max Planck Institute of Experimental Medicine, 37075 Göttingen, German

5 Institute of Neurophysiology, Charité-Universitätsmedizin Berlin, Berlin, Germany

6 Centre for Discovery Brain Sciences, Hugh Robson Building, George Square, University of Edinburgh, UK, EH9 9XD

7 Center for Behavioral Brain Science and Medical Faculty, Otto von Guericke University Magdeburg, Germany

8 Lead contact

# Present address: Centre for Discovery Brain Sciences, Hugh Robson Building, George Square, University of Edinburgh, UK, EH9 9XD

Corresponding author: Anna.Fejtova@uk-erlangen.de

\*Equally contributing authors

**Summary (150 words)** Compensatory endocytosis of released synaptic vesicles (SVs) relies on coordinated signaling at the lipid-protein interface. Here, we address the synaptic function of C-

terminal binding protein 1 (CtBP1), a ubiquitous regulator of gene expression and membrane trafficking, in cultured hippocampal neurons. In the absence of CtBP1 synapses formed in higher density and showed changes in SV distribution and size. The increased basal neurotransmission and enhanced synaptic depression could be attributed to a higher vesicular release probability and a smaller fraction of release-competent SVs, respectively. Rescue experiments with specifically targeted constructs indicated that while synaptogenesis and release probability were controlled by nuclear CtBP1, the efficient recycling of SVs relied on its synaptic expression. The ability of presynaptic CtBP1 to facilitate compensatory endocytosis depended on its membrane fission activity and the activation of the lipid-metabolizing enzyme PLD1. Thus, CtBP1 regulates SV recycling by promoting a permissive lipid environment for compensatory endocytosis.

**Keywords: (up to 10)**

Compensatory endocytosis, CtBP1, Bassoon, PLD1, synaptic vesicle recycling, membrane fission, short-term plasticity, synaptic vesicle pools, presynapse

**Introduction:**

C-terminal binding protein 1 (CtBP1) is a ubiquitously expressed dual-function protein that acts as a transcriptional corepressor in the cell nucleus and as a regulator of membrane fission in the cytoplasm (Chinnadurai, 2009; Valente et al., 2013). It is expressed in most types of neurons, where it shows a distinct localization to nuclei and presynapses (Hubler et al., 2012; tom Dieck et al., 2005). Presynaptic CtBP1 is localized in the vicinity of the active zone via its direct binding to two large, highly homologous active zone scaffolding proteins: bassoon (Bsn) and piccolo (Pclo) (Ivanova et al., 2015; tom Dieck et al., 2005). A dynamic synapto-nuclear shuttling of CtBP1, induced by changes in its affinity to Bsn and regulated by neuronal activity and cellular NAD/NADH ratio was shown to control the expression of a variety of neuroplasticity-related genes (Ivanova et al., 2016; Ivanova et al., 2015). While the importance of CtBP1-dependent transcriptional regulation of neuroplasticity genes emerged from recent studies (Garriga-Canut et al., 2006; Ivanova et al., 2016; Ivanova et al., 2015), the role of synaptic CtBP1 is still elusive. Here we hypothesize that in addition to being implicated in the remote control of gene expression, synaptic CtBP1 might directly contribute to neurotransmitter release and SV recycling. The involvement of CtBP1 in various membrane fission processes at the Golgi and plasma membrane in non-neuronal cells is in support of this view (Valente et al., 2013). Although the mechanism of CtBP1-mediated fission remains controversial, an increasing body of evidence suggests that it induces formation of vesicular carriers by recruiting and orchestrating numerous enzymes that



promote local lipid reorganization leading to membrane bending (Valente et al., 2013). This is mechanistically distinct from the principle of torsional force utilized in dynamin-mediated fission, most commonly implied in SV recycling (Antonny et al., 2016; Renard et al., 2018). Despite the well-established role of dynamin in SV fission, recent findings suggest that dynamin-independent forms of endocytosis might occur at hippocampal synapses (Gan and Watanabe, 2018; Wu et al., 2014). Moreover, a crosstalk and cooperativity between dynamin-mediated fission, actin cytoskeleton-mediated vesicle reformation and lipid reorganization by lipid-modifying enzymes in the execution of SV recycling were recently suggested (Puchkov and Haucke, 2013; Soykan et al., 2017; Wu et al., 2016).

In this study, we investigate the potential role of synaptic CtBP1 in the regulation of SV fusion and recycling. Using knock down (KD), knock out (KO) and complementation approaches we demonstrate that while loss of nuclear CtBP1 expression increases synaptogenesis and release probability of SVs, the depletion of synaptic CtBP1 leads to defects in SV retrieval, accompanied by an enlargement of the docked synaptic vesicles and pronounced synaptic depression during sustained neurotransmission. Functional experiments and super-resolution imaging indicate that synaptic CtBP1 acts at the same membrane domain as dynamin to promote SV recycling. Our results revealed a crucial requirement for CtBP1-mediated membrane fission and the activity of Phospholipase D1 (PLD1) in this process. Finally, we show that CtBP1 phosphorylation by the signaling kinase p21 (RAC1) activated kinase 1 (Pak1) provides a molecular switch controlling its re-distribution from the active zone protein Bsn to the endocytic effector PLD1, thus fine-tuning its membrane trafficking activity and potentially linking presynaptic exo- and endocytic processes.

## **Results:**

### **CtBP1 contributes to synaptic vesicle retrieval and regulates the size of the total recycling pool**

To assess whether the absence of CtBP1 affects synaptic structure and function we used a previously established RNA-interference approach in cultured hippocampal neurons (Ivanova et al., 2015). Significant downregulation of CtBP1, but no obvious differences in the morphology and the expression of pre- and post-synaptic markers or CtBP2, a close homologue of CtBP1, were observed between controls expressing scrambled shRNA (scr) and CtBP1 knock down (CtBP1KD) neurons expressing target shRNAs: CtBP1KD944 or CtBP1KD467 (Figure 1A,B, Figure S1A-D). Likewise, no regulation of synaptic proteins and CtBP2 were observed in homogenates or P2 fractions obtained from brains of CtBP1 knock out animals (Figure S2A,B).

To assess SV turnover in the absence of CtBP1 we applied a fluorophore-coupled antibody recognizing the luminal domain of the integral SV protein synaptotagmin 1 (Syt1 Ab) to living neurons. Syt1 Ab binds to its epitope which is transiently accessible upon SV fusion with the plasma membrane until its internalization during compensatory endocytosis. The fluorescence intensity of the internalized Syt1 Ab provides an estimate of SV recycling at individual synapses (Kraszewski et al., 1995; Lazarevic et al., 2011). The Syt1 Ab uptake driven by endogenous activity (network activity-driven release) was reduced by about 50% in CtBP1KD neurons as compared to controls (30 min incubation; Figure 1C,D). To address the potential contribution of an increased neuronal network activity to this phenotype and isolate presynaptic effects, we also measured the spontaneous (i.e. action potential-independent) SV recycling within 30 min in the presence of TTX and the pool of all fusion-competent vesicles (total recycling pool, TRP) upon brief depolarization with 50 mM KCl. In both conditions Syt1 Ab uptake was strongly reduced (~50%) in CtBP1KD (Figure 1C), indicating an impairment in both evoked and spontaneous SV recycling at CtBP1-deficient synapses.

To monitor SV recycling by an alternative approach we expressed scr and CtBP1KD944 and CtBP1KD467 from a bicistronic vector together with ratio:sypHy (sypHy) (Figure 1E). SypHy is an indicator composed of the SV protein synaptophysin 1, fused to pH-sensitive GFP in one of the luminal domains and tdimer 2 in the cytoplasmic domain which allows its visualization prior to stimulation (Granseth et al., 2006; Rose et al., 2013). The fluorescence of sypHy increases upon SV exocytosis and decays following SV endocytosis and re-acidification. To determine the sizes of the readily releasable pool (RRP) and the recycling pool (RP) we utilized bafilomycin A1, a blocker of the vesicular proton pump that prevents the re-acidification of endocytosed SVs and thus the decline of sypHy fluorescence (Burrone et al., 2006). Exocytosis of the SVs from RRP and RP was evoked by the sequential delivery of 40 and 200 action potentials (AP) at 20 Hz (Figure 1E-G). In CtBP1KD neurons around 14% of the sypHy positive SVs fused upon stimulation with 40 AP at 20 Hz (i.e. RRP), which was comparable to control neurons. The delivery of additional 200 AP triggered exocytosis of ~50% of all sypHy-labeled SVs in controls, but only ~30% in CtBP1KD neurons, indicating a role of CtBP1 in the control of TRP (comprising RRP and RP). Alkalization with ammonium chloride, which de-quenches all sypHy-positive SVs, revealed no differences in its expression between CtBP1KD and control neurons. (Figure 1E-G) An analogous analysis performed in cultured neurons isolated from constitutive *Ctbp1* KO mice recapitulated the results of the KD approach and confirmed the significant reduction of TRP in CtBP1-deficient synapses (Figure S2C-E).

To assess potential changes in the kinetics of SV exo-endocytosis in the absence of CtBP1, we monitored syHy responses evoked by a train of 200 AP at 5, 20 or 40 Hz in neurons expressing CtBP1KD944, CtBP1KD467 or scrambled shRNA (Figure 1H-K). Several stimulation rates were tested since distinct molecular mechanisms have been proposed to mediate SV retrieval at different stimulation frequencies (Cousin, 2017; Kononenko and Haucke, 2015; Soykan et al., 2017). Whereas the time course of exocytosis was indistinguishable between CtBP1KD and control groups, the syHy fluorescence decay was significantly slower in CtBP1KD neurons at all frequencies tested (Figure 1I-K) suggesting a role of CtBP1 in SV endocytosis. Analogous experiments in cultured neurons from constitutive *Ctbp1* KO mice confirmed this conclusion (Figure S2G). Taken together, these results suggest that CtBP1 contributes to SV retrieval at a broad range of neuronal firing frequencies and is specifically required for maintaining the size of TRP during sustained neuronal activity.

#### **Deletion of CtBP1 induces changes in SV size and distribution**

Next, we performed an ultrastructural analysis of small glutamatergic spine synapses in 4-5 weeks old cultured hippocampal slices obtained from *Ctbp1* KO mice and their wild-type (WT) siblings. A combination of rapid cryo-fixation, automated freeze substitution, and 3D-electron tomographic analysis was designed to accurately reveal vesicular organization at presynaptic active zones (AZ) with nanometer precision, while circumventing the introduction of morphological artefacts associated with conventional electron microscopy preparation methods requiring dehydration of the tissue at room temperature (Korogod et al., 2015; Murk et al., 2003). An analysis of gross synaptic morphology and the number of SVs in individual presynaptic glutamatergic terminals revealed no differences between *Ctbp1* KO and WT synaptic profiles (Figure 2A–G). Electron tomographic analysis, however, revealed changes in the distribution of SVs in KO versus WT synapses (Figure 2H-K). The KO synaptic profiles showed a significant increase in the number of membrane-proximal SVs (within 0-5, 0-40, 50-100 and 0-100 nm of the AZ, Figure 2L, P and Table 1). It is important to note that no statistically significant differences in the number of vesicles within 0-2nm of the AZ were observed (Figure 2M), which is the morphological correlate of RRP. Analyses of individual SVs revealed a small, but significant increase in the diameter of docked SVs (Figure 2O), however no change in SV size was seen when comparing all synaptic vesicles within 0-200 nm (Table1). Altogether, these data suggest that loss of CtBP1 does not affect the overall number of SVs in the presynaptic terminals, but triggers their redistribution from membrane-distal to membrane-proximal areas. They also indicate that CtBP1 regulates the size uniformity of docked SVs.

## Distinct roles of nuclear and synaptic CtBP1 in neurotransmission

Since we observed changes in the diameter of docked SVs and the size of TRP we next determined the effect of CtBP1 depletion on neurotransmission. We first compared the AP-evoked excitatory postsynaptic currents (EPSCs) in cultures of autaptic hippocampal neurons transduced with CtBP1KD944 shRNA or scrambled shRNA as a control. Unexpectedly, CtBP1KD944 neurons exhibited greater amplitudes of EPSC compared to controls (Figure 3A). To examine whether the increase in EPSC amplitude reflected an increase in the amount of glutamate loaded into SVs or changes in postsynaptic receptors we analyzed mEPSCs, which represent single fusion events. Neither the amplitudes nor the charges of mEPSCs were affected by CtBP1-depletion indicating that the observed increase in EPSC amplitude cannot be attributed to any major changes in vesicular neurotransmitter content or postsynaptic properties (Figure 3B,C, Table 2). In support of the latter conclusion, quantitative live immunolabeling of autaptic neurons with an antibody recognizing the extracellular epitope of GluAs did not uncover any significant differences in the surface expression of AMPA receptors between the groups (Figure 3E,F). The mEPSC frequency was not significantly altered in CtBP1KD944 neurons (Figure 3D). However, the number of morphological synapses assessed as a number of co-localizing synapsin-GluA puncta in CtBP1KD944 neurons was slightly higher suggesting increased synaptogenesis in the absence of CtBP1 (Figure 3E,G). The increased synapse number might contribute, at least in part, to the increase of EPSC amplitude observed in these neurons.

Next we measured postsynaptic current evoked by application of hypertonic sucrose, leading to the release of all docked SVs (RRP) (Rosenmund and Stevens, 1996). We detected unchanged sucrose-evoked currents (Figure 3H,I), which is in line with unchanged RRP measured by syHy imaging (Figure 1E-G) and with the unchanged number of morphologically docked SVs (Figure 2M). The unchanged total RRP charge, but significantly higher EPSC charge evoked by an injection of a single AP implies an increased mean vesicular release probability (P<sub>vr</sub>, Figure 3J). Increased P<sub>vr</sub> is predictive of an increased synaptic transmission upon isolated stimuli but leads to an enhanced short-term depression upon repeated stimulation. To explore this possibility, we recorded synaptic responses induced by a 25 ms spaced pair of APs (Figure 3K). In line with the elevated P<sub>vr</sub>, the paired pulse ratio (i.e. the ratio of the peak amplitude of the second to the first evoked EPSC; PPR), was significantly decreased in CtBP1KD944 neurons, confirming a higher degree of synaptic depression. We also analyzed the depression of neurotransmission during sustained neuronal activity by recording the EPSCs evoked by a train of 50 stimuli at 10 Hz (Figure 3L). At this frequency only minor depression of EPSC amplitudes was evident in controls

(scr), while a pronounced rundown of neurotransmission was measured upon depletion of CtBP1 (CtBP1KD944), which is in line with the high initial Pvr and increased PPR measured in CtBP1KD944 neurons. Thus, depletion of CtBP1 promotes synaptogenesis and elevates Pvr resulting in increased evoked neurotransmission and contributing to the strongly enhanced short-term depression.

We have previously shown that nuclear CtBP1 acts as a transcriptional corepressor and regulates the expression of plasticity-related genes which might affect synaptogenesis and neurotransmission (Ivanova et al., 2015). To discriminate between the effects of nuclear and synaptic CtBP1 on synaptic transmission, we expressed CtBP1944KD together with RNAi-resistant variants of CtBP1 that were sorted predominantly to the synapses (EGFP-CtBP1) or only to the nucleus (YFP-CtBP2(NLS)-CtBP1). In EGFP-CtBP1, the N-terminal fusion of EGFP interferes with its nuclear localization, while it leaves the synaptic targeting unaffected (Figure S3A) (Ivanova et al., 2015; Verger et al., 2006). The chimeric protein YFP-CtBP2(NLS)-CtBP1 which bears the NLS signal of CtBP2, the paralogue of CtBP1 in vertebrates, fused to almost full length CtBP1, showed a restricted nuclear localization (Figure S3A) (Verger et al., 2006). While expression of synaptic EGFP-CtBP1 on a KD background led to a further increase of EPSC amplitude, expression of nuclear YFP-CtBP2(NLS)-CtBP1 fully rescued the EPSC amplitude (Figure 3A). These data indicate that the increased size of the evoked response in CtBP1KD944 neurons is a result of the depletion of the nuclear rather than the synaptic pool of CtBP1. Similarly, the increased number of morphological synapses as well as Pvr and PPR were substantially normalized upon expression of nuclear YFP-CtBP2(NLS)-CtBP1, indicating that depletion of nuclear CtBP1 leads to increased synaptogenesis and elevated Pvr (Figure 3G,J,K). Expression of YFP-CtBP2(NLS)-CtBP1 also normalized the altered expression of the immediate early gene *Arc* and neurotrophin *BDNF* in CtBP1KD944 neurons (Figure S3B,C), suggesting a link between CtBP1-controlled gene expression and the regulation of synaptic efficacy. We observed an intermediate increase in Pvr and PPR upon expression of synaptic EGFP-CtBP1 (Figure 3G,J,K), which further supports the notion that nuclear and not synaptic CtBP1 controls synapse formation and/or maintenance and Pvr. The expression of EGFP-CtBP1 also led to an increase in mEPSC frequency, which might be a consequence of the concomitant strong elevation in synapse number and Pvr (Figure 3D,J,K).

To our surprise, the expression of the nuclear construct YFP-CtBP2(NLS)-CtBP1 in CtBP1KD944 neurons that normalized the evoked neurotransmission and significantly decreased Pvr assessed upon single or paired-pulse stimulation (Figure 3A,J,K), did not revert the strikingly elevated

depression during the train of 50 stimuli at 10Hz (Figure 3L). In contrast, expression of synaptic EGFP-CtBP1 in CtBP1KD944, which further enhanced the evoked neurotransmission and left the increased Pvr largely unaffected, increased the steady state response to 10Hz stimulation by about 7% (of initial response) compared to CtBP1KD944 (Figure 3L). This is comparable with data obtained at calyx of held, where complete block of endocytosis decreased steady state response by 10% (Hosoi et al., 2009). Taken together, the complementation experiments revealed that nuclear CtBP1 has an inhibitory effect on basal neurotransmission due to its negative effect on synapse number and SV fusion competency. Interestingly, the nuclear expression of CtBP1 (YFP-CtBP2(NLS)-CtBP1) left the enhanced depression of neurotransmission during repetitive stimulation unaffected, while expression of synaptic EGFP-CtBP1 ameliorated the effect of CtBP1 depletion. Since, the synaptic rundown during repetitive stimulation is determined not only by the Pvr, but also by the size and refill capacity of the total recycling pool of SVs, we next addressed the involvement of synaptic and nuclear CtBP1 in SV retrieval in the following imaging experiments.

#### **Synaptic CtBP1 is required for normal SV recycling and short-term plasticity of release.**

To directly determine the contribution of synaptic and nuclear CtBP1 to the defect in the retrieval of the fused SVs observed in CtBP1KD neurons we performed imaging experiments in neurons, where CtBP1 KD was complemented by expression of synaptic or nuclear rescue constructs. Synaptically-localized EGFP-CtBP1 expressed on CtBP1KD944 background led to ~80% restoration of Syt1 Ab uptake driven by network activity. In contrast, the expression of nuclear YFP-CtBP12(NLS)-CtBP1 failed to rescue Syt1 Ab uptake in CtBP1KD944 neurons (Figure 4A, B). In addition, the expression of EGFP-CtBP1 with aspartate 355-to-alanine mutation (D355A), which impairs the fission activities of CtBP1 (Bonazzi et al., 2005), also failed to restore the Syt1 Ab uptake in CtBP1KD neurons (Figure 4A,B), suggesting that the function of CtBP1 in fission is required for normal SV recycling. Next, we tested the ability of synaptic vs. nuclear CtBP1 expression to rescue the aberrant exo-endocytosis observed upon depletion of endogenous CtBP1 (Figure 1H-K) To this end we used a sensor composed of synaptophysin fused to the monomeric, orange pH-sensitive mOrange2 (sympOr2), which we co-expressed with the EGFP and YFP-labeled rescue constructs (Figure 4C,D). The fluorescence recovery after stimulation with 200 APs at 20 Hz was significantly retarded in CtBP1KD944: it did not reach full recovery during the time of imaging and had a greater recovery halftime compared to the controls (Figure 4C,D). The expression of synaptic EGFP-CtBP1 on CtBP1KD944 background fully rescued the normal SV retrieval, while nuclear YFP-CtBP2(NLS)-CtBP1 or the fission mutant EGFP-



CtBP1D355A failed to do so (Figure 4C,D). Altogether, these data indicate that synaptic localization and intact fission activities of CtBP1 are crucial for its role in SV retrieval.

To re-evaluate the altered short-term plasticity measured by the electrophysiological recordings of CtBP1-depleted autaptic neurons (Figure 3L), we monitored the exocytosis of endogenous syt1 during a train of 200 AP at 10 Hz using an antibody against its luminal domain coupled to CypHer5E (Syt1 Ab-CypHer). CypHer5E is a pH sensitive dye with maximal fluorescence at acidic pH in the vesicle lumen and fluorescence decline upon SV exocytosis (Hua et al., 2011). Experiments were performed in the presence of bafilomycin A1 (Figure 4E) or folimycin (Figure S4) to block SV reacidification and thus visualize net SV fusion. To normalize for potential differences in the initial release probability and thus uncover the contribution of SV retrieval, the response amplitudes after a reference train of 40 APs at 20 Hz, which leads to the release of RRP (unchanged between control and CtBP1KD, Figures 1G, 2I,M 3H,I), were used for normalization as described previously (Hua et al., 2013). This reference pulse was followed by a brief recovery period and a test stimulus of 200 AP at 10 Hz. The amplitudes of the fluorescence responses to 200 AP were strongly reduced in CtBP1KD944 compared to the control for stimuli delivered at 5, 10 or 40Hz (Figure 4E,F and S4A,B). The expression of YFP-CtBP2(NLS)-CtBP1 on CtBP1KD944 background did not improve this decrease, while the responses in KD neurons expressing EGFP-CtBP1 construct were not significantly different from control (Figure 4E,F). These experiments further supported the view that synaptic CtBP1 is required for efficient SV recycling during sustained neuronal activity.

#### **Dynamin-dependent SV recycling is unaffected in CtBP1-deficient neurons.**

The GTPase dynamin plays a key role in the reformation of SVs by catalyzing the fission of SV membranes from the plasma membrane and endosomal structures (Gan and Watanabe, 2018; Kononenko and Haucke, 2015). In non-neuronal cells, CtBP1 was described as an accessory protein in the assembly of dynamin-independent fission machinery, which includes molecules like ADP ribosylation factor (Arf), phospholipase D (PLD) and lysophosphatidic acid acyltransferase (LPAAT) (Haga et al., 2009; Pagliuso et al., 2016; Valente et al., 2012). To investigate a possible link of CtBP1 to the established presynaptic endocytic machinery, we assessed the nanoscale localization of CtBP1 in respect to other membranous structures implicated in SV recycling. To this end, we performed super-resolution dual-color STED microscopy of neurons labeled with antibodies against CtBP1, the SV protein Syt1 and several endocytic markers followed by co-localization modeling. Dynamin1 labeling was used to visualize the classic endocytic machinery

(Figure 5A). Since many of the components of the CtBP1-associated fission machinery were shown to coordinate the endosomal trafficking of membrane proteins, we also labeled the neurons with markers for early (rab5), late (rab7) and recycling (rab22) endosomes (Figure 5A). Prior to staining, neuronal cultures were first silenced with APV ((2*R*)-amino-5-phosphonovaleric acid; (2*R*)-amino-5-phosphonopentanoate) and CNQX (6-cyano-7-nitroquinoxaline-2,3-dione) for 10 minutes, in order to reduce the intersynaptic variability induced by the endogenous network activity. We analyzed the distance of CtBP1 to other markers at rest and also monitored the co-localization in cells fixed 30 seconds after stimulation with 200 AP at 40 Hz (Figure S5). Overall, CtBP1 localized in the proximity (0-200 nm) of dynamin1 and Syt1, while all endosome markers we probed for were much more distant (100-500 nm) (Figure 5A,B and S5A-E). Synaptic stimulation did not affect the co-localization of CtBP1 with dynamin1 and Syt1 but led to a significant increase in the distance between CtBP1 and endosome markers rab5 and rab7, but not rab22 (Figure S5A-E). Thus, CtBP1 likely acts at the membrane domain marked by Syt1 and dynamin1 indicating its potential role in the retrieval of exocytosed SVs. The poor baseline co-localization of CtBP1 with the endosomal markers rab5, rab7 and rab22, and subsequent increase of distance upon neuronal stimulation, suggests a role of CtBP1 in the formation of vesicular carriers rather than its constitutive association with intracellular membranous structures.

Given the fact that CtBP1 was reported to regulate membrane trafficking in dynamin-independent exocytic and endocytic pathways (Bonazzi et al., 2005), the high synaptic co-localization with dynamin1 was unexpected. Therefore, in order to test whether CtBP1 contributes to the presynaptic dynamin-dependent endocytosis, we quantified the Syt1 Ab-CypHer uptake in control and CtBP1KD944 neurons treated with the potent dynamin inhibitors dynole 34-2 (Figure 5C,D). As inhibition of dynamin increases the membrane stranding of SV proteins due to an impaired retrieval (Raimondi et al., 2011) we used Syt1 Ab-CypHer uptake to determine specifically the fraction of Syt1 retrieved through dynamin-independent endocytosis. Dynole 34-2 had a comparable effect in control and in CtBP1KD944 neurons, and reduced the Syt1 Ab-CypHer Ab uptake by more than 80% (Figure 5D). The large effect of dynamin inhibition in both conditions confirms the principal requirement of dynamin for efficient SV retrieval at the presynapse. However, as the effects of CtBP1KD and dynole 34-2 were not completely additive but rather cooperative and considering the high degree of co-localization observed for CtBP1 and dynamin, we propose that despite their involvement in independent machineries they might act in concert at the same membrane domain to mediate effective SV retrieval.

#### **CtBP1 promotes retrieval of SVs by activation of presynaptic PLD1**



Given the established role of CtBP1 in membrane trafficking in non-neuronal cells, we hypothesized a role of CtBP1-based fission machinery in SV recycling. To test this hypothesis, we first treated control and CtBP1-depleted neurons with brefeldin A (BFA), a fungal antibiotic interfering with the intracellular membrane trafficking. BFA targets several proteins involved in membrane trafficking, including CtBP1. It induces ADP-ribosylation of CtBP1 (also known as BFA-ADP-ribosylation substrate, shortly BARS), which interferes with the assembly of CtBP1-based fission complex and results in inhibition of endocytic vesicle formation (Colanzi et al., 2013; Spano et al., 1999). We applied BFA (2.5 $\mu$ M) only five minutes prior to and during the image acquisition, which we reasoned is a too short time period to influence synaptic function by changes in gene expression or soma-to-synapse trafficking. Thus, the effect of BFA treatment more likely reflected an acute inhibition of CtBP1 and the associated fission machinery at the presynapse. In agreement with previous reports (Kononenko et al., 2013; Park et al., 2016) (but see (Kim and Ryan, 2009) for lack of effect of BFA on vGLUT-pHluorin), BFA treatment affected significantly the post-stimulus fluorescence decay of sypHy in control neurons (Figure 6A) indicating that BFA slows down the retrieval of exocytosed SVs. In contrast, the sypHy fluorescence decay was not further affected by BFA in CtBP1KD neurons (Figure 6B), suggesting that CtBP1-based fission machinery mediates to a great extent the effect of BFA.

The precise molecular mechanism of CtBP1-mediated membrane trafficking is still not fully understood. It was suggested that CtBP1-based fission complex drives membrane budding and fission by catalyzing the remodeling of membrane lipids, which leads to formation of fission-prone membrane domains. In non-neuronal cells, CtBP1 was shown to interact and activate the phosphodiesterase activity of phospholipase D1 (PLD1), an enzyme catalyzing the conversion of phosphatidylcholine (PC) into the fusogenic phosphatidic acid (PA) (Donaldson, 2009; Haga et al., 2009; Raben and Barber, 2017). Although PLD1 was shown to play a role in the control of neurotransmitter release in Aplysia (Humeau et al., 2001) and in the secretion of neuropeptides in chromaffin cells (Zeniou-Meyer et al., 2007), its function in the regulation of SV recycling in mammalian synapses has not been investigated yet. Therefore, next we tested the involvement of PLD1 in SV recycling and its link to CtBP1-dependent SV retrieval. Acute application of VU 0155069 (1 $\mu$ M for 5 min), a specific inhibitor of PLD1, led to a two-fold decrease in the rate of sypHy retrieval in control neurons, while it had no effect on the endocytosis rate in CtBP1KD neurons (Figure 6C,D).

Considering the activity-induced recruitment of CtBP1 to nanodomains co-labeled with dynamin1 and Syt1 and its dissociation from the endosome markers rab5 and rab7 we hypothesized that

CtBP1 localizes to the membrane proximal regions, where endocytosis of newly released SV proteins takes place. To address this by independent means we performed imaging with fluorescently labeled mCLING: a lipophilic **reacidification-independent** probe suitable for STED nanoscopy of endocytic organelles (Revelo et al., 2014). We loaded mCLING into the synapses of APV and CNQX silenced (for 10min) control and CtBP1KD944 neurons by stimulation with 200 AP at 40 Hz and fixed them 30 seconds later. The mCLING labeling was notably reduced in the synapses in CtBP1KD944 neurons in comparison to the control (Figure 6E,F), but was again evident upon the expression of shRNA resistant EGFP-CtBP1 construct on CtBP1KD944 background (Figure 6G). We next performed dual-color STED nanoscopy followed by co-localization modelling to assess the co-distribution of mCLING and EGFP-CtBP1 (Figure 6G). This analysis revealed a significant negative correlation between the intensity of mCLING and the distance to individual EGFP-CtBP1 puncta, which supports a role of CtBP1 in SV endocytosis (Figure 6I).

Phosphorylation of CtBP1 at serine 147 (S147), mediated by the kinase Pak1, was found to strongly increase the capacity of CtBP1 to stimulate membrane fission by increasing its ability to activate PLD1 (Haga et al., 2009; Liberali et al., 2008). To test the importance of this regulation at the presynapse we compared the mCLING labeling in neurons expressing the RNAi resistant EGFP-CtBP1 or EGFP-CtBP1S147A construct on CtBP1KD944 background. The mCLING labeling was reduced by 80% in cells expressing EGFP-CtBP1S147A as compared to cells expressing EGFP-CtBP1 (Figure 6G,H) indicating lower ability of this mutant to rescue stimulus-induced membrane retrieval upon CtBP1KD. Moreover, the co-distribution between mCLING and S147A mutant was shifted towards higher distances compared to EGFP-CtBP1 (Figure 6J), which likely reflects impaired recruitment to the sites of endocytosis. Taken together these data indicate that the presence of CtBP1 at the endocytic sites and its phosphorylation at S147 are key factors determining the efficacy of SV retrieval.

### **Phosphorylation of CtBP1 regulates its distribution between the CAZ and the presynaptic endocytic sites.**

Previous studies showed that the presynaptic scaffolding proteins Bsn and Pclo recruit CtBP1 to synapses via a direct interaction (Ivanova et al., 2015; tom Dieck et al., 2005). Despite the tight functional coupling between SV fusion and endocytosis, it is well established that the two processes take place at distinct membrane domains within the presynapse (Haucke et al., 2011; Maritzen and Haucke, 2018). Thus, the association of CtBP1 with Bsn and Pclo, which are

established components of the SV release sites, is seemingly in disagreement with the proposed function of CtBP1 in SV endocytosis. To address this apparent ambiguity, we performed the following series of experiments. First, we performed co-immunoprecipitation (CoIP) of Bsn with EGFP-CtBP1, overexpressed in primary cortical cultures in basal state or upon a treatment with the Pak1 inhibitor IPA3 for 1 h (Figure 7A). At basal state a considerable CoIP of CtBP1 with PLD1 but only a low binding to Bsn were detected. The IPA3 treatment visibly reduced the overall serine/threonine phosphorylation of CtBP1 (Figure 7C,D). Consistent with the requirement for Pak1-dependent phosphorylation of CtBP1 for its association with PLD1, IPA3 reduced the CoIP of PLD1 with CtBP1 to an undetectable minimum but increased the association of CtBP1 with Bsn (Figure 7A and B). This indicates that the phosphorylation of CtBP1 by Pak1 acts as a molecular switch which triggers its dissociation from Bsn and binding to PLD1. To further test this hypothesis, we compared the nanoscale co-localization of EGFP-CtBP1 or S147A mutant with endogenous Bsn at synapses of acutely silenced neurons before and upon stimulation with 200 AP at 40 Hz. Consistent with our previously published observations, stimulation led to a tighter co-localization of EGFP-CtBP1 and Bsn (Figure 7E,F) (Ivanova et al., 2015). EGFP-CtBP1S147A showed a greater co-localization with Bsn than EGFP-CtBP1 in silenced cells and no effect on its co-distribution with Bsn was observed upon stimulation (Figure 7E,F). This supports our view that Pak1-mediated phosphorylation of S147 favors a redistribution of CtBP1 from Bsn towards PLD1, thus, promoting SV retrieval through activation of PLD1.

## Discussion:

### Nuclear CtBP1 restricts synaptogenesis, while synaptic CtBP1 promotes SV retrieval

In this study we investigated the effect of CtBP1 depletion on synaptic function using knock down and knock out approaches. Neurons lacking CtBP1 had normal overall morphology but showed a significant shift in the distribution of SVs towards the AZ and an enlargement of the docked SVs at rest. Interestingly, a similar change in the distribution of SVs was also observed after treatment with BFA (Ramperez et al., 2017), which as shown here inhibits SV recycling via CtBP1, and upon depletion of Arf6, a component of the CtBP1-dependent fission machinery and an alternative activator of PLD1 (Haga et al., 2009; Tagliatti et al., 2016; Valente et al., 2012). Thus, it is tempting to speculate that insufficient PLD1 activity in the absence of CtBP1 might cause this phenotype. The efficiency of fission during vesicle budding crucially affects the size of the resulting vesicular structures. In line with that, enlarged SVs were observed in mutants of dynamin, AP180 and syndapin, which have been implicated in different steps of SV reformation,

like fission, recruitment of the clathrin-coat or induction/sensing of membrane curvature (Ferguson et al., 2007; Koch et al., 2011; Zhang et al., 1998). Thus, an involvement of CtBP1 in the fission of the SV membranes, might explain the changes in SV size observed in *Ctbp1* KO synapses.

Interference of CtBP1 expression in cultured neurons revealed its multifaceted role in the regulation of synaptogenesis and neurotransmission. A rescue strategy with CtBP1 fusion proteins selectively sorted to nucleus or synapses revealed distinct roles for CtBP1 in these spatially separated neuronal compartments. **Nuclear CtBP1 restricted synaptogenesis and presynaptic vesicular release probability possibly by repressing the expression of plasticity-related genes, such as neurotrophins or neurotransmitter receptors (Ivanova et al., 2015).** In line with that, the expression of the nuclear rescue construct YFP-CtBP2(NLS)-CtBP1 could normalize the higher number of morphologically identified excitatory synapses, the enlarged amplitudes of the evoked EPSC and the higher Pvr and PPR that were observed in CtBP1KD944 neurons. Notably, the expression of the synaptic rescue (EGFP-CtBP1) on CtBP1KD944 background tended to enhance the effect of CtBP1 depletion on synapse density and EPSC amplitude, suggesting a dominant-negative effect of this construct on the nuclear functions of CtBP1. One possible explanation of this effect is that the EGFP-CtBP1 binds to the nuclear CtBP1-interacting partners and promotes their cytoplasmic retention. However, expression of this construct on CtBP1KD944 background compensated the defects in SV retrieval and ameliorated the enhanced short-term depression of neurotransmission upon repetitive stimulations. This indicates a positive effect of synaptic CtBP1 on neurotransmission. Based on this, we can speculate that the recently reported activity-induced redistribution of CtBP1 from nucleus to presynapses exerts a dual-positive effect on neurotransmission (Ivanova et al., 2015). Thus, during bursts of intense neuronal activity the reduced nuclear abundance of CtBP1 will lead to a release of the transcriptional block of neuroplasticity-related genes, while the enhanced synaptic targeting will facilitate SV recycling.

#### **CtBP1-mediated membrane fission and PLD1 activation are required for SV retrieval**

Our data indicate that CtBP1-mediated membrane fission and activation of PLD1 has an important contribution to the effective SV retrieval at the presynapse. We provide multiple evidences supporting this view: 1) CtBP1D355A fission-deficient mutant failed to rescue SV retrieval in CtBP1KD944, 2) CtBP1S147A mutant that cannot recruit PI4KIII $\beta$ /ARF6 and activate PLD1 failed to rescue endocytosis visualized with mCLING and 3) the pharmacological inhibition

of CtBP1-based fission complex using BFA or inhibition of PLD1 activity phenocopied the aberrant SV retrieval observed in CtBP1KD. Our data also indicate a role of PLD1 in SV recycling at hippocampal synapses. PLD1 was detected in synaptic plasma membranes isolated from rat synaptosomes and interference with PLD1 was shown to affect acetylcholine release from nerve ganglia in *Aplysia* (Humeau et al., 2001). However, PLD1 was mainly discussed in the context of exocytosis in neurons and chromaffin cells (Zenou-Meyer et al., 2007). Our data indicate a role of PLD1 in SV retrieval in hippocampal synapses and reveal a requirement for CtBP1-mediated activation of PLD1 in this process. The activation of PLD1 depends on Pak1-mediated phosphorylation of CtBP1. It is unclear whether and how Pak1 activity is regulated at the presynapse but based on our findings we can speculate that the level of presynaptic Pak1 activity could regulate the SV retrieval and thereby modulate short-term plasticity of neurotransmission. Interestingly, the phosphorylation of S147 of CtBP1 by Pak1, which is necessary for PLD1 activation, also induces dissociation of CtBP1 from Bsn, which anchors it to the active zones. This suggests that Pak1 activity might induce a rapid activation of PLD1 in the vicinity of presynaptic release sites and thereby link SV fusion and retrieval in time, space and extent.

#### **CtBP1-mediated lipid reorganization in SV retrieval**

CtBP1-based fission machinery was proposed to act in a dynamin-independent manner at the Golgi and plasma membrane in non-neuronal cells (Bonazzi et al., 2005; Haga et al., 2009; Yang et al., 2008). However, the fluid phase endocytosis switched from a CtBP1-dependent to a dynamin-dependent mechanism in fibroblasts in which CtBP1 was knocked out (Bonazzi et al., 2005), suggesting a tight interaction between these pathways. Thus, it is possible that CtBP1- and dynamin-based fission machineries converge in their action at the presynapse, where particularly potent endocytosis is required for sustained SV replenishment. CtBP1 was suggested to mediate fission of target membranes by activation of lipid enzymes such as PLD1 and LPAAT, that generate curvature-inducing lipid modifications (Haga et al., 2009; Liberali et al., 2008; Pagliuso et al., 2016), and by their recruitment to the machinery, that initiates vesicular budding and tubulation (Valente et al., 2012). PLD1 and LPAAT catalyze production of the fusogenic PA, which, due to its conical shape, promotes negative membrane curvature necessary for vesicle fusion and fission (Kooijman et al., 2003). Besides its structural role, PA was also linked to the generation of PI(4,5)P<sub>2</sub>, the phospholipid involved in the recruitment of numerous proteins involved in endocytosis, including dynamin (Puchkov and Haucke, 2013). Specifically, PA activates PI kinases necessary for PI(4,5)P<sub>2</sub> production (Jenkins et al., 1994; Moritz et al., 1992) and intriguingly, one of them, PI4KIIIβ, is a component of the CtBP1-based fission complex in

non-neuronal cells (Valente et al., 2012). Thus, it is likely that CtBP1 promotes SV retrieval by recruitment and activation of multiple lipid-modifying enzymes, which drive the formation of a lipid environment permissive for compensatory endocytosis. The tight co-localization of CtBP1 and dynamin as well as the cooperative effect of the interference with their functions on SV recycling support this view. However, future studies will be needed to gain more insight into the mechanisms linking and regulating the different fission machineries involved in SV recycling.

## LEAD CONTACT AND MATERIALS AVAILABILITY

Further information and requests for resources and reagents can be directed to and will be fulfilled by the Lead Contact, Anna Fejtova ([Anna.Fejtova@uk-erlangen.de](mailto:Anna.Fejtova@uk-erlangen.de)).

## EXPERIMENTAL MODEL AND SUBJECT DETAILS

### ***Animals***

Cells and tissues used in this study were obtained from Wistar rats, Sprague-Dawley rats, C57BL/6N mice and *Ctbp1*<sup>tm1Sor</sup> (*Ctbp1* KO) mouse strain (Hildebrand and Soriano, 2002) backcrossed to C57BL/6N. Animals of both sex were used. Animal handling was performed according to the regulations of the European Committees Council Directive 86/609/EEC, Landesverwaltungsamt Sachsen-Anhalt, (AZ: T LIN-AF/2009), Berlin state government agency for Health and Social Services and the animal welfare committee of Charité Medical University Berlin, Germany (license no. T 0220/09).

### ***Lentiviral particle production***

Lentiviral particles were produced as described previously with slight modifications (Ivanova et al., 2015). HEK293T cells (ATCC CRL-3216) were grown in media containing 10% fetal bovine serum (FBS) to 80% confluence and transfected using the calcium phosphate method (Fejtova et al., 2009) with three vectors: FUGW-based transfer, psPAX2 packaging, and p-CMV-VSV-G pseudotyping vectors (ratio 2:1:1). Cells were incubated for 8 h at 37°C in 5% CO<sub>2</sub> atmosphere, before the FBS medium was replaced by Neurobasal (NB) medium, containing B27, antibiotics, and 0.8 mM glutamine. Virus-containing media was collected at day 3 and 4, passed through 0.45 µm filter and used either directly for transducing primary neurons or stored at -80°C.

### ***Primary cultures and treatments***

Primary dissociated hippocampal and cortical cultures from rat embryos and C57BL/6N and *CtBP1* KO neonatal mice of were prepared as described in (Ivanova et al., 2015; Lazarevic et al., 2011).

Autaptic cultures from P0-P2 C57BL/6N mice were grown on coverslips with a dotted pattern of astrocytic microislands (Bekkers and Stevens, 1991). To grow neurons individually, 0.15% agarose solution was spread on 30 mm coverslips. Coating solution containing collagen and poly-D-lysine in acetic acid was stamped onto the agarose, thus creating small islands of substrate with a diameter of about 100  $\mu$ m. Hippocampi were dissected out and digested with 25 U/ml of papain for 60 min at 37°C. After papain inactivation, hippocampi were mechanically dissociated in Neurobasal-A medium containing B-27, Glutamax and penicillin/streptomycin. To obtain a desirable distribution of neurons, astrocytes and neurons were plated onto the coverslips with a density of 50000 and 3000 cells/coverslip, respectively. To knock down *CtBP1*, neurons were infected 24 hours later with lentiviruses expressing scrambled, shRNA against *CtBP1* or the rescue constructs EGFP-*CtBP1* and YFP-*CtBP2*(NLS)-*CtBP1*. Experiments were performed on DIV14 (electrophysiological recordings) or DIV16-21 (fixed and live-cell imaging).

Hippocampal neurons were co-transfected with syp mOrange2 and a plasmid expressing *CtBP1* scr, *CtBP1*KD944 or *CtBP1*KD944 along with shRNA-resistant EGFP-*CtBP1*, EGFP-*CtBP1*D355A or YFP-*CtBP2*(NLS)-*CtBP1* at DIV6 using Lipofectamine 2000 (Thermo Fisher Scientific) as recommended by the manufacturer. The neurons were used for live imaging 8 to 10 days after the transfection.

For the treatments, the following drugs were used: d-(-)-2-amino-5-phosphonopentanoic acid (APV, 50  $\mu$ M; Tocris), 6-cyano-7-nitroquinoxaline-2,3-dione disodium (CNQX, 10 $\mu$ M; Tocris), bafilomycin A1 (1 $\mu$ M, Merck/Millipore), folimycin/concanamycin A (80nM, Tocris), brefeldin A (2.5  $\mu$ M, Tocris), VU 0155069 (PLD1 inhibitor, 1 $\mu$ M, Tocris). Neurons were pre-treated with these inhibitors for 5 minutes before imaging and the inhibitors were kept in the imaging buffer during the whole imaging assay. IPA 3 (50  $\mu$ M, Tocris) was applied for 1h before the cells were collected or lysed for western blotting. The inhibitors of dynamin, Dynole 34-2 (30  $\mu$ M, Abcam) was applied for 1h during Syt1 Ab-CypHer uptake. The fixable endocytosis marker mCLING (ATTO647N-labelled in Figure 6G and H and DY654-labelled in Figure 6E and F, 1:100, Synaptic Systems) was applied to neurons in extracellular solution containing 50  $\mu$ M APV and 10  $\mu$ M CNQX, for 2 min before cells were stimulated with 200 AP at 40 Hz. To eliminate unspecific labeling neurons were washed three times with extracellular solution and fixed within 30 seconds after stimulation with a mixture of 4% paraformaldehyde (PFA) and 0.2% glutaraldehyde, as recommended by the manufacturer.

## METHOD DETAILS

### ***Antibodies***

The following primary antibodies were used in this study: **Mouse antibodies against:** CtBP1 (immunocytochemistry (ICC) 1:1,000, Western blotting (WB) 1:5,000, BD Biosciences, 612042), CtBP2 (WB 1:2000 BD Biosciences, 612044) synaptotagmin1 luminal domain Oyster 550 or CypHer5E-labeled (ICC 1:200, Synaptic Systems, 105311 and 105311CpH), rab5 (ICC 1:500, Synaptic Systems, cells stained with this antibody were fixed with ice-cold methanol for 10 min, followed by rehydration in PBS for 20 min, 108011), rab7 (ICC 1:1,000, Abcam, ab50533), phosphoserine/threonine (WB 1:1000, BD Biosciences, 612548), GluA Oyster 550-labeled (ICC 1:200, Synaptic Systems, 182411 C3),  $\alpha$ -tubulin (WB 1:1000, Sigma Aldrich); **Rabbit antibodies against:** CtBP1 (ICC 1:1,000, WB 1:1,000, Synaptic Systems, 222002), GFP (ICC 1:1,000, WB 1:5,000, Abcam, ab 6556), SV2B (ICC 1:200, Synaptic Systems, 119103), GAPDH (WB 1:3000, Abcam, ab37168), synaptotagmin1 luminal domain Oyster 550-labeled (ICC 1:200, Synaptic Systems, 105103C3), synaptotagmin 1 luminal domain (WB 1:1000, Synaptic Systems, 105102), dynamin1 (ICC 1:1000, Abcam, ab3456), rab22a (ICC 1:1000, Abcam, ab137093), Phospholipase D (WB 1:1000, Cell Signaling technologies, 3832S), , Homer1 (ICC 1:500, Synaptic Systems, 160003); **Guinea pig antibodies against:** synapsin 1, 2 (ICC 1:1,000, Synaptic Systems, 106004), synaptophysin 1 (ICC 1:1,000, Synaptic Systems, 101004), Piccolo (WB 1:2000, Dick et al, 2001).

The following secondary cross-adsorbed antibodies were used in this study: Alexa 488- (ICC: 1:1,000), Cy3-(ICC: 1:1,000), Cy5-(ICC: 1:2,000), Alexa 680- (WB 1:20,000) conjugated whole IgGs against mouse, rabbit and guinea pig were obtained from Invitrogen/Mol. Probes, IRDye™ 800CW (WB 1:20,000) and Atto 647N (1:500, 610-156-121 and 611-156-122) from Rockland and Abberior STAR 580 (1:100, 2-0002-005-1 and 2-0012-005-8) from Abberior GmbH.

### ***DNA constructs***

EGFP-tagged CtBP1 was generated by cloning the sequence for CtBP1-S into pEGFPC vector. Subsequently, the DNA cassette containing EGFP-CtBP1 was shuttled into FUGW H1 lentiviral vector (Leal-Ortiz et al., 2008), replacing EGFP coding sequence. The shRNAs against CtBP1 and YFP-CtBP2(NLS)-CtBP1 constructs were reported previously (Ivanova et al., 2015; Verger et al., 2006). All point mutations, including the silent point mutations for the rescue experiments,



were introduced by inverse PCR using primers containing the mutations and CtBP1-S coding sequence cloned in pBluescriptII SK-(AgilentTechnologies). The ratio:syHy construct and syp mOrange2 used in this study were reported in (Lazarevic et al., 2017; Rose et al., 2013) and (Egashira et al., 2015), respectively. All constructs were verified by sequencing.

### **Ultrastructural analysis**

Organotypic hippocampal slice cultures from *Ctbp1* KO and WT littermates were prepared at postnatal day 0 and were cryo-fixed after 4-5 weeks in vitro under cryo-protectant conditions (20% bovine serum albumin in culture medium) using the High Pressure Freezing device HPM100 (Leica), and cryo-substituted in Freeze Substitution Processor EM AFS2 (Leica) according to previously published protocols (Imig and Cooper, 2017; Imig et al., 2014). For 2D analyses of synaptic morphology, electron micrographs were acquired from 60 nm-thick plastic sections with a transmission electron microscope (Zeiss LEO 912-Omega) operating at 80 kV. For 3D electron tomographic analysis of docked SV, 200 nm-thick plastic sections were imaged in a JEM-2100 transmission electron microscope (JEOL) operating at 200 kV. SerialEM (Mastronarde, 2005) was used to acquire single-axis tilt series ( $-60^{\circ}/-55^{\circ}$  to  $\pm 55^{\circ}/\pm 60^{\circ}$ ;  $1^{\circ}$  increments) at 25,000 fold magnification with an Orius SC1000 camera (Gatan, Inc.). Tomograms reconstructed from tilt series using the IMOD package (Kremer et al., 1996) had a voxel size of  $x,y,z = 1.82$  nm. Tomogram acquisition and analyses were performed blindly. Quantifications were done manually using ImageJ (National Institutes of Health). The smallest SV distances from the outer leaflet of the SV membrane to the inner leaflet of the AZ plasma membrane were measured using the straight line tool of the ImageJ software. Only SVs observed to be in physical contact at their midline with the presynaptic membrane were considered docked (0-2 nm distance). The mean SV diameter was calculated from the area of the SV measured at its midline to the outer leaflet of the SV membrane using the elliptical selection tool of ImageJ.

For illustrative purposes, images depicting tomographic sub-volumes represent an overlay of seven consecutive tomographic slices produced using the slicer tool of the 3dmod software of the IMOD software package to generate an approximately 13 nm thick sub-volume.

### **Quantitative real-time PCR**

Quantitative real-time PCR was performed as described in (Ivanova et al., 2015). Total RNA was extracted from primary cortical cultures (DIV16) superinfected on the day of plating with lentiviral particles driving the expression of scrambled, shRNA944 and YFP-CtBP2(NLS)-CtBP1, using RNeasy Plus Mini Kit (Qiagen) and following the instructions of the manufacturer. The transcript

levels of BDNF and Arc were analyzed by a customized version of Rat Synaptic Plasticity RT<sup>2</sup> Profiler PCR Array (Qiagen). To calculate the expression of BDNF and Arc in relation to a reference gene we used  $\Delta\Delta$ CP method. We used the 'second derivative maximum analysis' method, available in the software of Roche LightCycler480, to determine the crossing point (CP) of the PCR. The expression of lactate dehydrogenase A was used as a reference to calculate the relative mRNA levels of BDNF and Arc.

### **Biochemical experimental work**

Cortical neurons with cell density 10 million per 75-cm<sup>2</sup> flask were superinfected with lentiviral particles, driving the expression of EGFP-CtBP1. Cells (DIV16) were lysed in 10mM Tris-HCl, 150mM NaCl, 2% SDS, 1% deoxycholate and 1% Triton X-100 containing complete protease inhibitors (Roche), and PhosStop (Roche) and co-immunoprecipitations were performed using MicroMACS anti-GFP MicroBeads and MicroColumns (Miltenyi Biotec) according to the instructions from the manufacturer.

Crude synaptosomal fraction (P2) was prepared as follows: First, cell or mouse brain homogenates were prepared in HEPES-buffered sucrose (4 mM HEPES pH 7.4, 0.32 M sucrose) and centrifuged at 1000 x g for 10 min to pellet the nuclear fraction (P1). The supernatant was then centrifuged at 12000 g for 20 min to give the crude synaptosomal pellet (P2). The crude synaptosomal fraction (P2) was lysed in 10 mM Tris-HCl, 150mM NaCl, 2% SDS, 1% deoxycholate and 1% Triton X-100 containing complete protease inhibitors (Roche), and PhosStop (Roche) and further subjected to IP or western blotting.

Protein samples were separated on 5–20% Tris-glycine gels, or 3.5–8% Tris-acetate gels as described previously (Ivanova et al., 2015) or on 10% (Bio-Rad TGX-Stain free gels) and blotted onto Millipore Immobilon FL PVDF membranes by tank or semidry blotting. Immunodetection was performed on Odyssey Infrared Scanner (LI-COR). For the quantification of the immunoblots the integrated density (ID) of signals was measured using ImageJ by setting rectangular ROIs with identical size around or using Image Studio Software (LI-COR). Samples of each experimental group were always loaded and quantified on the same membrane. TCE total protein stain used for normalization in Figure 1B. In Figure S2A GAPDH or  $\alpha$ -tubulin were used for normalization in homogenates and P2 fraction, respectively. The values for ID of CtBP1 or Pak1 (Figure 7A-D) were normalized to the corresponding expression levels of the two proteins in each experimental group. The antibodies used for immunodetection and the molecular weight of the markers are indicated in the figures.

## ***Microscopy and image analysis***

Immunostaining of neurons was performed as described in (Lazarevic et al., 2011). For quantifications, identical antibodies solutions were used for all coverslips from the same experiment. For the co-localization analysis, neurons were silenced with APV and CNQX for 10 minutes, in order to minimize the effect of the ongoing activity on the variance between synapses and then stimulated with 200 AP at 40 Hz. Cells were fixed within 30 seconds after the end of stimulation.

Staining with synaptotagmin 1 antibody (Syt1 Ab uptake) was performed by incubating the cells with fluorescently-labelled primary antibody dissolved in extracellular solution, containing 119 mM NaCl, 2.5 mM KCl, 2 mM CaCl<sub>2</sub>, 2 mM MgCl<sub>2</sub>, 30 mM glucose, and 25 mM HEPES, pH 7.4 for 30 min at 37°C (Lazarevic et al., 2011) before fixation. For the imaging with CypHer5E-labeled anti-synaptotagmin1 antibody, cells were incubated with the antibody diluted in a buffer containing 120 mM NaCl, 5 mM KCl, 2 mM MgCl<sub>2</sub>, 2 mM CaCl<sub>2</sub>, 10 mM glucose, and 18 mM NaHCO<sub>3</sub>, pH 7.4 for 2-3 hours at 37°C prior imaging.

Epifluorescence images were acquired on a Zeiss Axio Imager A2 microscope with Cool Snap EZ camera (Visitron Systems) controlled by VisiView (Visitron Systems GmbH) software.

Confocal images in Figure S2A were acquired on a Leica SP5 confocal microscope. The format of the images was 2048x2048 pixels display resolution, 8 bit dynamic range, for acquisition 63x objective, NA 1.40 and 2x optical zoom were used, which results in a voxel size of approximately 50 nm.

Dual-color STED images (1024x1024 pixels display resolution, 8 bit dynamic range) were acquired on a Leica TCS SP8-3X gated STED microscope using a HC APO CS2 100x objective, NA 1.40, and 5x optical zoom, corresponding to a voxel size of approximately 23 nm. 16 times line averaging was applied on frames acquired at a scan speed 600 Hz. The built-in pulsed white light laser of the setup was used to excite Abberior STAR 580 and Atto 647N at 561 nm and 650 nm, respectively. The detection was done at 580-620 nm for Abberior STAR 580 and 660-730 nm for Atto647N. Both dyes were depleted using a pulsed 775 nm depletion laser. Time-gated detection of 0.5-1 ns to 6 ns was set for both STED channels. All raw data were subsequently deconvolved using the calculated point spread function (PSF) of the system and the Classic Maximum Likelihood Estimation (CMLE) algorithm with Huygens Professional (SVI,15.10.1). In brief, after an automatic background correction, the signal to noise ratio was set to 15 and the optimized iteration mode of the CMLE was run until a quality threshold of 0.05 was reached. The deconvolved datasets were corrected for a chromatic aberration in z, using the Chromatic Aberration Corrector (CAC) in Huygens.

The co-localization analysis was performed on the deconvolved STED stacks using Imaris 8.3 (Bitplane, Oxford Instruments). To detect punctate staining as spots Imaris spot detection algorithm was applied as follows: the sensitivity for the detection of the spots in each channel was determined by an automatically generated threshold and the spots diameter was set to 0.06  $\mu\text{m}$ . The distances between the spots in the two channels were measured using a customized version of the Imaris XTension Spots Colocalize, which determines the co-localization between the spots within a user-defined distance (1  $\mu\text{m}$ ) and bins the data into several bins with equal width (100 nm).

For quantifications, the same detector settings were used for all coverslips quantified in one experiment. From each culture, images from at least two different coverslips were acquired and quantified to minimize experimental variability. The nuclear fluorescence was assessed as established before (Ivanova et al., 2015). ImageJ (NIH) and OpenView software (Tsurriel et al., 2006) were used for quantitative immunofluorescence analysis. After removing the background by threshold subtraction in ImageJ, synaptic puncta were defined with OpenView software by setting rectangular regions of interest (ROI) with identical dimensions around local intensity maxima in the channel with staining for synapsin or any of the other synaptic markers that were used (GluA, homer1, synaptophysin, SV2B). Mean immunofluorescence (IF) intensities were measured in the synaptic ROIs in all corresponding channels using the same software and normalized to the mean IF intensities of the control group for each of the experiments. The number of synapses per unit of dendrite length was determined as follows: First synapsin puncta along 30  $\mu\text{m}$  of proximal dendrite, was detected using Find Maxima function in ImageJ, by setting the same noise tolerance to all images quantified in one experiment; Mean IF intensities of GluA were measured in circular ROIs set around the local intensity maxima in the image with synapsin staining; The number of GluA puncta co-localizing with synapsin was calculated by applying an identical intensity threshold for GluA detection between the different conditions within an experiment.

### ***pHluorin imaging and analysis***

The pHluorin imaging was performed with hippocampal cultures DIV16 to 20, transduced with lentiviral particles on the day of plating.

The coverslips were removed from the cell culture plates and mounted in an imaging chamber (Warner instruments), supplied with a pair of platinum wire electrodes, 1 cm apart, for electrical stimulation. The imaging was performed at 26°C in extracellular solution, containing 119 mM NaCl, 2.5 mM KCl, 25 mM Hepes pH7.4, 30 mM glucose, 2 mM  $\text{MgCl}_2$  and 2 mM  $\text{CaCl}_2$ , 10  $\mu\text{M}$  6-cyano-7-nitroquinoxaline-2,3-dione disodium (CNQX, Tocris) and 50  $\mu\text{M}$  d-(-)-2-amino-5-

phosphonopentanoic acid (APV, Tocris), on inverted microscope (Observer. D1; Zeiss-as described above) equipped with an EMCCD camera (Evolve 512; Photometrics) controlled by MetaMorph Imaging (MDS Analytical Technologies) and VisiView (Visitron Systems GmbH) software, using 63x objective. EGFP ET filter set (exciter 470/40, emitter 525/50, dichroic 495 LP, Chroma Technology Corp.) and Cy5 ET filter set (exciter 620/60, emitter 700/75, dichroic 660 LP, Chroma Technology Corp.) were used for imaging of the pHluorin and CypHer5E, respectively. Cultures were stimulated with a train of 40 or 200 action potentials (1 ms, constant voltage pulses) at 5, 20 or 40 Hz using S48 stimulator (GRASS Technologies). The alkaline trapping method was used for quantification of the recycling vesicle pools. In brief, the stimulation of sypHy expressing neurons was done in presence of bafilomycin A1 (1  $\mu$ M, Merck/Millipore), a specific inhibitor of the vesicular V-type ATPase. Exocytosis of RRP was triggered by delivering of 40 AP at 20 Hz. Following a 2 min break after the end of the first train of stimuli TRP was released by stimulation with 200 AP at 20 Hz. The relative sizes of RRP and TRP were determined as fractions of the total sypHy-expressing pool measured after addition of alkaline imaging buffer (60 mM NaCl in the extracellular solution was replaced with 60 mM NH<sub>4</sub>Cl). Fluorescent images were acquired at 1 Hz (Figure 1I) and 10 Hz (Figures 1F,J,K, 4E, 6A-D, S2C,G, and S4). Imaging of hippocampal neurons transfected with syp mOrange2 (Figure 4C) was performed in a modified extracellular solution (136-mM NaCl, 2.5 mM KCl, 2 mM CaCl<sub>2</sub>, 1.3 mM MgCl<sub>2</sub>, 10 mM glucose, and 10 mM HEPES, 10  $\mu$ M CNQX, 50  $\mu$ M APV, pH 7.4) on inverted Zeiss Axio Observer.Z1 epifluorescence microscope, equipped with Zeiss AxioCam 506 camera controlled by ZEISS ZEN 2 software, using EC Plan-Neofluar 40x oil immersion objective (NA 1.3) and a DsRED filter set (exciter 538-562, beam splitter 570, emitter 570-640). Cultures were stimulated with a train of 200 AP delivered at 20 Hz (100 mA, 1 ms pulse width) and fluorescent images were acquired at 0.5 Hz. Synaptic puncta responding to stimulation were identified by subtracting an average of the first several frames of the baseline from an average of several frames at the end of stimulation. The mean IF intensities were measured in ROIs with an identical size, placed automatically over each responding synapse using a self-written macro in ImageJ. The data traces were determined after removing the background by threshold subtraction and correction for bleaching, calculated from the bleaching of unresponsive boutons from the same coverslip. The half times for endocytosis ( $t_{1/2}$ ) were determined by applying a single exponential fit to the decay phases of the data traces using GraphPad Prism5 and the following equation:  $F_t = F_{stim} \cdot \exp(-t/\tau)$ ,  $t_{1/2} = \ln(2) \cdot \tau$ , where  $F_{stim}$  is the fluorescence intensity at the end of stimulation and  $\tau$  is the time constant for endocytosis.

## Electrophysiology

Whole-cell voltage clamp recordings were performed between 14 and 18 days in vitro (DIV) in autaptic neurons at room temperature. Ionic currents were acquired using a Digidata 1440A digitizer and a Multiclamp 700B amplifier under the control of Clampex X software (Axon instrument). Series resistance was set at 70% and only neurons with series resistances below 10 M $\Omega$  were selected. Data were recorded at 10 kHz and low-pass filtered at 3 kHz. Borosilicate glass pipettes with a resistance around 3 M $\Omega$  were used and filled with an intracellular solution containing (in mM): 136 KCl, 17.8 HEPES, 1 EGTA, 4.6 MgCl<sub>2</sub>, 4 Na<sub>2</sub>ATP, 0.3 Na<sub>2</sub>GTP, 12 phosphocreatine, and 50 U/ml phosphocreatine kinase; 300 mOsm; pH 7.4. Autaptic neurons were continuously perfused with standard extracellular solution composed of (in mM): 140 NaCl, 2.4 KCl, 10 HEPES, 10 glucose, 2 CaCl<sub>2</sub>, 4 MgCl<sub>2</sub>; 300 mOsm; pH 7.4. Spontaneous release was measured by recording mEPSC for 30 s at a holding potential of -70 mV in the presence of 3 mM kynurenic acid to detect false positive events and for the equal amount of time in extracellular solution. Data were filtered at 1 kHz and analyzed using template-based miniature event detection algorithms implemented in the AxoGraph X software. Action potential-evoked release EPSCs were elicited by 2 ms somatic depolarization from -70 to 0 mV. To estimate the readily-releasable pool (RRP) size, 500 mM hypertonic sucrose added to standard extracellular solution, was applied for 5 s using a fast-flow system (Pyott and Rosenmund, 2002). For vesicular release probability (P<sub>vr</sub>) calculations, the ratio of EPSC charge to RRP charge was determined. Short-term plasticity was examined either by evoking 2 unclamped AP with 25 ms interval (40 Hz) or a train of 50 AP at an interval of 100 ms (10 Hz). All electrophysiological data were analyzed offline using Axograph X (Axograph Scientific).

## QUANTIFICATION AND STATISTICAL ANALYSIS

All quantitative results are given as means  $\pm$  standard errors of the mean (SEM) and normalised to the values of control. Statistical analyses were performed with Prism 7 and 8 (GraphPad Software, Inc.). The sample sizes (n numbers) were adjusted based on published studies using similar methodology. In the plots the interquartile range and median are depicted as boxes, minimal and maximal values as whiskers and + indicates mean. In Figure 2 F and G scatter dot plots show mean and 95% CI, and in 2 L and N bars indicate mean and SEM. Data points in curves in Figure 3L, 4C and E, 6A-D, are depicted as means and SEM. n numbers correspond to the number of cells (fixed cell imaging and electrophysiology experiments), individual coverslips (live cell imaging experiments), synaptic profiles (EM data), number of independent

immunoprecipitations (IP) or samples from independent animals (WB) and are indicated for each group in graphs. In graphs comparisons with the control are indicated above each box and, comparisons between the conditions are given as horizontal bars. The statistical tests were chosen after the distribution of the data sets was explored. The scoring and the statistical tests used to compute the P values are specified in the datatable. Significance is indicated using asterisks: nsP>0.05, \*P<0.05, \*\*P<0.01, \*\*\*P<0.001, \*\*\*\* P<0.0001.

## DATA AND CODE AVAILABILITY

Requests for data and the scripts used for the main steps of the analysis of the pHluorin and STED data should be directed to the Lead Contact Anna Fejtova and will be made available upon reasonable request.

**Acknowledgments:** The YFP-CtBP2(NLS)-CtBP1 construct was kindly provided by M.Crossley, University of Sydney, Australia. We thank Anika Dirks for help with maintenance of the *Ctbp1* KO mouse colony, Christiana Kontaxi for help with animal handling, Maria Jose for help with imaging, Oliver Kobler, Torsten Stoeter and SL ELMI for providing expertise in STED imaging and tools for analysis and Janina Juhle, Bettina Kracht, Anita Heine and Isabel Herbert for excellent technical assistance. We also thank Renato Frischknecht, all members of the Presynaptic plasticity group and the Department Neurochemistry and molecular biology at LIN for useful discussions. This research was supported by the German Research Council grant GRK2162 and FE1335-1 to AF, SFB 779 to AF, SFB958 to CR, Wellcome Trust grant to MAC (204954/Z/16/Z) and Leibniz SAW grants to AF and EDG.

## Author contributions:

Conceptualization: DI and AF; Methodology: DI, CI, MC, CMV, DG, MAC, BC, AF; Investigation: DI, CI, MC, AR, DG, BC; Writing original draft: DI and AF; Writing-Review-Editing: all authors; Funding acquisition: MAC, CR, EDG and AF

## Declaration of interest:

"The authors declare no competing interests"

## Figure legends

### Figure 1

#### Knock down of CtBP1 reduces SV recycling.

- A) Representative images showing that the general neuronal morphology and the localization of synaptic markers are not changed in CtBP1KD neurons.
- B) Representative Western blots of samples from rat neurons transduced with viruses expressing shRNAs: scr, CtBP1KD944 and KD467 together with syphHy. The immunoreactivity for CtBP1 and CtBP2 and TCE total protein stain used as a loading control are shown. While notable downregulation of CtBP1 is evident in KD samples compared to scr, no changes were detected for CtBP2.
- C) Quantification of the Syt1 Ab uptake driven by basal network activity, depolarization with 50 mM KCl or in the presence of 1  $\mu$ M TTX in scr, and knockdown cultures.
- D) Representative images of Syt1 Ab uptake driven by basal neuronal network activity in control (scr), CtBP1KD944 and CtBP1KD467 cultures.
- E) Representative images of neurons expressing syphHy used to determine SV pool sizes. Cells were imaged in the presence of bafilomycin A1 during stimulation with 40 AP at 20 Hz to release RRP. After a rest for 2 min a train of 200 AP at 20 Hz triggered the exocytosis of all release-competent vesicles (TRP). A final NH<sub>4</sub>Cl-pulse that visualized all released and non-released syphHy-positive vesicles (total pool: TP) was used for normalization.
- F) Average syphHy-fluorescence (FsyphHy) traces reporting SV pool sizes from control and CtBP1KD neurons. RRP and TRP are given as fractions of TP.
- G) The mean values of RRP in scr, CtBP1KD944 and CtBP1KD467 did not differ significantly, but KD of CtBP1 leads to a significant reduction of TRP size.
- H) Images of syphHy showing SV exo-endocytosis at synapses in response to 200 AP at 5 Hz. The upper image shows the reference F of tdimer 2 before stimulation and the lower three the green F of syphHy before, during and after the stimulation.
- I-K) CtBP1 deletion results in slower retrieval of exocytosed SV. Peak-normalized syphHy responses to 200 AP at 5 Hz (I), 200 AP at 20 Hz (J) and 200 AP at 40 Hz (K) and respective single exponential fits of fluorescence decay are shown for each group. The estimated half times of endocytosis ( $t_{1/2}$ ) are plotted.
- Overlays are shown in the indicated colors. Scale bar is 10  $\mu$ m in A and 5  $\mu$ m in D, E and H.

### Figure 2

#### Ultrastructural analysis of synaptic morphology and SV distribution in *Ctbp1* KO and wild-type (WT) neurons

Synaptic profiles of glutamatergic spine synapses in high-pressure frozen and freeze substituted hippocampal organotypic slice cultures of *Ctbp1* knock out (KO) and wild-type (WT) animals were



analysed in electron micrographs of 60 nm-thick ultrathin sections (A-G) and by 3D electron tomography (H-P).

A and B) Electron micrographs of WT and respective *Ctbp1* KO synaptic profiles.

C to G) Mean values for number of SVs per synaptic profile(C), SV density(D), postsynaptic density (PSD) length (E), number of endosomes per synaptic profile(F,) and number of large dense-core vesicles (LDCVs) per synaptic profile(G).

H and I) Electron tomography sub-volumes of wild-type (H) and *Ctbp1* KO (I) synapses.

J and K) 3D models of synaptic profiles including orthogonal views of the active zone (AZ, white; docked SVs, red; nonattached SVs, gray).

L to P) Graphs show spatial distribution of SVs within 100 nm of the AZ (L), mean number of docked SVs (within 0–2 nm of the AZ) per AZ area (M), frequency distribution of SV diameters within 200 nm of the AZ (N), mean diameter of docked SVs (O) and mean number SV within 0–40 nm of the AZ per AZ area.

Scale bars: 200 nm in B) and 100 nm in I)

Figure 3

### **Synaptic and nuclear CtBP1 have distinct effects on neurotransmission and their deletion leads to pronounced short-term depression**

A) Averaged normalized evoked EPSC amplitudes from control, CtBP1KD944, EGFP-CtBP1 and YFP-CtBP2(NLS)-CtBP1 expressed in CtBP1KD944 neurons.

B) Example traces showing spontaneous EPSCs from control, CtBP1KD944 neurons, or neurons expressing EGFP-CtBP1 and YFP-CtBP2(NLS)-CtBP1 on CtBP1KD background.

C) Respective quantifications of average mEPSC amplitudes from the groups shown in (B).

D) Respective quantifications of mEPSC frequency from the groups shown in (B).

E) Autaptic neurons expressing the scrambled and CtBP1KD944 shRNA or the rescue variants: EGFP-CtBP1 or YFP-CtBP2(NLS)-CtBP1 on CtBP1KD944 background, were live stained for surface AMPA receptors and post fixation for synapsin to label presynapses. The overlays are shown in the indicated colors. Scale bar: 5µm

F and G) Quantification of the experiment in E. IF intensity of surface expressed GluA at synapses does not differ between conditions, but CtBP1KD944 and expression of EGFP-CtBP1 in CtBP1KD944 neurons increase the number of synapses.

H and I) Typical responses to application of 500mOsmM sucrose for 10sec (H) and average normalized sizes of RRP (I).

J) and K) Averaged normalized vesicular release probability (J) and PPR (K) in control, CtBP1KD944, and EGFP-CtBP1 and YFP-CtBP2(NLS)-CtBP1 expressed in CtBP1KD944 neurons.

L) Averaged normalized amplitudes of EPSC evoked by a train of stimuli at 10Hz.

Figure 4

### **Synaptic CtBP1 regulates SV recycling and short-term plasticity**

A) Syt1 Ab uptake was used to evaluate the efficacy of SV recycling in control, CtBP1KD944 and CtBP1KD944 neurons expressing the rescue constructs: EGFP-CtBP1 and YFP-

CtBP2(NLS)-CtBP1. Neurons were stained for synapsin to label synapses. Colored images represent overlays. Scale bar: 5µm.

- B) Expression of EGFP-CtBP1 rescues the Syt1 Ab uptake in CtBP1KD944 neurons up to 80% of the control levels. The fission deficient mutant EGFP-CtBP1D355A has a reduced rescue capacity compared to EGFP-CtBP1. Expression of the nuclear rescue: YFP-CtBP2(NLS)-CtBP1, does not compensate for the decreased Syt1 Ab uptake in CtBP1KD944.
- C) Average sympOrange2 responses to 200 AP at 20 Hz from control, CtBP1KD944 or CtBP1KD944 neurons expressing EGFP-CtBP1, EGFP-CtBP1D355A or YFP-CtBP2(NLS)-CtBP1.
- D) The endocytic half times,  $t_{1/2}$  from the experiment in (C) indicated that the rate of endocytosis was significantly lower in CtBP1KD944 compared to control. While expression of EGFP-CtBP1 in CtBP1KD944 cells rescued the endocytosis rate, expression of EGFP-CtBP1D355A or YFP-CtBP2(NLS)-CtBP1 did not.
- E) Visualization of short-term depression of exocytosis in CtBP1KD944 and upon expression of rescue constructs. Plotted are average Syt1 Ab-CypHer responses to 40AP at 20Hz (a reference response), followed by a 60s rest period and 200 AP at 10 Hz in the presence of bafilomycin A1. The traces were normalized to the amplitudes of the reference responses in each condition.
- F) The absence of synaptic CtBP1 led to a reduction of the plateau fluorescence responses in experiment E.

Figure 5

### **CtBP1 and dynamin act at the same membrane domain in an independent but likely cooperative manner**

- A) Orthographic views of the distribution of synaptic CtBP1 and the endocytic markers dynamin1, rab5, rab7, rab22 in neurons stimulated with 200 AP at 40 Hz. Punctate staining was detected as 'spots' and the co-localization was assessed as a distance from the CtBP1-labeled spots (synaptic distance) < 1 µm.
- B) The histogram shows the distribution of synaptic puncta co-localizing with CtBP1, binned according to the distance to CtBP1. A significantly smaller distance to CtBP1 is evident for dynamin1 (0-100 and 100-200 nm distance to CtBP1) compared to the other endosome markers.
- C) Images of Syt1 Ab-CypHer uptake in control and CtBP1KD944 neurons untreated or treated with dynole 34-2 (C, 30 µM) for 1h. Live staining for surface GluA receptors was used to mark synapses. Overlays are shown as colored images.
- D) Dynole 34-2 inhibits endocytosis in control and in CtBP1KD944 neurons. The residual endocytosis is significantly lower upon Dynole 34-2 application in CtBP1KD944 suggesting an interaction of treatments.

Scale bar is 0.1 µm in (A) and 5µm in (C).

Figure 6

### **CtBP1 promotes SV retrieval by activation of PLD1**

- A to D) Average syHy responses to 200 AP at 20 Hz were recorded and quantification of  $t_{1/2}$  of recovery was performed upon treatment with BFA (A,B) or PLD1 inhibitor (C,D) in control (A,C) or CtBP1KD944 neurons (B,D). SV retrieval was significantly delayed in BFA-treated neurons (A) but not further affected in BFA treated CtBP1KD944 neurons (B). Treatment with a PLD1 inhibitor affected SV retrieval in control neurons (C) but not in CtBP1KD944 neurons (D). The same controls were plotted in (A) and (C) as well as in (B) and (D), respectively.
- E) The endocytic probe mCLING-DY654 was loaded by stimulation of control and CtBP1KD944 neurons with 200AP at 40Hz. Synapses were stained with synapsin Ab. Synapses in CtBP1KD944 neurons show a reduction in the mCLING labeling.
- F) Quantification of synaptic mCLING IF in (E).
- G) Orthographic views of synaptic EGFP-CtBP1 or EGFP-CtBP1S147A (S147A) expressed in CtBP1KD944 neurons and the endocytic probe mCLING-ATTO647N, loaded by stimulation with 200 AP at 40 Hz.
- H) Quantification of the mCLING intensities from EGFP-CtBP1- and S147A-labeled synapses in G.
- I) Correlation of mCLING intensities and the distances to EGFP-CtBP1. The intensity of the endocytic probe was inversely correlated with the distance to EGFP-CtBP1.
- J) The histogram shows the distribution of mCLING puncta co-localizing with EGFP-CtBP1 or S147A, binned according to the distance mCLING-CtBP1. Note the shift in the histogram of EGFP-CtBP1 towards closer distances.

Scale bar is 2  $\mu$ m in E and 0.1  $\mu$ m in G.

Figure 7

#### **PAK1 phosphorylation mediates a switch in the association of CtBP1 with Bsn and PLD1**

- A and B) Inhibition of Pak1 increases the binding of EGFP-CtBP1 to Bsn and reduces its binding to PLD1. (A) Co-IP with EGFP antibodies was performed from neuronal cultures expressing EGFP-CtBP1 and treated or not with the Pak1 inhibitor IPA3 (50 $\mu$ M, 1h). (B) Quantification of the binding of Bsn to CtBP1.
- C and D) IP with EGFP antibodies was performed from whole cell lysates or P2 fractions of neuronal cultures expressing EGFP-CtBP1 and treated or not with the Pak1 inhibitor IPA3 (50 $\mu$ M for 1h). The Western blots were probed with a pan anti Ser/Thr Ab to visualize the phospho-Ser/Thr levels of CtBP1. Quantification of the Ser/Thr phosphorylation of CtBP1.
- E) The 2 color-STED images show a tighter co-localization of EGFP-CtBP1 with Bsn after stimulation with 200 AP at 40 Hz compared to cells at rest. EGFP-CtBP1S147A displays a tight co-localization with Bsn independently of neuronal activity.
- F) The histogram shows the relative distribution of Bsn puncta co-localizing with EGFP-CtBP1 or S147A at rest and upon stimulation.

Scale bar is 40 nm.

Figure S1

**Knock down of CtBP1 does not affect the overall expression of synaptic proteins and CtBP2**

- A) Synaptic abundance of pre- (SV2B, synapsin, synaptophysin) and post-synaptic markers (homer1, GluA) does not change in CtBP1KD neurons.
- B) Quantification of the effects shown in A)
- C) Nuclear CtBP2 does not change in CtBP1KD neurons.
- D) Quantification of the effects shown in C)

Scale bar is 5  $\mu$ m in A, and 10  $\mu$ m in C.

**Figure S2**

***Ctbp1* KO synapses have a reduced rate of SV endocytosis and a lower number of release-competent vesicles.**

- A) Immunoblot detection of synaptic proteins in brain homogenates (H) and crude synaptosomes (P2) from WT and *CtBP1* KO mice. GAPDH and  $\alpha$ -tubulin are loading controls.
- B) Quantification of the effects shown in A)
- C) Average syHy-fluorescence traces reporting SV pool sizes from neurons derived from WT and *Ctbp1*<sup>-/-</sup> mice.
- D) The mean values of RRP in WT and *Ctbp1*<sup>-/-</sup> did not differ significantly.
- E) Quantification of TRP size in WT and *Ctbp1*<sup>-/-</sup>.
- F) Neurons prepared from *Ctbp1*<sup>-/-</sup> animals and their WT siblings stained with an anti synapsin Ab, to label presynaptic terminals and pan anti GluA Ab to label postsynapses. Number of co-localizing synapsin and GluA puncta was slightly but not significantly increased in KO compared to control. The overlays are shown in the indicated colors. Scale bar: 5 $\mu$ m.
- G) Peak-normalized syHy responses to 200 AP at 20Hz. The half times: t<sub>1/2</sub> of endocytosis (bar graph) were smaller in WT neurons compared to *Ctbp1*<sup>-/-</sup>.

**Figure S3**

**Expression of YFP-CtBP2(NLS)-CtBP1 reverts the effect of CtBP1KD944 on gene expression.**

- A) Perspective views of 3D reconstructions of hippocampal neurons showing the synapto-nuclear distribution of the endogenous CtBP1 and the expressed rescue variants. Synapsin staining labels presynaptic terminals; DAPI labels nuclei. Note that EGFP-CtBP1 shows a decreased nuclear and an increased synaptic localization, whereas YFP-CtBP2(NLS)-CtBP1 is expressed only in the nucleus. For better visualization several EGFP-CtBP1-positive spots were removed from the planes above the nucleus. Overlays are shown in the indicated colors. Scale bar: 7 $\mu$ m.

B and C) YFP-CtBP2(NLS)-CtBP1 counteracts the increased expression of BDNF and Arc in CtBP1KD944 neuronal cultures.

Figure S4

### Frequency-dependent short-term synaptic depression at CtBP1-deficient synapses

A) and B) Average Syt1 Ab-CypHer responses to 50 AP at 20 Hz (a reference response), followed by a 60s rest period and 200 AP at 5 Hz (A) or 40 Hz (B) in the presence of 80 nM folimycin. The traces were normalized to the amplitudes of the reference response. KD of CtBP1 reduces the fluorescence responses to 200 AP at 5 Hz and even more pronouncedly at 40 Hz.

Figure S5

### Effect of synaptic stimulation on the co-localization of CtBP1 with the endocytic markers dynamin1, rab5, rab7, rab22 and the SV protein Syt1.

A - E) Cumulative plots showing the % of dynamin1, rab5, rab7, rab22 and Syt1 puncta co-localizing with CtBP1 in control (treated with 50μM APV and 10μM CNQX for 10 min) and stimulated (200AP at 40Hz) neurons, binned according to the distance to the CtBP1 labeled spots.

### Table 1: Ultrastructural analysis of synaptic morphology

#### 2D EM Analysis of Synaptic Morphology

	WT (N=3, n=159)	KO (N=4, n=146)	
# of SVs per profile	80.72 ± 3.244	89.21 ± 3.721	P = 0.098
terminal area ( x 0.01 μm <sup>2</sup> )	40.38 ± 1.182	41.19 ± 1.303	P = 0.845
# SVs / 0.01 μm <sup>2</sup> terminal area	1.993 ± 0.054	2.159 ± 0.064	P = 0.065
PSD length (nm)	373.7 ± 9.261	379.4 ± 9.421	P = 0.627
# of endosomes / terminal	0.843 ± 0.077	0.726 ± 0.082	P = 0.140
# of LDCVs / terminal	0.151 ± 0.034	0.24 ± 0.043	P = 0.083

N, number of animals; n, number of synaptic profiles; SV, synaptic vesicle; PSD, postsynaptic density; LDCV, large dense-core vesicle. (red P-values = Mann-Whitney test, black P-values = unpaired t-test)

#### 3D Electron Tomographic Analysis of Synaptic Vesicle Pools

	WT (N=3, n=26)	KO (N=4, n=25)	
# SVs within 0-2 nm of AZ	0.605 ± 0.092	0.876 ± 0.117	P = 0.075
# SVs within 0-5 nm of AZ	0.797 ± 0.109	1.213 ± 0.142	*P = 0.043
# SVs within 0-40 nm of AZ	1.821 ± 0.12	2.496 ± 0.168	**P = 0.002
# SVs within 0-100 nm of AZ	5.876 ± 0.267	7.307 ± 0.382	**P = 0.003

# SVs within 0-200 nm of AZ	14.65 ± 0.817	15.31 ± 0.811	P = 0.572
# SVs within 5-10 nm of AZ	0.214 ± 0.041	0.292 ± 0.07	P = 0.621
# SVs within 10-20 nm of AZ	0.264 ± 0.058	0.162 ± 0.037	P = 0.354
# SVs within 20-30 nm of AZ	0.213 ± 0.051	0.363 ± 0.069	P = 0.072
# SVs within 30-40 nm of AZ	0.345 ± 0.052	0.465 ± 0.07	P = 0.170
# SVs within 40-50 nm of AZ	0.531 ± 0.053	0.596 ± 0.081	P = 0.503
# SVs within 50-100 nm of AZ	3.54 ± 0.196	4.215 ± 0.245	*P = 0.036
# SVs within 100-150 nm of AZ	4.408 ± 0.331	4.175 ± 0.251	P = 0.579
# SVs within 150-200 nm of AZ	4.34 ± 0.328	3.827 ± 0.291	P = 0.249
AZ area (nm <sup>2</sup> )	40.900 ± 1.775	44.240 ± 2.276	P = 0.569
SV diameter (SVs within 0-200 nm of AZ)	44.95 ± 0.347	45.77 ± 0.38	P = 0.114
SV diameter (SVs within 0-100 nm of AZ)	44.98 ± 0.381	45.82 ± 0.426	P = 0.15

N, number of animals; n, number of tomograms; SV, synaptic vesicle; AZ, active zone. SV numbers within a certain distance of the AZ are normalized to 0.01  $\mu\text{m}^2$  of AZ area. Values indicate mean  $\pm$  SEM. (red P-values = Mann-Whitney test, black P-values = unpaired t-test)

	WT (n=63)	KO (n=100)	
SV diameter (docked SVs, 0-2 nm of AZ)	44.17 ± 0.64	46.08 ± 0.485	*P = 0.012

n, number of docked SVs averaged over all tomograms of a given genotype

Table 2: Electrophysiological analysis of autaptic cultures from CtBP1944KD and scr and upon expression of selective synaptic or nuclear rescue constructs

	SC	Kruskal-Wallis test	CtBP1KD944	Kruskal-Wallis test	EGFP-CtBP1	Kruskal-Wallis test	YFP-CtBP2(NLS)-CtBP1	Kruskal-Wallis test
mEPSC charge (fC)	110.5 ± 4.2 (n=69/5)	CtBP1KD944 P>0.99	104.4 ± 4.1 (n=70/5)	SC P>0.99	119.4 ± 9.8 (n=64/5)	SC P>0.99	110.3 ± 4.1 (n=62/5)	SC P>0.99
		EGFP-CtBP1 P>0.99		EGFP-CtBP1 P>0.99		CtBP1KD944 P>0.99		CtBP1KD944 P>0.99
		YFP-CtBP2(NLS)-CtBP1 P>0.99		YFP-CtBP2(NLS)-CtBP1 P>0.99		YFP-CtBP2(NLS)-CtBP1 P>0.99		EGFP-CtBP1 P>0.99
EPSC	35.4	CtBP1KD944	55.2	SC	78.1	SC	51.3	SC P=0.072

Charge (pC)	± 4.5 (n=77/5)	P=0.0018	± 5.9 (n=72/5)	P=0.0018	± 8.5 (n=62/5)	<0.0001	± 6.2 (n=63/5)	
		EGFP-CtBP1 P<0.0001		EGFP- CtBP1 P=0.4137		CtBP1KD94 4 P=0.4137		CtBP1KD944 P>0.99
		YFP- CtBP2(NLS)- CtBP1 P=0.072		YFP- CtBP2(NLS) -CtBP1 P>0.99		YFP- CtBP2(NLS) -CtBP1 P=0.0436		EGFP-CtBP1 P=0.0436
Pvr (%)	7.0 ± 0.5 (n=73/5)	CtBP1KD944 P<0.0001	15.8 ± 0.9 (n=64/5)	SC P<0.0001	14.2 ± 1.1 (n=52/5)	SC P<0.0001	11.6 ± 1.0 (n=62/5)	SC P>0.006
		EGFP-CtBP1 P<0.0001		EGFP- CtBP1 P>0.999		CtBP1KD94 4 P>0.999		CtBP1KD944 P=0.011
		YFP- CtBP2(NLS)- CtBP1 P>0.006		YFP- CtBP2(NLS) -CtBP1 P=0.011		YFP- CtBP2(NLS) -CtBP1 P=0.1925		EGFP-CtBP1 P=0.1925

1031 n, number of neurons / independent cultures analyzed

## 1032 References:

- 1033 Antonny, B., Burd, C., De Camilli, P., Chen, E., Daumke, O., Faelber, K., Ford, M., Frolov, V.A., Frost, A.,  
1034 Hinshaw, J.E., *et al.* (2016). Membrane fission by dynamin: what we know and what we need to know.  
1035 EMBO J 35, 2270-2284.
- 1036 Bekkers, J.M., and Stevens, C.F. (1991). Excitatory and inhibitory autaptic currents in isolated hippocampal  
1037 neurons maintained in cell culture. Proc Natl Acad Sci U S A 88, 7834-7838.
- 1038 Bonazzi, M., Spano, S., Turacchio, G., Cericola, C., Valente, C., Colanzi, A., Kweon, H.S., Hsu, V.W.,  
1039 Polishchuck, E.V., Polishchuck, R.S., *et al.* (2005). CtBP3/BARS drives membrane fission in dynamin-  
1040 independent transport pathways. Nat Cell Biol 7, 570-580.
- 1041 Burrone, J., Li, Z., and Murthy, V.N. (2006). Studying vesicle cycling in presynaptic terminals using the  
1042 genetically encoded probe synaptopHluorin. Nat Protoc 1, 2970-2978.
- 1043 Chinnadurai, G. (2009). The transcriptional corepressor CtBP: a foe of multiple tumor suppressors. Cancer  
1044 Res 69, 731-734.
- 1045 Colanzi, A., Grimaldi, G., Catara, G., Valente, C., Cericola, C., Liberali, P., Ronci, M., Lalioti, V.S., Bruno, A.,  
1046 Beccari, A.R., *et al.* (2013). Molecular mechanism and functional role of brefeldin A-mediated ADP-  
1047 ribosylation of CtBP1/BARS. Proc Natl Acad Sci U S A 110, 9794-9799.
- 1048 Cousin, M.A. (2017). Integration of Synaptic Vesicle Cargo Retrieval with Endocytosis at Central Nerve  
1049 Terminals. Front Cell Neurosci 11, 234.
- 1050 Dick O, Hack I, Altrock WD, Garner CC, Gundelfinger ED, Brandstatter JH (2001) Localization of the  
1051 presynaptic cytomatrix protein Piccolo at ribbon and conventional synapses in the rat retina: comparison  
1052 with Bassoon. J Comp Neurol 439: 224-234
- 1053 Donaldson, J.G. (2009). Phospholipase D in endocytosis and endosomal recycling pathways. Biochim  
1054 Biophys Acta 1791, 845-849.

1055 Egashira, Y., Takase, M., and Takamori, S. (2015). Monitoring of vacuolar-type H<sup>+</sup> ATPase-mediated proton  
1056 influx into synaptic vesicles. *J Neurosci* 35, 3701-3710.

1057 Fejtova, A., Davydova, D., Bischof, F., Lazarevic, V., Altmann, W.D., Romorini, S., Schone, C., Zuschratter, W.,  
1058 Kreutz, M.R., Garner, C.C., *et al.* (2009). Dynein light chain regulates axonal trafficking and synaptic levels  
1059 of Bassoon. *J Cell Biol* 185, 341-355.

1060 Ferguson, S.M., Brasnjo, G., Hayashi, M., Wolfel, M., Collesi, C., Giovedi, S., Raimondi, A., Gong, L.W., Ariel,  
1061 P., Paradise, S., *et al.* (2007). A selective activity-dependent requirement for dynamin 1 in synaptic vesicle  
1062 endocytosis. *Science* 316, 570-574.

1063 Gan, Q., and Watanabe, S. (2018). Synaptic Vesicle Endocytosis in Different Model Systems. *Front Cell*  
1064 *Neurosci* 12, 171.

1065 Garriga-Canut, M., Schoenike, B., Qazi, R., Bergendahl, K., Daley, T.J., Pfender, R.M., Morrison, J.F., Ockuly,  
1066 J., Stafstrom, C., Sutula, T., and Roopra, A. (2006). 2-Deoxy-D-glucose reduces epilepsy progression by  
1067 NRSF-CtBP-dependent metabolic regulation of chromatin structure. *Nat Neurosci* 9, 1382-1387.

1068 Granseth, B., Odermatt, B., Royle, S.J., and Lagnado, L. (2006). Clathrin-mediated endocytosis is the  
1069 dominant mechanism of vesicle retrieval at hippocampal synapses. *Neuron* 51, 773-786.

1070 Haga, Y., Miwa, N., Jahangeer, S., Okada, T., and Nakamura, S. (2009). CtBP1/BARS is an activator of  
1071 phospholipase D1 necessary for agonist-induced macropinocytosis. *EMBO J* 28, 1197-1207.

1072 Haucke, V., Neher, E., and Sigrist, S.J. (2011). Protein scaffolds in the coupling of synaptic exocytosis and  
1073 endocytosis. *Nat Rev Neurosci* 12, 127-138.

1074 Hildebrand, J.D., and Soriano, P. (2002). Overlapping and unique roles for C-terminal binding protein 1  
1075 (CtBP1) and CtBP2 during mouse development. *Mol Cell Biol* 22, 5296-5307.

1076 Hosoi N, Holt M, Sakaba T (2009) Calcium dependence of exo- and endocytotic coupling at a glutamatergic  
1077 synapse. *Neuron* 63: 216-229

1078 Hua, Y., Sinha, R., Thiel, C.S., Schmidt, R., Huve, J., Martens, H., Hell, S.W., Egner, A., and Klingauf, J.  
1079 (2011). A readily retrievable pool of synaptic vesicles. *Nat Neurosci* 14, 833-839.

1080 Hua, Y., Woehler, A., Kahms, M., Haucke, V., Neher, E., and Klingauf, J. (2013). Blocking endocytosis  
1081 enhances short-term synaptic depression under conditions of normal availability of vesicles. *Neuron* 80,  
1082 343-349.

1083 Hubler, D., Rankovic, M., Richter, K., Lazarevic, V., Altmann, W.D., Fischer, K.D., Gundelfinger, E.D., and  
1084 Fejtova, A. (2012). Differential spatial expression and subcellular localization of CtBP family members in  
1085 rodent brain. *PLoS One* 7, e39710.

1086 Humeau, Y., Vitale, N., Chasserot-Golaz, S., Dupont, J.L., Du, G., Frohman, M.A., Bader, M.F., and Poulain,  
1087 B. (2001). A role for phospholipase D1 in neurotransmitter release. *Proc Natl Acad Sci U S A* 98, 15300-  
1088 15305.

1089 Imig, C., and Cooper, B.H. (2017). 3D Analysis of Synaptic Ultrastructure in Organotypic Hippocampal Slice  
1090 Culture by High-Pressure Freezing and Electron Tomography. *Methods Mol Biol* 1538, 215-231.

1091 Imig, C., Min, S.W., Krinner, S., Arancillo, M., Rosenmund, C., Sudhof, T.C., Rhee, J., Brose, N., and Cooper,  
1092 B.H. (2014). The morphological and molecular nature of synaptic vesicle priming at presynaptic active  
1093 zones. *Neuron* 84, 416-431.

1094 Ivanova, D., Dirks, A., and Fejtova, A. (2016). Bassoon and piccolo regulate ubiquitination and link  
1095 presynaptic molecular dynamics with activity-regulated gene expression. *J Physiol* 594, 5441-5448.

1096 Ivanova, D., Dirks, A., Montenegro-Venegas, C., Schone, C., Altmann, W.D., Marini, C., Frischknecht, R.,  
1097 Schanze, D., Zenker, M., Gundelfinger, E.D., and Fejtova, A. (2015). Synaptic activity controls localization  
1098 and function of CtBP1 via binding to Bassoon and Piccolo. *EMBO J* 34, 1056-1077.

1099 Jenkins, G.H., Fiset, P.L., and Anderson, R.A. (1994). Type I phosphatidylinositol 4-phosphate 5-kinase  
1100 isoforms are specifically stimulated by phosphatidic acid. *J Biol Chem* 269, 11547-11554.

1101 Kim, S.H., and Ryan, T.A. (2009). Synaptic vesicle recycling at CNS synapses without AP-2. *J Neurosci* 29,  
1102 3865-3874.



1103 Koch, D., Spiwoks-Becker, I., Sabanov, V., Sinning, A., Dugladze, T., Stellmacher, A., Ahuja, R., Grimm, J.,  
 1104 Schuler, S., Muller, A., *et al.* (2011). Proper synaptic vesicle formation and neuronal network activity  
 1105 critically rely on syndapin I. *EMBO J* 30, 4955-4969.  
 1106 Kononenko, N.L., Diril, M.K., Puchkov, D., Kintscher, M., Koo, S.J., Pfuhl, G., Winter, Y., Wienisch, M.,  
 1107 Klingauf, J., Breustedt, J., *et al.* (2013). Compromised fidelity of endocytic synaptic vesicle protein sorting  
 1108 in the absence of stonin 2. *Proc Natl Acad Sci U S A* 110, E526-535.  
 1109 Kononenko, N.L., and Haucke, V. (2015). Molecular mechanisms of presynaptic membrane retrieval and  
 1110 synaptic vesicle reformation. *Neuron* 85, 484-496.  
 1111 Kooijman, E.E., Chupin, V., de Kruijff, B., and Burger, K.N. (2003). Modulation of membrane curvature by  
 1112 phosphatidic acid and lysophosphatidic acid. *Traffic* 4, 162-174.  
 1113 Kraszewski, K., Mundigl, O., Daniell, L., Verderio, C., Matteoli, M., and De Camilli, P. (1995). Synaptic  
 1114 vesicle dynamics in living cultured hippocampal neurons visualized with CY3-conjugated antibodies  
 1115 directed against the luminal domain of synaptotagmin. *J Neurosci* 15, 4328-4342.  
 1116 Kremer, J.R., Mastronarde, D.N., and McIntosh, J.R. (1996). Computer visualization of three-dimensional  
 1117 image data using IMOD. *Journal of structural biology* 116, 71-76.  
 1118 Lazarevic, V., Fienko, S., Andres-Alonso, M., Anni, D., Ivanova, D., Montenegro-Venegas, C., Gundelfinger,  
 1119 E.D., Cousin, M.A., and Fejtova, A. (2017). Physiological Concentrations of Amyloid Beta Regulate Recycling  
 1120 of Synaptic Vesicles via Alpha7 Acetylcholine Receptor and CDK5/Calcineurin Signaling. *Front Mol Neurosci*  
 1121 10, 221.  
 1122 Lazarevic, V., Schone, C., Heine, M., Gundelfinger, E.D., and Fejtova, A. (2011). Extensive remodeling of the  
 1123 presynaptic cytomatrix upon homeostatic adaptation to network activity silencing. *J Neurosci* 31, 10189-  
 1124 10200.  
 1125 Leal-Ortiz, S., Waites, C.L., Terry-Lorenzo, R., Zamorano, P., Gundelfinger, E.D., and Garner, C.C. (2008).  
 1126 Piccolo modulation of Synapsin1a dynamics regulates synaptic vesicle exocytosis. *J Cell Biol* 181, 831-846.  
 1127 Liberali, P., Kakkonen, E., Turacchio, G., Valente, C., Spaar, A., Perinetti, G., Bockmann, R.A., Corda, D.,  
 1128 Colanzi, A., Marjomaki, V., and Luini, A. (2008). The closure of Pak1-dependent macropinosomes requires  
 1129 the phosphorylation of CtBP1/BARS. *Embo J* 27, 970-981.  
 1130 Maritzen, T., and Haucke, V. (2018). Coupling of exocytosis and endocytosis at the presynaptic active zone.  
 1131 *Neurosci Res* 127, 45-52.  
 1132 Mastronarde DN (2005) Automated electron microscope tomography using robust prediction of specimen  
 1133 movements. *Journal of structural biology* 152: 36-51  
 1134 Moritz, A., De Graan, P.N., Gispen, W.H., and Wirtz, K.W. (1992). Phosphatidic acid is a specific activator of  
 1135 phosphatidylinositol-4-phosphate kinase. *J Biol Chem* 267, 7207-7210.  
 1136 Pagliuso, A., Valente, C., Giordano, L.L., Filograna, A., Li, G., Circolo, D., Turacchio, G., Marzullo, V.M.,  
 1137 Mandrich, L., Zhukovsky, M.A., *et al.* (2016). Golgi membrane fission requires the CtBP1-S/BARS-induced  
 1138 activation of lysophosphatidic acid acyltransferase delta. *Nature communications* 7, 12148.  
 1139 Park, J., Cho, O.Y., Kim, J.A., and Chang, S. (2016). Endosome-mediated endocytic mechanism replenishes  
 1140 the majority of synaptic vesicles at mature CNS synapses in an activity-dependent manner. *Scientific*  
 1141 *reports* 6, 31807.  
 1142 Puchkov, D., and Haucke, V. (2013). Greasing the synaptic vesicle cycle by membrane lipids. *Trends Cell*  
 1143 *Biol* 23, 493-503.  
 1144 Pyott, S.J., and Rosenmund, C. (2002). The effects of temperature on vesicular supply and release in  
 1145 autaptic cultures of rat and mouse hippocampal neurons. *J Physiol* 539, 523-535.  
 1146 Raben, D.M., and Barber, C.N. (2017). Phosphatidic acid and neurotransmission. *Advances in biological*  
 1147 *regulation* 63, 15-21.  
 1148 Raimondi, A., Ferguson, S.M., Lou, X., Armbruster, M., Paradise, S., Giovedi, S., Messa, M., Kono, N.,  
 1149 Takasaki, J., Cappello, V., *et al.* (2011). Overlapping role of dynamin isoforms in synaptic vesicle  
 1150 endocytosis. *Neuron* 70, 1100-1114.

1151 Ramperez, A., Sanchez-Prieto, J., and Torres, M. (2017). Brefeldin A sensitive mechanisms contribute to  
1152 endocytotic membrane retrieval and vesicle recycling in cerebellar granule cells. *J Neurochem* 141, 662-  
1153 675.

1154 Renard, H.F., Johannes, L., and Morsomme, P. (2018). Increasing Diversity of Biological Membrane Fission  
1155 Mechanisms. *Trends Cell Biol* 28, 274-286.

1156 Revelo, N.H., Kamin, D., Truckenbrodt, S., Wong, A.B., Reuter-Jessen, K., Reisinger, E., Moser, T., and  
1157 Rizzoli, S.O. (2014). A new probe for super-resolution imaging of membranes elucidates trafficking  
1158 pathways. *J Cell Biol* 205, 591-606.

1159 Rose, T., Schoenenberger, P., Jezek, K., and Oertner, T.G. (2013). Developmental refinement of vesicle  
1160 cycling at Schaffer collateral synapses. *Neuron* 77, 1109-1121.

1161 Rosenmund, C., and Stevens, C.F. (1996). Definition of the readily releasable pool of vesicles at  
1162 hippocampal synapses. *Neuron* 16, 1197-1207.

1163 Soykan, T., Kaempf, N., Sakaba, T., Vollweiler, D., Goerdeler, F., Puchkov, D., Kononenko, N.L., and  
1164 Haucke, V. (2017). Synaptic Vesicle Endocytosis Occurs on Multiple Timescales and Is Mediated by Formin-  
1165 Dependent Actin Assembly. *Neuron* 93, 854-866 e854.

1166 Spano, S., Silletta, M.G., Colanzi, A., Alberti, S., Fiucci, G., Valente, C., Fusella, A., Salmona, M., Mironov, A.,  
1167 Luini, A., *et al.* (1999). Molecular cloning and functional characterization of brefeldin A-ADP-ribosylated  
1168 substrate. A novel protein involved in the maintenance of the Golgi structure. *J Biol Chem* 274, 17705-  
1169 17710.

1170 Tagliatti, E., Fadda, M., Falace, A., Benfenati, F., and Fassio, A. (2016). Arf6 regulates the cycling and the  
1171 readily releasable pool of synaptic vesicles at hippocampal synapse. *eLife* 5.

1172 tom Dieck, S., Altroch, W.D., Kessels, M.M., Qualmann, B., Regus, H., Brauner, D., Fejtova, A., Bracko, O.,  
1173 Gundelfinger, E.D., and Brandstatter, J.H. (2005). Molecular dissection of the photoreceptor ribbon  
1174 synapse: physical interaction of Bassoon and RIBEYE is essential for the assembly of the ribbon complex. *J*  
1175 *Cell Biol* 168, 825-836.

1176 Tsuruel, S., Geva, R., Zamorano, P., Dresbach, T., Boeckers, T., Gundelfinger, E.D., Garner, C.C., and Ziv, N.E.  
1177 (2006). Local sharing as a predominant determinant of synaptic matrix molecular dynamics. *PLoS biology*  
1178 4, e271.

1179 Valente, C., Luini, A., and Corda, D. (2013). Components of the CtBP1/BARS-dependent fission machinery.  
1180 *Histochemistry and cell biology* 140, 407-421.

1181 Valente, C., Turacchio, G., Mariggio, S., Pagliuso, A., Gaibisso, R., Di Tullio, G., Santoro, M., Formiggini, F.,  
1182 Spano, S., Piccini, D., *et al.* (2012). A 14-3-3gamma dimer-based scaffold bridges CtBP1-S/BARS to  
1183 PI(4)KIIIbeta to regulate post-Golgi carrier formation. *Nat Cell Biol* 14, 343-354.

1184 Verger, A., Quinlan, K.G., Crofts, L.A., Spano, S., Corda, D., Kable, E.P., Braet, F., and Crossley, M. (2006).  
1185 Mechanisms directing the nuclear localization of the CtBP family proteins. *Mol Cell Biol* 26, 4882-4894.

1186 Wu, X.S., Lee, S.H., Sheng, J., Zhang, Z., Zhao, W.D., Wang, D., Jin, Y., Charnay, P., Ervasti, J.M., and Wu,  
1187 L.G. (2016). Actin Is Crucial for All Kinetically Distinguishable Forms of Endocytosis at Synapses. *Neuron* 92,  
1188 1020-1035.

1189 Wu, Y., O'Toole, E.T., Girard, M., Ritter, B., Messa, M., Liu, X., McPherson, P.S., Ferguson, S.M., and De  
1190 Camilli, P. (2014). A dynamin 1-, dynamin 3- and clathrin-independent pathway of synaptic vesicle  
1191 recycling mediated by bulk endocytosis. *eLife* 3, e01621.

1192 Yang, J.S., Gad, H., Lee, S.Y., Mironov, A., Zhang, L., Bezoussenko, G.V., Valente, C., Turacchio, G., Bonsra,  
1193 A.N., Du, G., *et al.* (2008). A role for phosphatidic acid in COPI vesicle fission yields insights into Golgi  
1194 maintenance. *Nat Cell Biol* 10, 1146-1153.

1195 Zeniou-Meyer, M., Zabari, N., Ashery, U., Chasserot-Golaz, S., Haeberle, A.M., Demais, V., Bailly, Y.,  
1196 Gottfried, I., Nakanishi, H., Neiman, A.M., *et al.* (2007). Phospholipase D1 production of phosphatidic acid  
1197 at the plasma membrane promotes exocytosis of large dense-core granules at a late stage. *J Biol Chem*  
1198 282, 21746-21757.

1199 Zhang, B., Koh, Y.H., Beckstead, R.B., Budnik, V., Ganetzky, B., and Bellen, H.J. (1998). Synaptic vesicle size  
1200 and number are regulated by a clathrin adaptor protein required for endocytosis. *Neuron* 21, 1465-1475.

1201

1202

**KEY RESOURCES TABLE**

REAGENT or RESOURCE	SOURCE	IDENTIFIER
<b>Antibodies</b>		
Mouse anti-CtBP1	BD Biosciences	Cat#612042; RRID:AB_399429
Mouse anti-CtBP2	BD Biosciences	Cat#612044; RRID: AB_399431
Mouse anti-synaptotagmin1 luminal domain Oyster550	Synaptic Systems	Cat#105311; RRID:AB_993036
Mouse anti-synaptotagmin1 luminal domain CypHer5E-labeled	Synaptic Systems	Cat#105311CpH; RRID:AB_2199307
Mouse anti-rab5	Synaptic Systems	Cat#108011; RRID:AB_887773
Mouse anti-rab7	Abcam	Cat#ab50533; RRID:AB_882241
Mouse anti-phosphoserine/threonine	BD Biosciences	Cat#612548; RRID:AB_399843
Mouse anti-GluA Oyster 550-labeled	Synaptic Systems	Cat#182411C3; RRID:AB_2619877
Mouse anti- $\alpha$ -tubulin	Sigma Aldrich	Cat# T9026; RRID:N/A
Rabbit anti-CtBP1	Synaptic Systems	Cat#222002; RRID:AB_2086638
Rabbit anti-GFP	Abcam	Cat#ab6556; RRID:AB_305564
Rabbit anti-SV2B	Synaptic Systems	Cat#119103; RRID:AB_2725759
Rabbit anti-GAPDH	Abcam	Cat#ab37168; RRID:AB_732652
Rabbit anti-synaptotagmin1 luminal domain Oyster 550-labeled	Synaptic Systems	Cat#105103C3; RRID:AB_887829
Rabbit anti-synaptotagmin 1 luminal domain	Synaptic Systems	Cat#105102; RRID:AB_887835
Rabbit anti-dynamin1	Abcam	Cat#ab3456; RRID:AB_303818
Rabbit anti-rab22a	Abcam	Cat#ab137093; RRID:N/A

Rabbit anti-Phospholipase D1	Cell Signaling technologies	Cat#3832S; RRID:AB_2172256
Rabbit anti-Homer1	Synaptic Systems	Cat#160003; RRID:AB_887730
Guinea pig anti-synapsin 1, 2	Synaptic Systems	Cat#106004; RRID:AB_1106784
Guinea pig anti-synaptophysin 1	Synaptic Systems	Cat#101004; RRID:AB_1210382
Guinea pig anti-Piccolo	Dick et al, 2001	N/A
Alexa Fluor 488 donkey anti-mouse secondary antibody	ThermoFisher Scientific	Cat#A21202; RRID:AB_141607
Alexa Fluor 488 donkey anti-rabbit secondary antibody	ThermoFisher Scientific	Cat#A21206; RRID:AB_141708
Alexa Fluor 488 donkey anti-guinea pig secondary antibody	Dianova/Jackson ImmunoResearch Labs	Cat#706-545-148; RRID:AB_2340472
Cy3 donkey anti-mouse secondary antibody	Dianova/Jackson ImmunoResearch Labs	Cat#715-165-150; RRID:AB_2340813
Cy3 donkey anti-rabbit secondary antibody	Dianova/Jackson ImmunoResearch Labs	Cat#711-165-152; RRID:AB_2307443
Cy3 donkey anti-guinea pig secondary antibody	Dianova/Jackson ImmunoResearch Labs	Cat#706165-148; RRID:AB_2340460
647 donkey anti-mouse secondary antibody	ThermoFisher Scientific	Cat#A31571; RRID:AB_162542
Cy5 donkey anti-rabbit secondary antibody	Dianova/Jackson ImmunoResearch Labs	Cat#711-175-152; RRID:AB_2340607
Cy5 donkey anti-guinea pig secondary antibody	Dianova/Jackson ImmunoResearch Labs	Cat#706-175-148; RRID:AB_2340462
IRDye® 680 Donkey Anti-Mouse secondary antibody	LI-COR	Cat#926-68072; AB_10953628
IRDye 680RD Goat anti-Rabbit secondary antibody	LI-COR	Cat#926-68071; RRID:AB_10956166
IRDye 800CW Donkey anti-guinea pig secondary antibody	LI-COR	Cat#926-32411; RRID:AB_1850024

Atto 647N- goat anti mouse secondary antibody	Rockland	Cat#610-156-121; RRID:AB_10894200
Atto 647N- goat anti rabbit secondary antibody	Rockland	Cat#611-156-122; RRID:AB_10893043
Abberior STAR 580- anti mouse secondary antibody	Abberior GmbH	Cat#2-0002-005-1; RRID:AB_2620153
Abberior STAR 580- anti rabbit secondary antibody	Abberior GmbH	Cat#2-0012-005-8; RRID:AB_2810981
<b>Bacterial and Virus Strains</b>		
<b>Biological Samples</b>		
<b>Chemicals, Peptides, and Recombinant Proteins</b>		
APV	Tocris	0106 CAS: 79055-68-8
CNQX	Tocris	1045 CAS: 479347-85-8
bafilomycin A1	Merck/Millipore	196000 CAS: 88899-55-2
concanamycin A	Tocris	2656 CAS: 80890-47-7
brefeldin A	Tocris	1231 CAS: 20350-15-6
VU 0155069	Tocris	3575 CAS: 1781834-89-6
Dynole 34-2	Abcam	ab120463 CAS: 1128165-88-7
IPA 3	Tocris	3622 CAS: 42521-82-4
cOmplete™ ULTRA Tablets	Roche/Merck	05892791001
PhosSTOP™	Roche/Merck	PHOSS-RO
mCLING-ATTO647N	Synaptic Systems	710 006AT1
mCLING-DY654	Synaptic Systems	710 006DY1

Critical Commercial Assays		
RT <sup>2</sup> Profiler™ PCR Array Rat Synaptic Plasticity	Qiagen	PARN-126Z
RNeasy Plus Mini Kit	Qiagen	74134
μMACS GFP Isolation Kit	Miltenyi Biotec	130-091-125
μ Columns	Miltenyi Biotec	130-042-701
Deposited Data		
Raw and analyzed data	This paper	N/A
Experimental Models: Cell Lines		
HEK293T (human, embryonic kidney)	ATCC	CRL-3216
Experimental Models: Organisms/Strains		
Rat: Wistar	Charles River	Wistar IGS Rat
Rat: Sprague-Dawley	Charles River	CD® (Sprague Dawley) IGS Rat
Mouse: C57BL/6N	Charles River	C57BL/6NCrl
Mouse: <i>Ctbp1</i> <sup>tm1Sor</sup> ( <i>Ctbp1</i> KO)	Jackson Lab	(Stock No: 011054)
Oligonucleotides		
CtBP1KD944 shRNA target sequence: GCTTCAACGTCCTCTTCTA	Ivanova et al, 2015	N/A
CtBP1KD467 shRNA target sequence: GCACAGTGGAGATGCCTAT	Ivanova et al, 2015	N/A
scrambled shRNA sequence: GACTTTACTGCCCCTTACT	Ivanova et al, 2015	N/A
Genotyping primers for CtBP1KO animals ctbp1_common; GAAGTACCAGTACAGGGGACG ctbp1_korev; GTTATCGCCGCTCCCGATTCTG ctbp1_wtrev; CCCAGCTGACTTGATGTCTG	Hildebrand and Soriano, 2002	N/A
Recombinant DNA		
Plasmid: ratio:syPHy	Rose et al., 2013	N/A
Plasmid: syP mOrange2	Egashira et al., 2015	N/A

Lentiviral Plasmid: pCtBP1KD944	Ivanova et al., 2015	N/A
Lentiviral Plasmid: scrambled	Ivanova et al., 2015	
Lentiviral Plasmid: pCtBP1KD467	Ivanova et al., 2015	N/A
Lentiviral Plasmid: pCtBP1KD944 + EGFP-CtBP1	This paper	N/A
Lentiviral Plasmid: pCtBP1KD944 + YFP-CtBP2(NLS)-CtBP1	This paper	N/A
Lentiviral Plasmid: pCtBP1KD944 + EGFP-CtBP1D355A	This paper	N/A
Lentiviral Plasmid: pCtBP1KD944 + EGFP-CtBP1S147A	This paper	N/A
psPAX2	gift from Didier Trono	Addgene Plasmid #12260
p-CMV-VSV-G	Stewart et al., 2003	Addgene Plasmid #8454
<b>Software and Algorithms</b>		
ImageJ	National Institute of Health	<a href="https://imagej.nih.gov/">https://imagej.nih.gov/</a>
Openview	Tsuriel et al., 2006	N/A
custom script for STED analysis (MATLAB)	This paper	N/A
custom script for pHluorin analysis (ImageJ)	This paper	N/A
IMOD package	Kremer et al., 1996	<a href="https://bio3d.colorado.edu/imod/">https://bio3d.colorado.edu/imod/</a>
Huygens Professional (SVI,15.10.1)	Scientific Volume Imaging	<a href="https://svi.nl/Huygens-Professional">https://svi.nl/Huygens-Professional</a>
Imaris 8.3	Bitplane, Oxford Instruments	<a href="https://imaris.oxinst.com/">https://imaris.oxinst.com/</a>
LightCycler® 480 Software	Roche	<a href="https://www.roche.com/">https://www.roche.com/</a>
AxoGraph X software	Axograph Scientific	<a href="https://axograph.com/">https://axograph.com/</a>
Prism 7 and 8 software	GraphPad Software	<a href="https://www.graphpad.com/">https://www.graphpad.com/</a>
<b>Other</b>		



Figure	condition	mean±SEM	n = number of cells or coverslips/ N= number of neuronal preparations	Comparison	P	Statistical test
Fig1B	scr	1.00±0.10	3 experiments	scr vs CtBP1KD944	<0,0001	one-way ANOVA with Dunnett's multiple comparison test
	CtBP1KD944	0.28±0.02		scr vs CtBP1KD467	<0,0001	
	CtBP1KD467	0.55±0.04				
Fig1C	scr basal	1.00±0.05	27 cells/3	scr basal vs CtBP1KD944 basal	<0,0001	one-way ANOVA with Dunnett's multiple comparisons test
	CtBP1KD944 basal	0.49±0.03	27 cells/3	scr basal vs CtBP1KD467 basal	<0,0001	
	CtBP1KD467 basal	0.45±0.04	27 cells/3			
	scr KCl	1.00±0.03	10 cells/2	scr KCl vs CtBP1KD944 KCl	<0,0001	one-way ANOVA with Dunnett's multiple comparisons test
	CtBP1KD944 KCl	0.44±0.02	10 cells/2	scr KCl vs CtBP1KD467 KCl	<0,0001	
	CtBP1KD467 KCl	0.66±0.03	9 cells/2			
	scr TTX	1.00±0.14	10 cells/2	scr TTX vs CtBP1KD944 TTX	<0,0001	one-way ANOVA with Dunnett's multiple comparisons test
	CtBP1KD944 TTX	0.39±0.04	10 cells/2	scr TTX vs CtBP1KD467 TTX	<0,0001	
	CtBP1KD467 TTX	0.20±0.02	9 cells/2			
Fig1G: RRP	scr	0.17±0.03	10 coverslips/3	scr vs CtBP1KD944	ns	unpaired t test
	CtBP1KD944	0.14±0.03	8 coverslips/3	scr vs CtBP1KD467	ns	
	RRCtBP1KD467	0.14±0.03	8 coverslips/3			
Fig1H: TRP	scr	0.51±0.05	10 coverslips/3	scr vs CtBP1KD944	0,0067	unpaired t test
	CtBP1KD944	0.30±0.04	8 coverslips/3	scr vs CtBP1KD467	0,0076	
	CtBP1KD467	0.31±0.04	8 coverslips/3			
Fig1J	scr 5Hz	25.26±3.22	7 coverslips/3	scr 5Hz vs CtBP1KD944 5Hz	0,0389	unpaired t test
	CtBP1KD944 5Hz	44.33±6.63	10 coverslips/3	scr vs CtBP1KD467	0,0207	
	CtBP1KD467 5Hz	43.11±2.80	7 coverslips/3			
Fig1K	scr 20Hz	24.76±4.11	6 coverslips/2	scr 20Hz vs CtBP1KD944 20Hz	0,0064	unpaired t test
	CtBP1KD944 20Hz	43.11±2.80	5 coverslips/2	scr 20Hz vs CtBP1KD467 20Hz	0,0332	
	CtBP1KD467 20Hz	53.65±10.96	6 coverslips/2			
Fig1L	scr 40Hz	28.13±2.60	7 coverslips/2	scr 40Hz vs CtBP1KD944 40Hz	0,0213	unpaired t test
	CtBP1KD944 40Hz	85.58±25.16	5 coverslips/2	scr 40Hz vs CtBP1KD467 40Hz	0,0312	
	CtBP1KD467 40Hz	70.43±18.40	6 coverslips/2			

Data related to the Figure 2 can be find in the Table 1

Figure	condition	mean±SEM	n = number of cells or coverslips/ N= number of neuronal preparations	Comparison	P	Statistical test
Fig.3A	scr	1.00±0.09	76 cells/5	scr vs CtBP1KD944	<0,0001	Kruskal-Wallis one-way ANOVA with Dunn's multiple comparison test
	CtBP1KD944	1.59±0.12	72 cells/5			
	EGFP-CtBP1 in CtBP1KD944	2.11±0.12	62 cells/5	scr vs EGFP-CtBP1 in CtBP1KD944	<0,0001	
	YFP-CtBP2(NLS)-CtBP1 in CtBP1KD944	1.22±0.11	63 cells/5	scr vs YFP-CtBP2(NLS)-CtBP1 in CtBP1KD944	ns	
Fig.3C	scr	30.25±1.55	69 cells/5	scr vs CtBP1KD944	ns	Kruskal-Wallis one-way ANOVA with Dunn's multiple comparison test
	CtBP1KD944	28.91±1.19	70 cells/5			
	EGFP-CtBP1 in CtBP1KD944	30.04±1.10	64 cells/5	scr vs EGFP-CtBP1 in CtBP1KD944	ns	
	YFP-CtBP2(NLS)-CtBP1 in CtBP1KD944	28.81±1.22	62 cells/5	scr vs YFP-CtBP2(NLS)-CtBP1 in CtBP1KD944	ns	
Fig.3D	scr	8.24±0.83	69 cells/5	scr vs CtBP1KD944	ns	Kruskal-Wallis one-way ANOVA with Dunn's multiple comparison test
	CtBP1KD944	9.06±0.75	70 cells/5			
	EGFP-CtBP1 in CtBP1KD944	12.14±0.91	64 cells/5	scr vs EGFP-CtBP1 in CtBP1KD944	0,0003	
	YFP-CtBP2(NLS)-CtBP1 in CtBP1KD944	9.45±0.87	61 cells/5	scr vs YFP-CtBP2(NLS)-CtBP1 in CtBP1KD944	ns	
Fig.3F	scr		29 cells/2	scr vs CtBP1KD944	ns	one-way ANOVA with Sidak test
	CtBP1KD944		29 cells/2			
	EGFP-CtBP1 in CtBP1KD944		25 cells/2	scr vs EGFP-CtBP1 in CtBP1KD944	ns	
	YFP-CtBP2(NLS)-CtBP1 in CtBP1KD944		28 cells/2	scr vs YFP-CtBP2(NLS)-CtBP1 in CtBP1KD944	ns	
Fig.3G	scr	1.00±0.12	29 cells/2	scr vs CtBP1KD944	0,0358	one-way ANOVA with Sidak test
	CtBP1KD944	1.76±0.22	29 cells/2			
	EGFP-CtBP1 in CtBP1KD944	2.17±0.25	25 cells/2	scr vs EGFP-CtBP1 in CtBP1KD944	0,0006	
	YFP-CtBP2(NLS)-CtBP1 in CtBP1KD944	1.34±0.22	28 cells/2	scr vs YFP-CtBP2(NLS)-CtBP1 in CtBP1KD944	ns	
Fig.3I	scr	1.00±0.15	73 cells/5	scr vs CtBP1KD944	ns	Kruskal-Wallis one-way ANOVA with Dunn's multiple comparison test
	CtBP1KD944	0.80±0.09	64 cells/5			
	EGFP-CtBP1 in CtBP1KD944	0.98±0.11	57 cells/5	scr vs EGFP-CtBP1 in CtBP1KD944	ns	
	YFP-CtBP2(NLS)-CtBP1 in CtBP1KD944	0.89±0.71	63 cells/5	scr vs YFP-CtBP2(NLS)-CtBP1 in CtBP1KD944	ns	
Fig.3J	scr	1±0.07	73 cells/5	scr vs CtBP1KD944	<0,0001	Kruskal-Wallis one-way ANOVA with Dunn's multiple comparison test
	CtBP1KD944	2.27±0.14	64 cells/5	CtBP1KD944 vs YFP-CtBP2(NLS)-CtBP1 in CtBP1KD944	0,0021	
	EGFP-CtBP1 in CtBP1KD944	2.00±0.19	57 cells/5	scr vs EGFP-CtBP1 in CtBP1KD944	<0,0001	
	YFP-CtBP2(NLS)-CtBP1 in CtBP1KD944	1.70±0.16	63 cells/5	scr vs YFP-CtBP2(NLS)-CtBP1 in CtBP1KD944	0,0009	

Fig.3K	scr	1.02±0.03	78 cells/5	scr vs CtBP1KD944	<0,0001	Kruskal-Wallis one-way ANOVA with Dunn's multiple comparison test
	CtBP1KD944	0.74±0.02	73 cells/5	CtBP1KD944 vs YFP-CtBP2(NLS)-CtBP1 in CtBP1KD944	<0,0001	
	EGFP-CtBP1 in CtBP1KD944	0.81±0.03	66 cells/5	scr vs EGFP-CtBP1 in CtBP1KD944	<0,0001	
	YFP-CtBP2(NLS)-CtBP1 in CtBP1KD944	0.92±0.03	64 cells/5	scr vs YFP-CtBP2(NLS)-CtBP1 in CtBP1KD944	ns (0,0511)	
Fig.3L (averaged EPSC of last 20 stimuli)	scr	0.79±0.04	78 cells/5	scr vs CtBP1KD944	<0,0001	Kruskal-Wallis one-way ANOVA with Dunn's multiple comparison test
	CtBP1KD944	0.53±0.02	73 cells/5	CtBP1KD944 vs YFP-CtBP2(NLS)-CtBP1 in CtBP1KD944	<0,0001	
	EGFP-CtBP1 in CtBP1KD944	0.59±0.03	66 cells/5	scr vs EGFP-CtBP1 in CtBP1KD944	0,0027	
	YFP-CtBP2(NLS)-CtBP1 in CtBP1KD944	0.52±0.02	64 cells/5	scr vs YFP-CtBP2(NLS)-CtBP1 in CtBP1KD944	<0,0001	

Figure	condition	mean±SEM	n = number of cells or coverslips/ N= number of neuronal preparations	Comparison	P	Statistical test
Fig.4B	scr	1.00±0.05	48 cells/5	scr vs CtBP1KD944	<0,0001	one-way ANOVA with Dunnett's T3 multiple comparison test
	CtBP1KD944	0.37±0.04	49 cells/5	CtBP1KD944 vs YFP-CtBP2(NLS)-CtBP1 in CtBP1KD944	ns	
				CtBP1KD944 vs EGFP-CtBP1 in CtBP1KD944	<0,0001	
				CtBP1KD944 vs EGFP-CtBP1D355A in CtBP1KD944	ns	
	EGFP-CtBP1 in CtBP1KD944	0.80±0.07	29 cells/5	scr vs EGFP-CtBP1 in CtBP1KD944	ns	
	EGFP-CtBP1 D355A in CtBP1KD944	0.50±0.06	30 cells/5	scr vs EGFP-CtBP1D355A in CtBP1KD944	<0,0001	
	YFP-CtBP2(NLS)-CtBP1 in CtBP1KD944	0.44±0.04	29 cells/5	scr vs YFP-CtBP2(NLS)-CtBP1 in CtBP1KD944	<0,0001	

Fig.4D	scr	23.20±2.27	19 coverslips/5	scr vs CtBP1KD944	P=0,0008	Unpaired t test
	CtBP1KD944	45.66±5.66	19 coverslips/5	CtBP1KD944 vs YFP-CtBP2(NLS)-CtBP1 in CtBP1KD944	ns	
				CtBP1KD944 vs EGFP-CtBP1 in CtBP1KD944	P=0,0033	
				CtBP1KD944 vs EGFP-CtBP1D355A in CtBP1KD944	ns	
	EGFP-CtBP1 in CtBP1KD944	24.42±2.25	15 coverslips/5	scr vs EGFP-CtBP1 in CtBP1KD944	ns	
	EGFP-CtBP1 D355A in CtBP1KD944	38.70±5.55	19 coverslips/5	scr vs EGFP-CtBP1D355A in CtBP1KD944	P=0,0137	
	YFP-CtBP2(NLS)-CtBP1 in CtBP1KD944	53.03±7.04	17 coverslips/5	scr vs YFP-CtBP2(NLS)-CtBP1 in CtBP1KD944	P=0,0002	
Fig.4F	scr	1.67±0.17	10 coverslips/3	scr vs CtBP1KD944	P=0,0040	unpaired t test
	CtBP1KD944	1.02±0.08	9 coverslips/3	CtBP1KD944 vs YFP-CtBP2(NLS)-CtBP1 in CtBP1KD944	ns	
				CtBP1KD944 vs EGFP-CtBP1 in CtBP1KD944	P=0,0448	
	EGFP-CtBP1 in CtBP1KD944	1.41±0.16	10 coverslips/3	scr vs EGFP-CtBP1 in CtBP1KD944	ns	
	YFP-CtBP2(NLS)-CtBP1 in CtBP1KD944	1.08±0.04	11 coverslips/3	scr vs YFP-CtBP2(NLS)-CtBP1 in CtBP1KD944	P=0,0025	

Figure	condition	mean±SEM	n = number of cells or coverslips/ N= number of neuronal preparations	Comparison	P	Statistical test
Fig.5B 0-100nm	dynamin1	43±3	5 cells/2	dynamin1 vs rab5	<0,0001	two-way ANOVA with Turkey's multiple comparison test
	rab5	7±1	6 cells/2			
	rab7	8±1	6 cells/2	dynamin1 vs rab7	<0,0001	
	rab22	6±1	5 cells/2	dynamin1 vs rab22	<0,0001	
100-200 nm	dynamin1	42±1	5 cells/2	dynamin1 vs rab5	<0,0001	two-way ANOVA with Turkey's multiple comparison test
	rab5	21±1	6 cells/2			
	rab7	21±3	6 cells/2	dynamin1 vs rab7	<0,0001	
	rab22	21±2	5 cells/2	dynamin1 vs rab22	<0,0001	
Fig.5D	scr	1.00±0.05	26 coverslips/3	scr vs CtBP1KD944	<0,0001	one-way ANOVA with Dunnett's T3 multiple comparison test
	scr + Dynole 34-2	0.18±0.05	30 coverslips/3	scr vs scr + Dynole 34-2	<0,0001	
	CtBP1KD944	0.52±0.04	26 coverslips/3	CtBP1KD944 vs. CtBP1KD944 + Dynole 34-2	<0,0001	
	CtBP1KD944 + Dynole 34-2	0.09±0.01	28 coverslips/3	scr + Dynole 34-2 vs CtBP1KD944 + Dynole 34-2	<0,0001	

Figure	condition	mean±SEM	n = number of cells or coverslips/ N= number of neuronal preparations	Comparison	P	Statistical test
Fig.6A	scr	23.84±3.65	7 coverslips/2	scr vs scr + BFA	P=0,0261	unpaired t tests
	scr + BFA	40.93±5.88	5 coverslips/2			
Fig.6B	CtBP1KD944	44.64±7.75	7 coverslips/2	CtBP1KD944 vs CtBP1KD944 + BFA	ns	unpaired t tests
	CtBP1KD944 + BFA	50.97±7.08	7 coverslips/2			
Fig.6C	scr	23.84±3.65	7 coverslips/2	scr vs scr + PLD1inh	P=0,0359	unpaired t tests
	scr + PLD1inh	46.41±9.33	6 coverslips/2			
Fig.6D	CtBP1KD944	44.64±7.75	7 coverslips/2	CtBP1KD944 vs CtBP1KD944 + PLD1inh	ns	unpaired t tests
	CtBP1KD944 + PLD1inh	40.60±8.85	6 coverslips/2			
Fig.6F	scr	1.00 ± 0.07	19 cells/2	scr vs CtBP1KD944	<0,0001	unpaired t tests
	CtBP1KD944	0.32 ± 0.06	15 cells/2			
Fig.6H	EGFP-CtBP1 in CtBP1KD944	1.00±0.18	5 cells/2	EGFP-CtBP1 vs EGFP-CtBP1-S147A	P=0,0050	unpaired t tests
	EGFP-CtBP1-S147A in CtBP1KD944	0.22±0.10	5 cells/2			
Fig.6J 100-200nm	EGFP-CtBP1 in CtBP1KD944	44.17±1.93	5 cells/2	EGFP-CtBP1 vs EGFP-CtBP1-S147A	P=0,0073	two-way ANOVA with Sidak's multiple comparison test
	EGFP-CtBP1-S147A in CtBP1KD944	37.69±1.99	5 cells/2			

Figure	condition	mean±SEM	n = number of cells or coverslips/ N= number of neuronal preparations	Comparison	P	Statistical test
Fig.7B	control	1.00±0.02	8 experiments	control vs IPA3	P=0,0013	Welch's t-test
	IPA3	1.73±0.14	8 experiments			
Fig.7D	control	1.00±0.02	7 experiments	control vs IPA3	P=0,0015	Welch's t-test
	IPA3	0.53±0.08	6 experiments			
Fig.7F 0-100nm	EGFP-CtBP1 control	31.91±3.45	5 cells/2	EGFP-CtBP1 control vs. EGFP-CtBP1 stimulated	<0,0001	two-way ANOVA with Turkey's multiple comparison test
	EGFP-CtBP1 stimulated	42.62±158	5 cells/2			
	EGFP-CtBP1S147A control	44.18±0.84	5 cells/2	EGFP-CtBP1 control vs. EGFP-CtBP1S147A control	<0,0001	
	EGFP-CtBP1S147A stimulated	42.43±1.99	5 cells/2	EGFP-CtBP1 control vs. EGFP-CtBP1S147A stimulated	<0,0001	

Figure		condition	mean±SEM	n = number of cells or coverslips/ N= number of neuronal preparations	Comparison	P	Statistical test
FigS1B	SV2B	scr	1.00±0.06	9 cells/2	scr vs CtBP1KD944	ns	one-way ANOVA with Dunnett's multiple comparisons test
		CtBP1KD944	1.00±0.08	14 cells/2			
		CtBP1KD467	1.18±0.09	20 cells/2	scr vs CtBP1KD467	ns	
	sph	scr	1.00±0.06	12 cells/2	scr vs CtBP1KD944	ns	one-way ANOVA with Dunnett's multiple comparisons test
		CtBP1KD944	0.99±0.08	12 cells/2			
		CtBP1KD467	1.18±0.07	12 cells/2	scr vs CtBP1KD467	ns	
	Syn	scr	1.00±0.06	9 cells/2	scr vs CtBP1KD944	ns	one-way ANOVA with Dunnett's multiple comparisons test
		CtBP1KD944	1.06±0.10	14 cells/2			
		CtBP1KD467	1.23±0.16	20 cells/2	scr s CtBP1KD467	ns	
	homer <sub>1</sub>	scr	1.00±0.16	10 cells/2	scr vs CtBP1KD944	ns	one-way ANOVA with Dunnett's multiple comparisons test
		CtBP1KD944	0.93±0.07	10 cells/2			
		CtBP1KD467	0.83±0.09	10 cells/2	scr vs CtBP1KD467	ns	
	GluA1	scr	1.00±0.08	10 cells/2	scr vs CtBP1KD944	ns	one-way ANOVA with Dunnett's multiple comparisons test
		CtBP1KD944	1.14±0.12	10 cells/2			
		CtBP1KD467	1.06±0.23	10 cells/2	scr vs CtBP1KD467	ns	
FigS1D	CtBP2	scr	1.00±0.08	41 cells/2	scr CtBP2 vs CtBP1KD944 CtBP2		one-way ANOVA with Dunnett's multiple comparisons test
		CtBP1KD944	0.78±0.04	38 cells/2			
		CtBP1KD467	0.86±0.06	38 cells/2	scr CtBP2 vs CtBP1KD467 CtBP2		

Figure		condition	mean±SEM	n = number of cells or coverslips/ N= number of neuronal preparations	Comparison	Adjusted P	Statistical test
FigS2B H	CtBP1	WT	1.00±0.13	3 mice	WT vs KO	P=0,010525	multiple t-test with Holm-Sidak method for significance testing
		KO	0.04±0.03	3 mice			
	CtBP2	WT	1.00±0.14	3 mice	WT vs KO	ns	
		KO	1.22±0.16	3 mice			
	Bsn	WT	1.00±0.09	3 mice	WT vs KO	ns	
		KO	0.87±0.07	3 mice			
	Pclo	WT	1.00±0.02	3 mice	WT vs KO	ns	
		KO	0.83±0.04	3 mice			
	Stg1	WT	1.00±0.15	3 mice	WT vs KO	ns	
		KO	0.79±0.14	3 mice			
P2	CtBP1	WT	1.00±0.04	3 mice	WT vs KO	P=0,000090	multiple t-test with Holm-Sidak method for significance testing
		KO	0.01±0.01	3 mice			
	CtBP2	WT	1.00±0.14	3 mice	WT vs KO	ns	
		KO	0.84±0.01	3 mice			
	Bsn	WT	1.00±0.05	3 mice	WT vs KO	ns	
		KO	1.1±0.07	3 mice			
	Pclo	WT	1.00±0.02	3 mice	WT vs KO	ns	
		KO	0.87±0.09	3 mice			
	Sy11	WT	1.00±0.01	3 mice	WT vs KO	ns	
		KO	0.92±0.03	3 mice			
Fig.S2D		WT	0.19±0.02	5 coverslips/2	WT vs KO	ns	unpaired Student's t test
		KO	0.15±0.01	6 coverslips/2			
Fig.S2E		WT	0.57±0.05	5 coverslips/2	WT vs KO	P=0,0043	Mann Whitney test
		KO	0.45±0.01	6 coverslips/2			
Fig.S2F		WT	1.00±0.12	11 cells/2	WT vs KO	ns	unpaired Student's

	KO	1.23±0.15	11 cells/2			t test
Fig.S2G	WT	15.11±1.45	7 coverslips/2	WT vs KO	P=0,0036	unpaired Student's t test
	KO	22.18±1.32	7 coverslips/2			

Figure	condition	mean±SEM	n = number of neuronal preparations	Comparison	P	Statistical test
Fig.S3B	scr	1.00±0	4	scr vs CtBP1KD944	<0,0001	One-way ANOVA with Turkey's multiple comparison test
	CtBP1KD944	1.24±0.02	4	CtBP1KD944 vs CtBP1KD944 + YFP-CtBP2(NLS)-CtBP1	<0,0001	
	CtBP1KD944 + YFP-CtBP2(NLS)-CtBP1	0.59±0.02	4	scr vs CtBP1KD944 + YFP-CtBP2(NLS)-CtBP1	<0,0001	
Fig.S3C	scr	1.00±0	4	scr vs CtBP1KD944	P=0,0002	One-way ANOVA with Turkey's multiple comparison test
	CtBP1KD944	2.11±0.04	4	CtBP1KD944 vs CtBP1KD944 + YFP-CtBP2(NLS)-CtBP1	ns	
	CtBP1KD944 + YFP-CtBP2(NLS)-CtBP1	1.34±0.20	4	scr vs CtBP1KD944 + YFP-CtBP2(NLS)-CtBP1	P=0,0030	

Figure	bin	condition	mean	n	Comparison	P	Statistical test
Fig.S5A	dynamin1		N/A	5	effect of stimulation	ns	Two way ANOVA with Sidak's test
	dynamin 1 stim		N/A	5			
Fig.S5B	Syt1		N/A	5	effect of stimulation	ns	Two way ANOVA with Sidak's test
	Syt1 stim		N/A	5			
Fig.S5C	rab5			6	effect of stimulation	<0,0001	Two way ANOVA with Sidak's test
	rab5 stim			6			
	0-300nm	rab5	60,55		rab5 vs. rab5 stim	<0,0001	
		rab5 stim	52,81				
	0-400nm	rab5	79,94			<0,0001	
		rab5 stim	72,27				
	0-500nm	rab5	90,38			P=0,0059	
		rab5 stim	84,88				
Fig.S5D	rab7			6	effect of stimulation	<0,0001	Two way ANOVA with Sidak's test
	rab7 stim			6			
	0-300nm	rab7	64,75		rab5 vs. rab5 stim	P=0,0046	
		rab7 stim	48,81				
	0-400nm	rab7	80,65			P=0,0040	
		rab7 stim	64,53				
	0-500nm	rab7	89,87			P=0,0244	
		rab7 stim	76,20				
Fig.S5E	rab21			6	effect of stimulation	ns	Two way ANOVA with Sidak's test
	rab21 stim			6			

Figure1

Figure 1

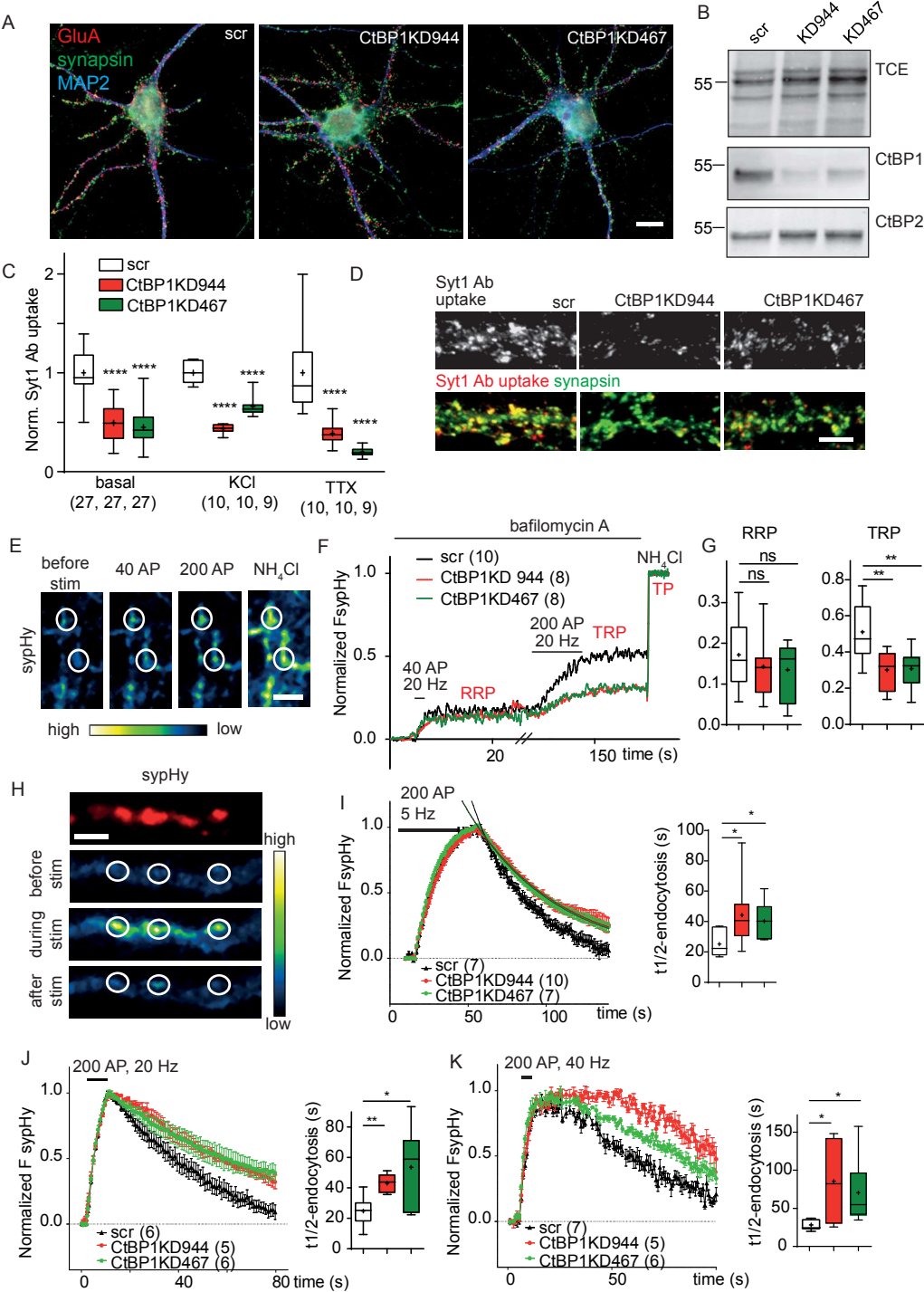




Figure2

Figure 2

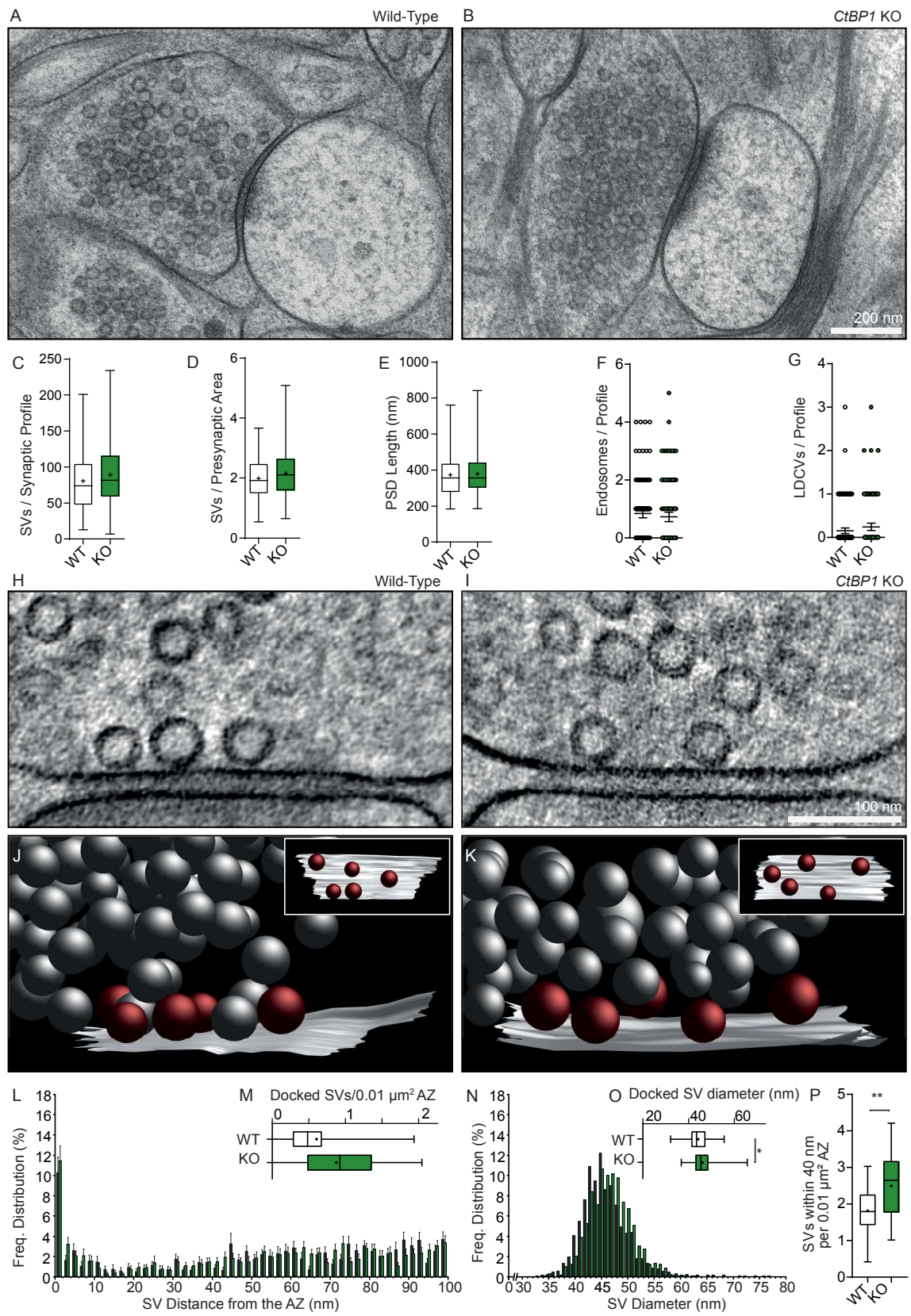


Figure3

Figure 3

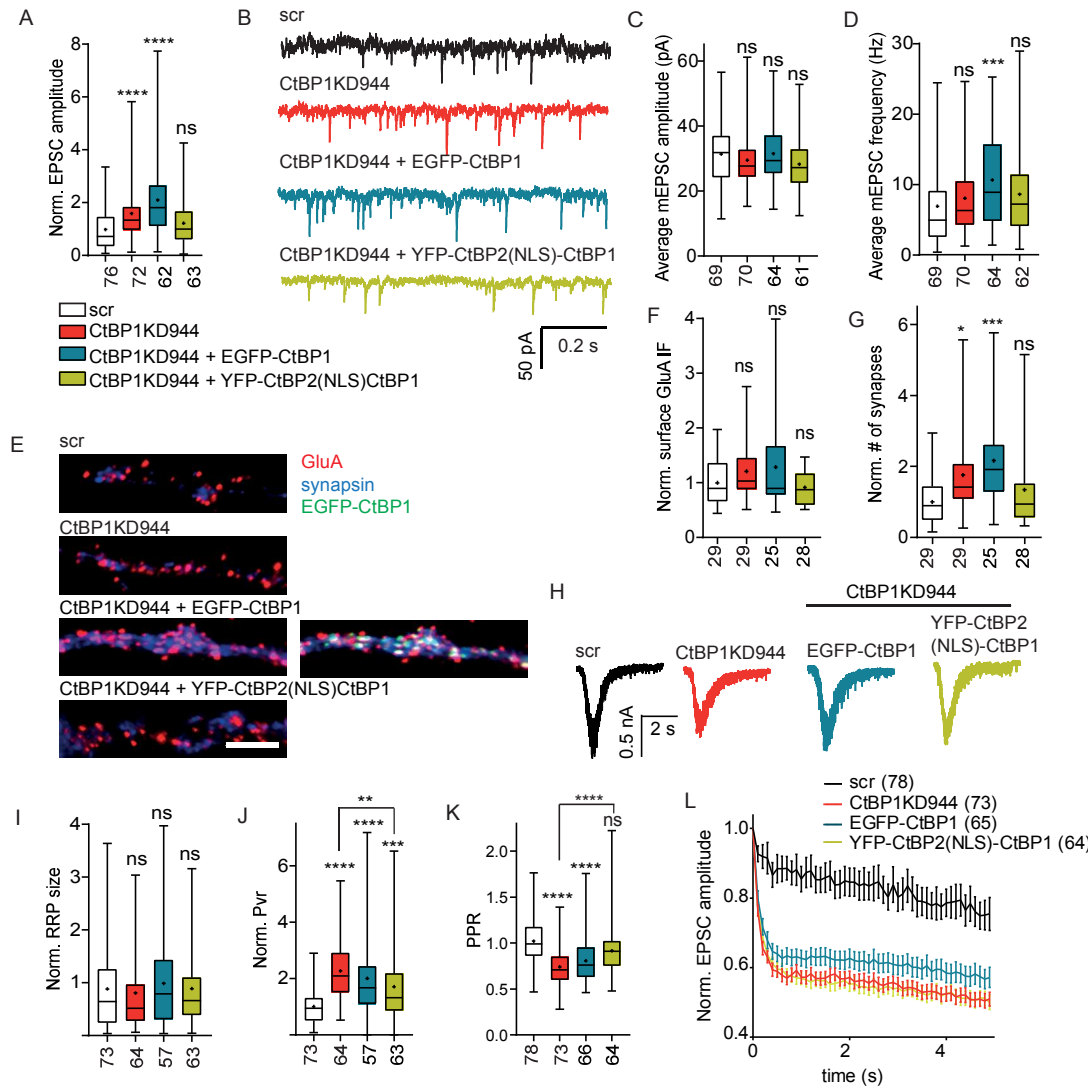


Figure 4



Figure5

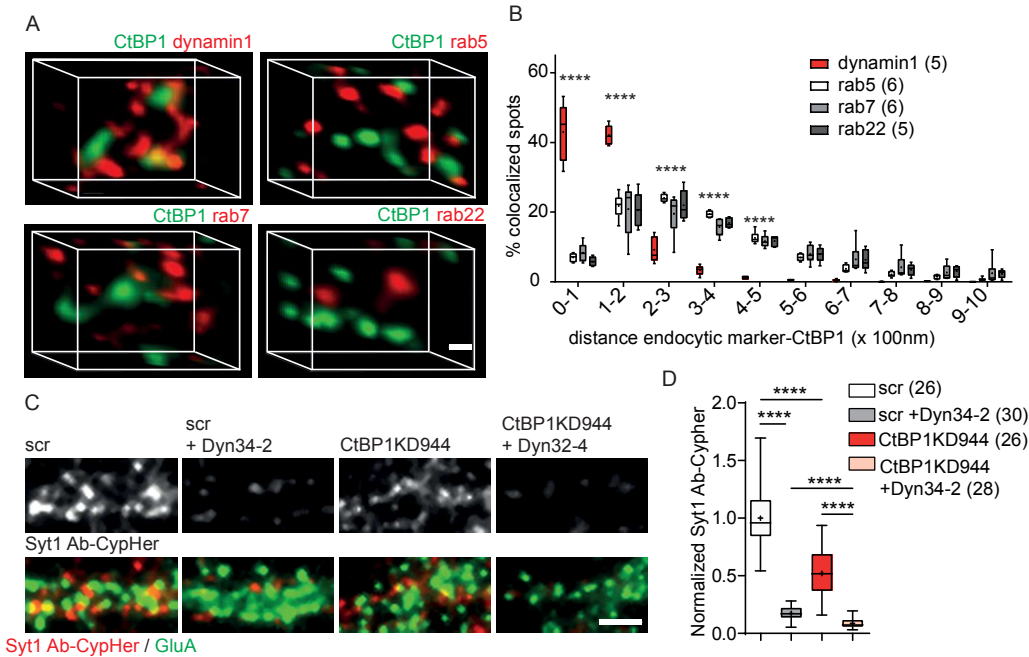


Figure 6

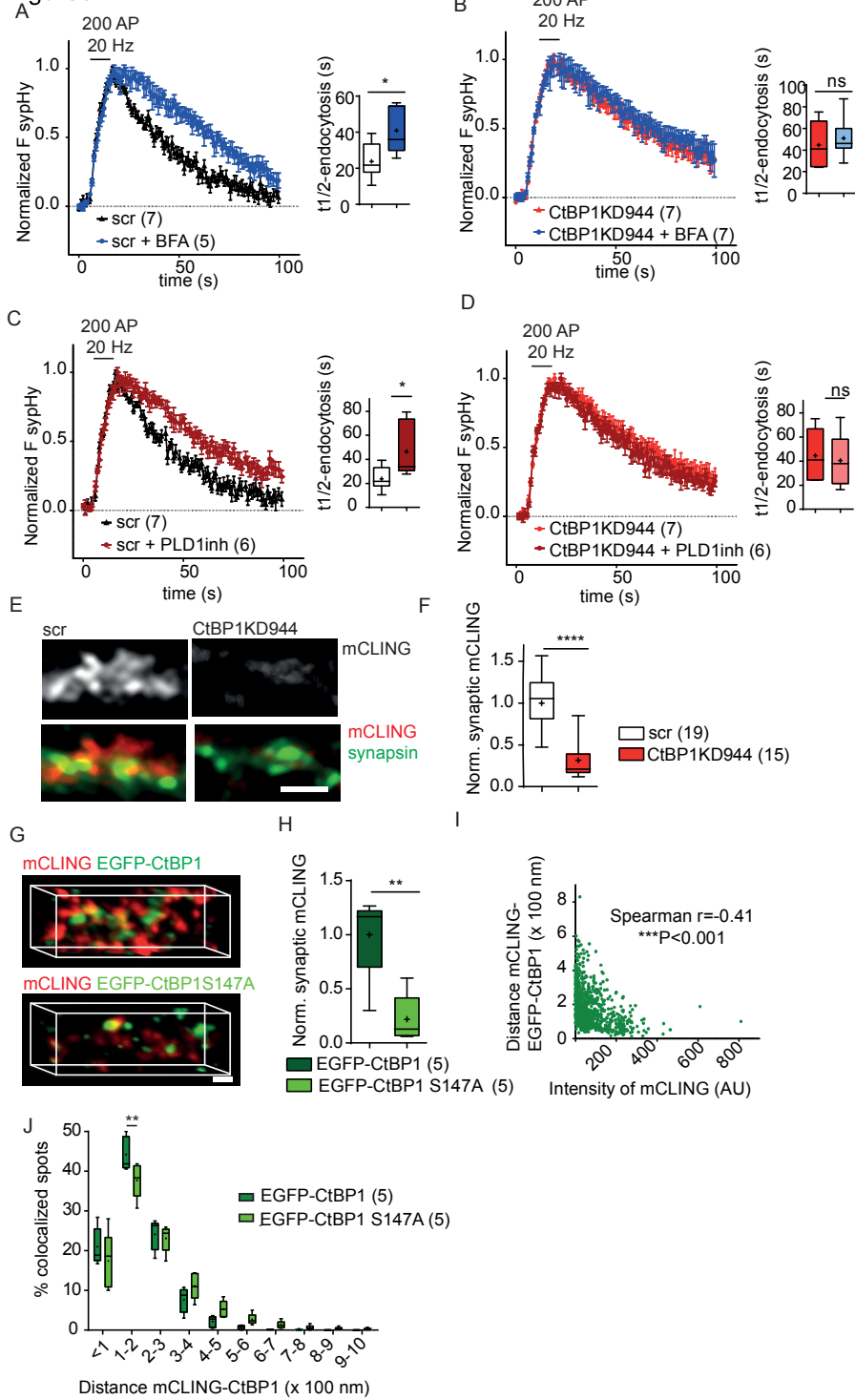
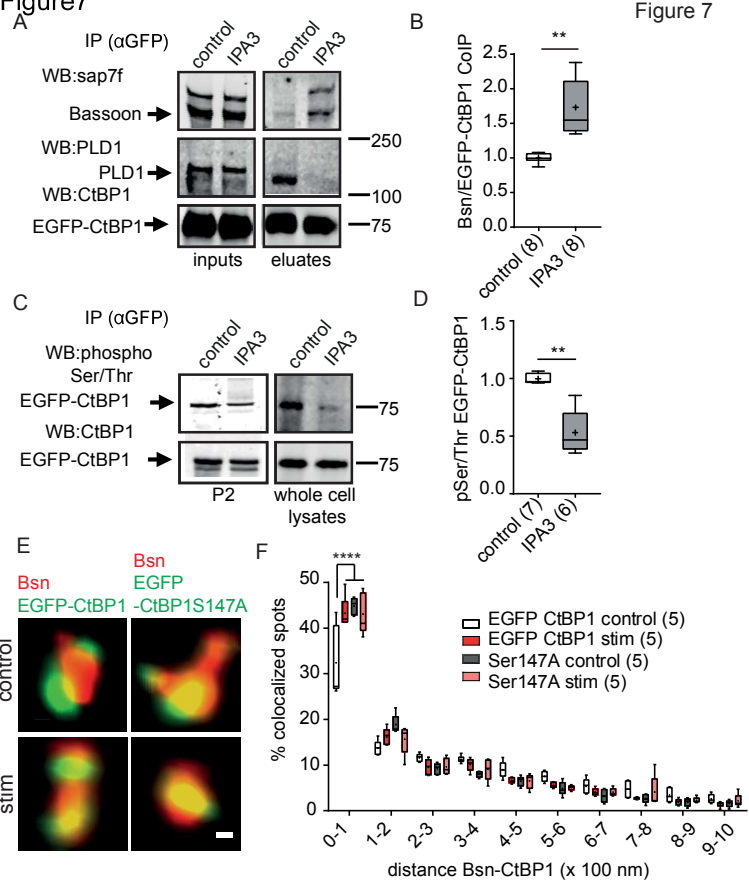


Figure 7



FigureS1

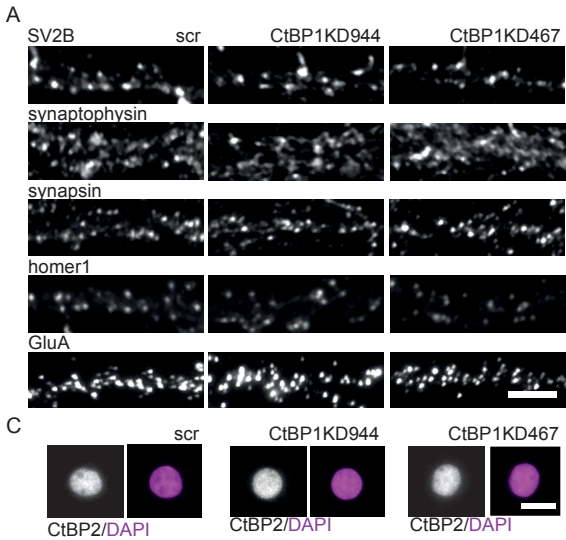
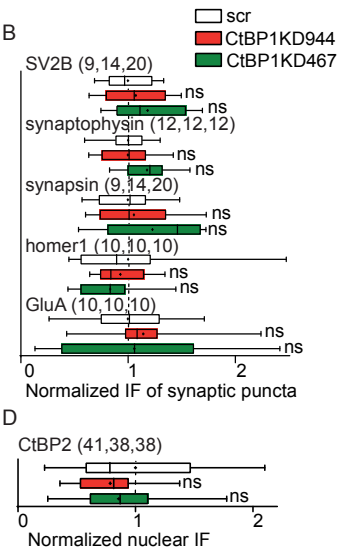
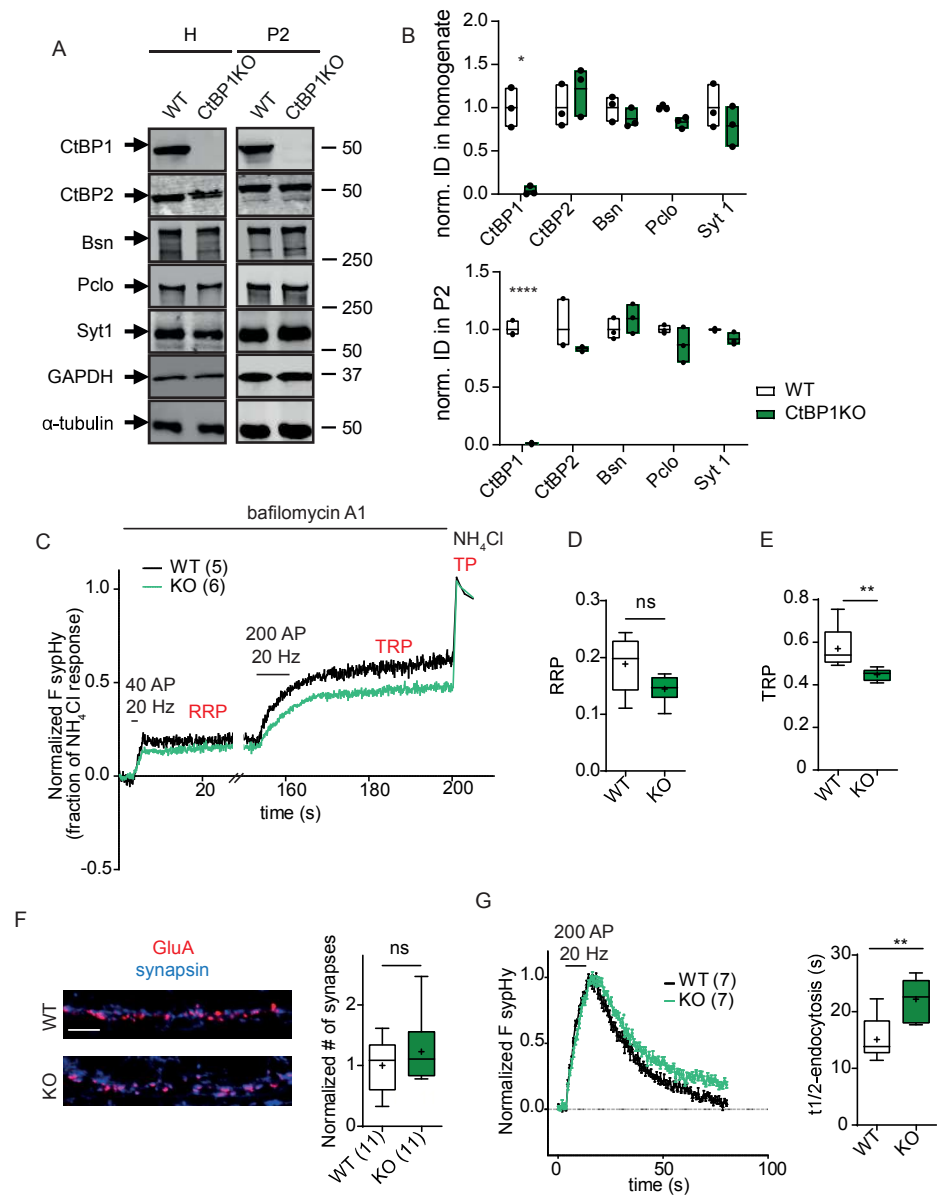


Figure S1



FigureS2

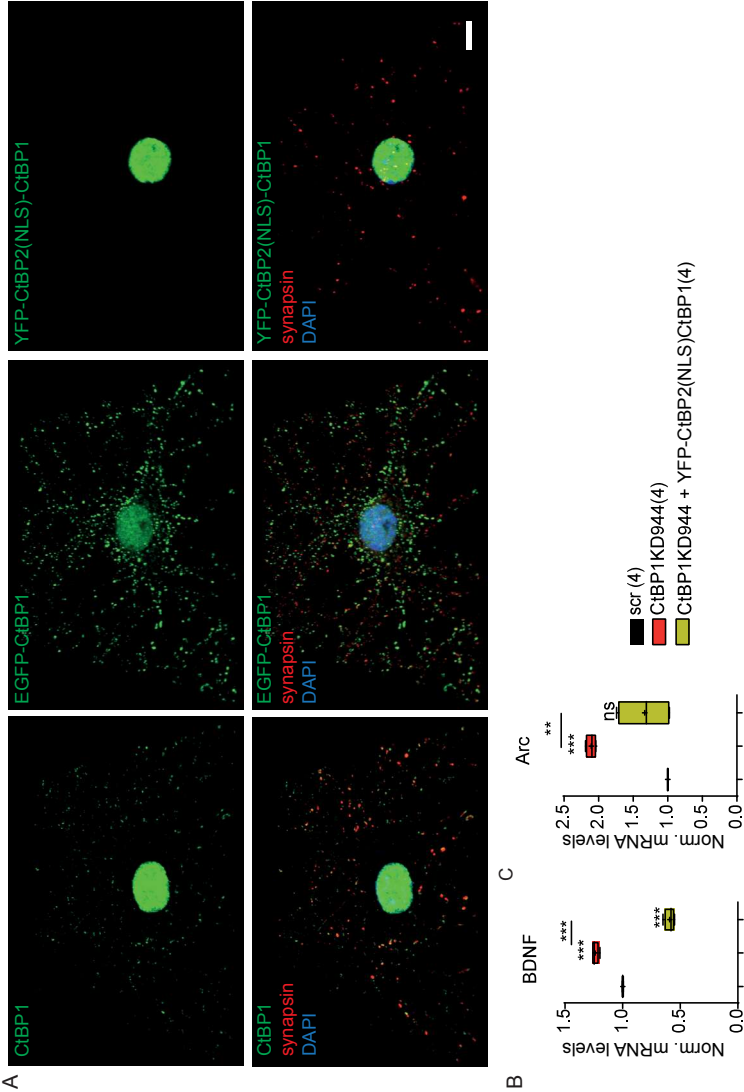
Figure S2





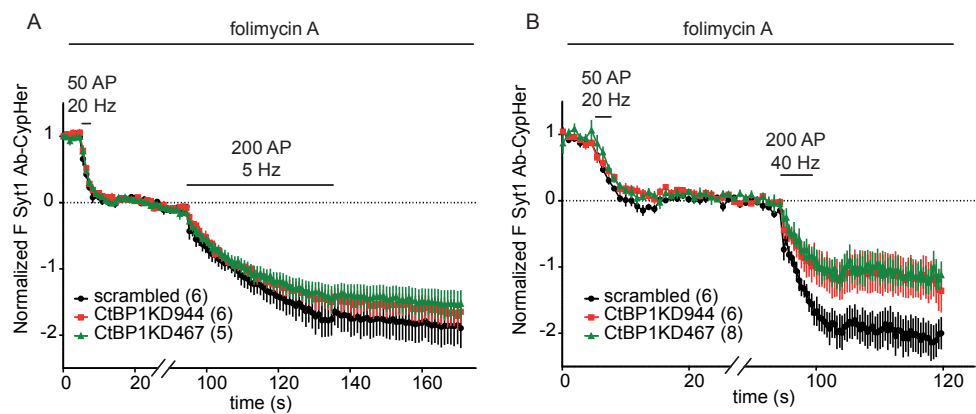
FigureS3

Figure S3



FigureS4

Figure S4



FigureS5

